IOP Concise Physics | A Morgan & Claypool Publication

High Power Microwave Tubes: Basics and Trends

Vishal Kesari
B N Basu

VOLUME TWO

IOP ebooks

High Power Microwave Tubes: Basics and Trends

Volume 2

High Power Microwave Tubes: Basics and Trends

Volume 2

Vishal Kesari
Microwave Tube Research and Development Centre, Bangalore, India

B N Basu
Sir J C Bose School of Engineering, Mankundu, India

Morgan & Claypool Publishers

ISBN 978-1-6817-4704-0 (ebook)
ISBN 978-1-6817-4705-7 (print)
ISBN 978-1-6817-4706-4 (mobi)

DOI 10.1088/978-1-6817-4704-0

Version: 20180101

IOP Concise Physics
ISSN 2053-2571 (online)
ISSN 2054-7307 (print)

A Morgan & Claypool publication as part of IOP Concise Physics
Published by Morgan & Claypool Publishers, 1210 Fifth Avenue, Suite 250, San Rafael, CA, 94901, USA

IOP Publishing, Temple Circus, Temple Way, Bristol BS1 6HG, UK

Dedicated to the Late Professor N C Vaidya, who established the Centre of Research in Microwave Tubes at Banaras Hindu University

Contents

Preface

This is volume 2 of the book. The development of this book is due to the initiative and inspiration of Professor Akhlesh Lakhtakia of Pennsylvania State University. It is a continuation of volume 1, which described the historical timeline of the development of microwave tubes (MWTs), the high-frequency limitations of traditional electron tubes and the means of overcoming them, the factors making MWTs superior to solid-state devices (chapter 1), the classification, applications and trends of research and development in MWTs (chapter 2), some judiciously-selected enabling concepts that will help newcomers to understand the behavior of MWTs (chapter 3), the basic concepts of electron guns, magnetic focusing structures and collectors for the formation, confinement and collection of an electron beam (chapter 4), and the analyses of the beam-absent and beam-present interaction structures of MWTs (chapter 5).

This volume begins with chapter 6, in which we have discussed conventional MWTs (TWTs, klystrons, including multi-cavity and multi-beam klystrons, klystron variants including reflex klystron, IOT, EIK, EIO and twystron, and crossed-field tubes, namely, magnetron, CFA and carcinotron). In chapter 7 we have explored fast-wave tubes (gyrotron, gyro-BWO, gyro-klystron, gyro-TWT, CARM, SWCA, hybrid gyro-tubes and peniotron). In chapter 8 we have discussed vacuum microelectronic tubes (klystrino module, THz gyrotron and clinotron BWO); plasma-assisted tubes (PWT, plasma-filled TWT, BWO, including PASOTRON and gyrotron); and HPM (high power microwave) tubes (relativistic TWT, relativistic BWO, RELTRON (a variant of relativistic klystron), relativistic magnetron, high power Cerenkov tubes including SWO, RDG or orotron, MWCG and MWDG, bremsstrahlung radiation type tube, namely, vircator, and the M-type tube MILO). In chapter 9 one can find handy information about the frequency and power ranges of common MWTs, though more such information has been provided at relevant places in the rest of the book as and where necessary. Chapter 10 sums up the authors' attempt to elucidate the various aspects of the basics of, and developmental trends in, high power MWTs.

The scope of ever-expanding applications of MWTs in the high-power and high-frequency regimes will continue to sustain and intensify the research and development in MWTs in the coming years. We will be happy if our effort to present the basics and trends of MWTs in this book proves to be useful.

Acknowledgment

We profusely express our gratitude to Professor Akhlesh Laktakia for stimulating us to write this book. Mr Wayne Yuhasz has provided us with constant guidance in liaison with Professor Laktakia in the development of the manuscript. We sincerely thank Mr Joel Claypool of Morgan & Claypool Publishers for his suggestions to improve the presentation of the book. We sincerely acknowledge the support we have received from Mr B GuhaMallick, Chairman, SKFGI, and Dr S Kamath, Director, MTRDC.

We sincerely thank Mr Amit Varshney for drawing the figures, and Mr Raktim Guha, Dr Udit Narayan Pal, Dr S Maurya, Dr Ranjan Kumar Barik, Dr S K Datta, and Dr Vishnu Srivastava for helping us to develop the reference section of the book. We wish to record our sincere thanks to Ms Sreelatha Menon for editing some portions of the manuscript of this book.

We would also like to acknowledge Ms M Jayalaxmi, Librarian MTRDC, for her support in providing us with the published literature available at the Technical Information Centre of MTRDC.

Vishal Kesari and B N Basu

Author biographies

Vishal Kesari

Vishal Kesari received a MSc (Physics) degree from Purvanchal University, India, and a PhD (Electronics Engineering) degree from the Institute of Technology, Banaras Hindu University (IT-BHU) (now known as IIT-BHU), India, in 2001 and 2006, respectively. He has worked as a Research Fellow at the Centre of Advanced Study, Electronics Engineering Department, IT-BHU, and significantly contributed to sponsored research projects at the Centre of Research in Microwave Tubes, IT-BHU. He served as a lecturer at the Birla Institute of Technology, Ranchi, India, and the Indian Institute of Information Technology, Allahabad, India, before joining as a scientist at the Microwave Tube Research and Development Centre, Defence Research and Development Organisation, Bengaluru, India. His research interests include microwave and millimeter-wave vacuum electronic devices. He has authored two books: (i) *Analysis of Disc-loaded Circular Waveguides for Wideband Gyro-TWTs* (Lambert Academic Publishing AG & Co., Germany, 2009), and (ii) *High Power Microwave Tubes: Basics and Trends* (IOP Concise Physics; Morgan & Claypool Publishers, London, 2018) (with B N Basu as the co-author), and numerous research papers in peer-reviewed journals and conference proceedings. He has, to his credit, a number of international and departmental level awards including the DRDO Young Scientist Award, 2012. He has acted as a reviewer for various peer-reviewed journals and conference proceedings. He is a life member of the Vacuum Electronic Devices and Application Society, India.

B N Basu

B N Basu received BTech, MTech and PhD degrees from the Institute of Radiophysics and Electronics, Calcutta University in 1965, 1966 and 1976, respectively. He served several organizations in India: RIT, Jamshedpur; CSIR-CEERI, Pilani; DRDO-DLRL, Hyderabad; IT-BHU, Varanasi; IFTM University, Moradabad; and SKFGI, Mankundu. He took visiting assignments abroad at Lancaster University, UK; Seoul National University, Korea; and KIT, Karlsruhe, Germany. He was the CSIR Distinguished Visiting Scientist at CSIR-CEERI, Pilani, and Consultant at DRDO-MTRDC, Bengaluru. He played a pivotal role in establishing MOUs (i) between the Department of Electronics Engineering, BHU and CSIR-CEERI, Pilani; (ii) between Seoul National University and CSIR-CEERI, Pilani; and (iii) between SKFGI, Mankundu and CSIR-CEERI, Pilani. He was President of the Vacuum Electron Devices and Application Society, Bengaluru. He has authored (or co-authored) more than a

hundred research papers in journals of international repute (including 37 in *IEEE Transactions*) and six monograph chapters in the area of microwave tubes. He has authored four books: (i) *Electromagnetic Theory and Applications in Beam-Wave Electronics* (World Scientific, Singapore/New Jersey/London/Hong Kong, 1996) (ii) *Technical Writing* (Prentice-Hall of India, New Delhi, 2007), (iii) *Engineering Electromagnetics Essentials* (Universities Press, Hyderabad, 2015) (distributed by Orient Blackswan, India) and (iv) *High Power Microwave Tubes: Basics and Trends* (IOP Concise Physics; Morgan & Claypool Publishers, London, 2018) (with Vishal Kesari as the co-author). He is on the Editorial Board of the *Journal of Electromagnetic Waves and Applications* and he guest-edited a Special Issue on Microwave Tubes and Applications: Issue 17, Vol 31, 2017 of the *Journal of Electromagnetic Waves and Applications* (Taylor and Francis publication). He served on the Technical Committee on Vacuum Electronic Devices of the IEEE Electron Devices Society. He is a recipient of the SVC Aiya Memorial Award of IETE, Lifetime Achievement Award of the Vacuum Electronic Devices and Application Society, India and ISM Microwave Pioneer Award, Bengaluru.

IOP Concise Physics

High Power Microwave Tubes: Basics and Trends

Volume 2

Vishal Kesari and B N Basu

Chapter 6

Qualitative description of conventional and familiar microwave tubes

The enabling basic concepts in microwave tubes (chapter 3, volume 1), as well as the basic principles of the formation, confinement and collection of an electron beam (chapter 4, volume 1), as well as interaction structures (chapter 5, volume 1) have already been discussed. Therefore, in this chapter let us present a phenomenological description of some conventional and familiar microwave tubes.

6.1 Travelling-wave tubes

The travelling-wave tube (TWT) may be classified as a linear beam/TPO or O/Cerenkov radiation/slow-wave/kinetic energy conversion/distributed interaction type, etc in the family of microwave tubes (see table 2.1 in chapter 2, volume 1). TWTs are mostly available as a helix-TWT or a coupled-cavity TWT (CC-TWT) depending on whether the interaction structure used in the device is the helix or the coupled-cavity structure (figure 5.1 in chapter 5, volume 1). The helical SWS of a helix-TWT usually has positive dispersion characteristics (phase velocity decreasing with frequency). However, wideband device performance calls for the structure to be nearly dispersion-free, more precisely, having slightly negative dispersion characteristics (phase velocity slightly increasing with frequency). CC-TWT usually operates in the fundamental backward-wave mode of the coupled-cavity SWS (see chapter 5, volume 1). Power capabilities of typical TWTs are given in table 9.2 of chapter 9, volume 2.

6.1.1 Phenomenological description

A TWT consists of an electron gun (see section 4.1) to form an electron beam; a slow-wave structure (SWS) (interaction structure) (see chapter 5, volume 1) into which the beam is thrown by the gun for interaction with RF waves; a magnetic focusing structure (see section 4.2) to confine the beam in the SWS; and a collector

doi:10.1088/978-1-6817-4704-0ch6

(single-staged or multi-staged; see section 4.3). The device is also provided with a system of RF input and output couplers connected to the two ends of the SWS (figure 6.1). A built-in attenuator in the form of a resistive coating on the dielectric helix-support rods of a helix-TWT (figure 6.1) prevents the tube, which is essentially an amplifying device, from oscillations caused either by the reflection of RF waves at the RF input and output couplers due to imperfect impedance matching or due to backward wave interaction. The attenuating layer can be deposited on dielectric helix-support rods by pyrolytic cracking of hydrocarbons such as benzene and heptane in a low pressure and inert, say, argon atmosphere, in the vicinity of the work piece which is uniformly heated all around, say, by resistance heating. The thickness of the coating is gradually tapered to zero at the ends of the attenuating region to obtain a good impedance match over a wide range of frequencies [1]. In a CC-TWT, the attenuator is provided in the form of a lossy ceramic button on the spacer-cavity wall of the coupled-cavity structure (figure 5.1 in chapter 5, volume 1). In early helix-TWTs using a glass envelope, a coupled-helix attenuator was used to prevent the device from oscillation [2]. In this type of attenuator, a helix concentric and contra-wound with respect to the main helix is wrapped over a lossy sleeve around the envelope barely touching it. The RF power is thus coupled out from the main helix to the coupled helix and gets absorbed in the lossy sleeve. Care is taken to minimize reflections by terminating both ends of the coupler helix in matched loads and optimizing the parameters such as the resistivity of the sleeve material, separation between the main and the coupler helices, pitch angles of the two helices, length of the coupler helix, etc [3]. There is yet another type of attenuator, namely, the ferrite attenuator which may be realized by placing a cylinder made of non-reciprocal ferrite around the helix forming a part of the tube envelope itself, using either an axial or a circumferential DC magnetic field to magnetize the ferrite. If it is axial the required magnetic field can be obtained from the main focusing field used to confine the electron beam in the device. The circumferential magnetic field (if required) can be produced by an external axial conduction current which can be removed after the magnetization. In a CC-TWT, the slots of the cavity wall may be ferrite-loaded to achieve non-reciprocal attenuation.

Interestingly, the attenuation constant of the attenuator of the TWT in its operating condition, which is referred to as the 'hot' (beam-present) attenuation constant, is not very significant even if its 'cold' (beam-absent) attenuation constant

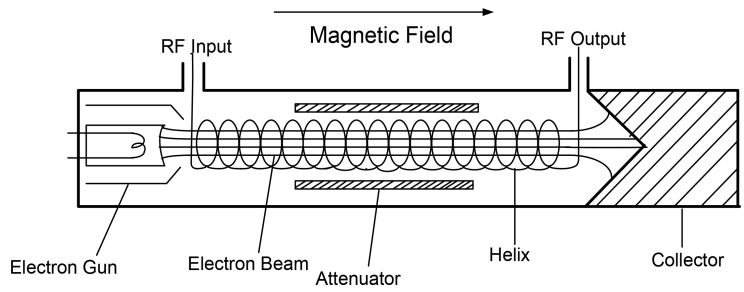

Figure 6.1. Schematic of a travelling-wave tube (TWT).

is very large. The TWTs in their various ranges of power and frequency (see chapter 9, volume 2) enjoy a maximum share in various applications of microwave tubes (see chapter 2, volume 1). The advent of innovative concepts and new technology has made it possible to continually improve the performance of TWTs for various applications.

The phase velocity supported by the SWS in a TWT is made slightly less than the DC electron beam velocity to ensure (i) that the bunch of electrons formed in the device (see section 3.4) continues to remain in the decelerating phase of the RF wave and (ii) that the slow space-charge wave of the beam (see figure 3.1, section 3.3) gets coupled to a forward-wave mode of the SWS so that, according to Chu's kinetic power transfer theorem [2, 4, 5], power is delivered by the beam to the SWS. The operating point of the TWT corresponds to the intersection between the dispersion line of the slow space-charge-wave mode on the electron beam (figure 3.1 in chapter 3, volume 1) and the $\omega - \beta$ dispersion plot of the helix SWS (chapter 5, volume 2) obtainable from its dispersion relation (figure 6.2).

The helix-TWT using a non-resonant helix SWS has a wideband potential. The CC-TWT using a non-resonant coupled-cavity SWS has a lesser bandwidth potential than a helix-TWT. Further, the CC-TWT, being more massive and thermally better than a helix-TWT, can deliver a larger RF output power than a helix-TWT.

6.1.2 Wideband performance

In order to achieve wide bandwidths of a helix-TWT for frequency agility in electronic warfare systems, the dispersion characteristics of the helix SWS are flattened either by vane loading the envelope [6–9] or by tapering the cross section of the dielectric helix-support bars [7] (see chapter 5, volume 1) that makes the phase velocity synchronous with the DC beam velocity. More precisely, instead of

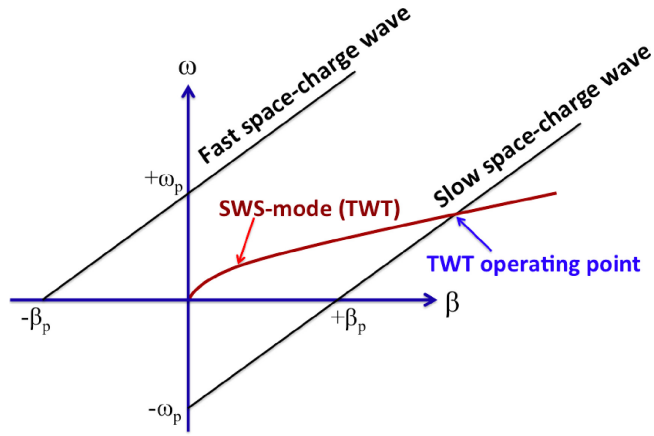

Figure 6.2. Intersection between the slow space-charge-wave mode and the forward SWS mode representing the operating point of a TWT.

flat dispersion characteristics, the helix SWS should have slightly negative dispersion (that is, the RF phase velocity of the SWS slightly increasing with frequency). This in turn makes the Pierce's velocity synchronization parameter $b(= (v_0 - v_p)/(v_pC))$ (see section 5.3 in chapter 5, volume 1) constant for a wide range of frequencies thereby ensuring wideband electron bunching in the device, where v_0 and v_p are the DC beam and RF phase velocities, respectively, and $C(= (KI_0/4V_0)^{1/3})$ is the Pierce's gain parameter, K being the interaction impedance of the SWS and I_0 and V_0 being the DC beam current and accelerating voltage, respectively [2]. However, care needs to be taken to see that the interaction impedance of the helix (chapter 5, volume 1) does not deteriorate while optimizing the helical structure in order to control the helix dispersion for widening the device bandwidth since such deterioration is accompanied by the reduction of the device gain and efficiency as well. There is yet another bandwidth limiting factor of the device, namely, the pi-point (π-point) frequency which satisfies the relation $\beta p' = \pi$, where β is the axial phase propagation constant of the helix SWS and p' is the helix pitch. It corresponds to a peak point of the $\omega - \beta$ dispersion plot of the SWS where the slope representing the group velocity $d\omega/d\beta$ of the SWS is zero. In fact, the TWT and the backward-wave oscillator (BWO) operate below and above the pi-point frequency where the slopes are positive and negative, respectively [10]. Thus, the pi-point frequency is the potential backward-mode oscillation frequency of a TWT.

The gain of a TWT in dB (ignoring the launching loss) is directly proportional to the parameter CN, where $N(= \beta_e l/2\pi = (\omega/v_0)l/2\pi = l/\lambda_e)$ is the interaction length l, expressed in terms of the operating frequency $\omega(= 2\pi f)$ or the number of beam wavelength $\lambda_e(= v_0/f)$ (see section 5.3 in chapter 5, volume 1). Since the value of N decreases with the 'decrease' of the operating frequency f and the value of K decreases, making in turn $C(= (KI_0/4V_0)^{1/3})$ also decrease, with the 'increase' of f, the value of CN decreases, thereby making the device gain also fall, both at lower and higher values of f. If the value of l is increased to increase the value of N and hence enhance the device gain at lower frequencies, then the value N at higher frequencies would become too large to make the device gain too high to make the device prone to oscillations at higher frequencies [11, 12]. The problem is alleviated in the approach of using multi-section, multi-dispersion SWS for realizing wideband TWT performance. In this approach, one of the sections has the conventional structure with positive dispersion (that is, with phase velocity decreasing with frequency). The phase velocity of this section is made synchronous with the DC beam velocity at lower frequencies. The second section is made to have flat dispersion with its phase velocity made synchronous with the DC beam velocity for a wide band of frequencies. As a result, the interaction length of the second section remains effective for the entire band of frequencies, while the first section becomes effective only at lower frequencies such that the effective interaction length of the first section progressively gets shortened with the operating frequency. Thus, this will prevent the device from having enhanced gain at higher frequencies that would otherwise cause oscillation in the device [12].

6.1.3 Efficiency considerations

High efficiency, together with long life and light weight, is as important in the design of a space-TWT for satellite communication as the wide bandwidth in the design of a TWT for electronic warfare. A S Gilmour [13] has depicted the various efficiency terminologies, namely, the collector efficiency $\eta_{\text{collector}}$, the electronic efficiency $\eta_{\text{electronic}}$, the circuit efficiency η_{circuit} and the overall efficiency η_{overall} [13]:

$$\left.\begin{aligned}\eta_{\text{collector}} &= \frac{P_{\text{recovered}}}{P_{\text{spent}}}\\ \eta_{\text{electronic}} &= \frac{P_{\text{output}} + P_{\text{circuit}}}{P_{\text{beam}}}\\ \eta_{\text{circuit}} &= \frac{P_{\text{output}}}{P_{\text{output}} + P_{\text{circuit}}}\\ \eta_{\text{overall}} &= \frac{P_{\text{output}}}{P_{\text{input}}}\end{aligned}\right\}, \tag{6.1}$$

where P_{output} is the useful RF output power. $P_{\text{recovered}}$ is the power recovered by the collector. P_{circuit} is the power loss in the SWS, the later described an equivalent 'circuit' in the absence of the electron beam. P_{spent} is the power in the spent beam being the beam power P_{beam} less the power removed from the beam, given by

$$P_{\text{spent}} = P_{\text{beam}} - \left(P_{\text{interecpt}} + P_{\text{circuit}} + P_{\text{nonlnear}} + P_{\text{output}}\right), \tag{6.2}$$

where $P_{\text{interecpt}}$ is the part of the beam power lost in the physical structure such as the SWS intercepting the beam. $P_{\text{nonlinear}}$ is the 'non-useful' RF power generated in the device due to nonlinear effects in the devices such as harmonic generation and inter-modulation distortion. P_{input} is the total power P_{total} minus $P_{\text{recovered}}$ given by

$$P_{\text{input}} = P_{\text{total}} - P_{\text{recovered}}, \tag{6.3}$$

where

$$P_{\text{total}} = P_{\text{beam}} + P_{\text{heater}} + P_{\text{solenoid}} \tag{6.4}$$

are the powers inputted into the electron beam via an electron gun: P_{beam}, cathode heater: P_{heater} and solenoid (if used as a focusing structure): P_{solenoid} taken together. With the help of (6.1)–(6.4) one can therefore obtain a relation between the device efficiencies as follows:

$$\eta_{\text{overall}} = \frac{\eta_{\text{circuit}}\eta_{\text{electronic}}}{(P_{\text{total}}/P_{\text{beam}}) - \eta_{\text{collector}}(1 - \eta_{\text{electronic}} - (P_{\text{intercept}} + P_{\text{nonlinear}})/P_{\text{beam}}} \tag{6.5}$$

If we (i) take $\eta_{\text{circuit}} = 1$ ignoring the circuit loss (which can be appreciated putting $P_{\text{circuit}} = 0$ in (6.1)) and put it in (6.5); (ii) ignore the contribution of power by the heater and solenoid P_{heater} and P_{solenoid}, respectively, in (6.4) thereby enabling us to

put $P_{\text{total}}/P_{\text{beam}} \approx 1$ in (6.5); and (iii) ignore $P_{\text{intercept}}$ and $P_{\text{nonlinear}}$ each in (6.5), we obtain the approximate relation between the device efficiencies as

$$\eta_{\text{overall}} = \frac{\eta_{\text{electronic}}}{1 - \eta_{\text{collector}}(1 - \eta_{\text{electronic}})} \left(P_{\text{circuit}} = P_{\text{intercept}} = P_{\text{nonlinear}} = 0\right). \tag{6.6}$$

Typically, the value η_{overall} of a helix-TWT can vary from 30% to 50% and that of $\eta_{\text{collector}}$ from 50% to 90% depending, as can be appreciated with the help of (6.5), on the values of P_{total} and $P_{\text{intercept}}$ and $P_{\text{nonlinear}}$, each relative to the value of P_{beam} [13].

The efficiency of a TWT can be increased by the method of 're-synchronization'. In this method for a helix-TWT, the helix pitch is decreased near the output end which enables the RF phase velocity of the SWS to continue to remain synchronized with the DC velocity of the electron beam that slows down after delivering its kinetic energy to RF waves [14]. In a CC-TWT, the required re-synchronization for efficiency improvement can be implemented by reducing the spacing between cavities near the output end of the tube. An alternative is to provide a velocity-jump cavity to boost the operating beam voltage in the so-called the voltage-jump TWT (figure 6.3) [13–15]. The enhancement of the efficiency of a TWT using a multistage depressed collector (MDC) to collect the electrons of various energy classes in the spent beam has been discussed earlier (see section 4.3).

6.1.4 Thermal management and output power

Due attention may be given to the thermal dissipation in a TWT so that the SWS does not get heated to its melting point and the magnetic material of the PPM structure used for beam confinement (see section 4.2) does not reach its Curie temperature both leading the tube close to destruction. In fact, proper thermal management of the TWT is necessary to increase its average RF output power capability. From the standpoint of thermal management of the interaction structure, a helix-derived structure such as the ring-and-bar structure is superior to a helix while a coupled-cavity structure is superior to a ring-and-bar structure (see figure 5.1 in chapter 5, volume 1). Further, the dielectric materials having a good thermal

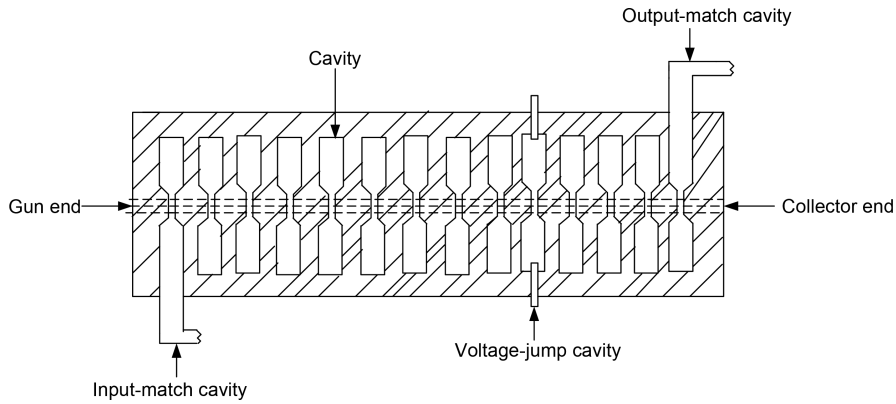

Figure 6.3. Velocity-jump TWT [15].

conductivity such as isotropic boron nitride (IBN), anisotropic pyrolytic boron nitride (APBN), beryllia, alumina and diamond should be used for helix supports. Also, the thermal resistances at the interfaces between the helix and the supports and between the supports and the envelope, which become enhanced in vacuum, need to be reduced. This reduction of thermal resistances can be implemented by the brazed-helix technology which proves to be better from thermal considerations—thereby making it more effective in increasing the average RF output of the device—than the force-fitting technology of the helix in the support-assembly. In the brazed-helix technology [16, 17], the helix made of copper, which has a better electrical and thermal conductivity than the usual tungsten, tungsten-rhenium, etc, is supported by rods made of beryllia, which has poor electrical conductivity but good thermal conductivity and which can be easily brazed to the copper helix and the copper envelope of the structure. The brazed-helix technology also ensures the reduction of hot RF losses of the structure due to a lower temperature, higher electrical conductivity and lower temperature coefficient of resistivity of the copper helix. Further, the non-intercepting gridded gun technology to reduce the grid intercept current also increases the average RF output power of a 'pulsed' TWT of high pulse repetition frequency [14]. The peak power of a TWT can be increased by increasing the beam voltage, which can be better implemented in a coupled-cavity TWT than in a helix-TWT.

6.1.5 Backward-wave excitation, its suppression and role of attenuators

Further, for a helix-TWT, the circumference of the helix relative to the free-space wavelength sets the limit of the beam voltage above which the first backward space-harmonic mode of the helix gets accentuated such that BWO at the pi-point frequency becomes a major source of instability in the device. Such BWO at a high beam voltage can cause in-band power holes and can drive induced oscillations and thus prevent the device from achieving high peak power [12]. One of the methods to suppress BWO in a helix-TWT is to use a frequency-sensitive attenuator which is implemented by printing a gold meander line with a titanium adhesive thin layer on one or two dielectric helix-support rods, say, made of boron nitride (substrate), between helix turns, using the standard MIC lift-off technique [18]. If the distributed loss is to be provided over and above the resonant loss, one can provide two types of loss on the opposite faces of the rod if it is of rectangular cross section. Alternatively, one can provide the resonant loss on one or two of the helix support rods and the distributed loss on the remaining rod(s) [18]. The total un-wrapped length meander line of the attenuator should be made equal to half the wavelength of the BWO frequency so that the lowest resonant frequency is the BWO frequency [13]—the resonant frequency decreasing almost linearly with the ratio of the unwrapped length-to-pattern width. Since the meander line is not printed on all three helix-support rods, an asymmetry in the structure geometry is caused resulting in a stop-band in the $\omega - \beta$ dispersion plot of the structure (see section 5.1 in chapter 5, volume 1) centered at the pi-point frequency. However, since this stop-band enhances the loss at this frequency such

an asymmetric arrangement appears to be beneficial [18–21]. Apart from the method of resonant attenuation to suppress BWO in the helix-TWT, one can try the method of pitch tapering, more precisely, by constructing a pitch step-up at the output end of the helix. In the increased pitch section, the phase velocity of the backward-wave mode supported by the SWS becomes synchronous with the fast space-charge wave on the beam, which, according to Chu's kinetic power transfer theorem, becomes responsible for the transfer of energy from the backward-wave mode to the electron beam [12], thereby attenuating the mode. However, the degradation of the tube performance by the coupling of the forward-wave mode of the SWS along with the backward-wave mode with the fast space-charge wave on the beam is a drawback of the method [22]. Moreover, the pitch step-up for the attenuation of the backward-wave mode being opposite to the pitch step-down for the improvement of tube efficiency becomes another design concern. Yet another method of the suppression of BWO in a helix-TWT is to use a conical helix, the diameter of which varies along its length so that its pitch-to-circumference ratio remains constant [22]. The phase velocity of the forward wave of such a helix, the value of which normalized with the speed of light being approximately the same as this ratio, remains constant along the length though the phase velocity of the space harmonics, including the first negative harmonic (backward-wave), changes along the length. As a result, in this method, useful interaction takes place only with the forward wave and not with the backward wave of the helix thereby suppressing BWO in the device [22]. Apart from BWO, another bandwidth limiting factor in a helix TWT is the band-edge oscillation [9, 18–22, 28] due to a stop-band in the dispersion plot, which is caused by the asymmetry in the dielectric helix-support rods and which can be stabilized against by providing a distributed loss. The issue has already been discussed earlier (see section 5.1 in chapter 5, volume 1) [2].

The attenuator not only does the function of absorbing reflected energy but also absorbs the useful forward energy. The quantitative effect of the attenuator in terms of 'hot' attenuation or beam-present attenuation will be given due consideration later while discussing beam-wave interaction mechanism in a TWT. In order to compensate for the length occupied by the attenuator which does not contribute to the device gain, it becomes necessary to increase the interaction length. However, for a high-power, high-efficiency tube the most common technique of suppressing the backward wave is to sever the SWS typically into two sections, roughly in the middle. The input section is terminated in a load of approximately the characteristic impedance of the SWS at the point where the structure is severed. The output section of the structure is also terminated in a load similarly at the point of division so that the severed loads of the two input and output sections face each other. For high-power tubes, the power absorbed by the severed loads must be carried out of the tube properly through matched transmission lines and subsequently dissipated in dummy loads that are external to the tube structure. For higher gains requiring longer interaction length, the tube needs to be severed into more than two sections and the rule of thumb is to use one section per about 20 dB gain.

6.1.6 Extension of the design to the millimeter-wave regime

The conventional design of a TWT can be extended to the millimeter-wave regime with due consideration to the reduction of the transverse dimension of the SWS at high frequencies. This calls for precision and tight tolerances for the required tiny parts of the SWS. Correspondingly, the electron beam's cross-sectional area has also to be reduced in proportion to the reduced transverse dimension of the SWS. This, in turn, calls for a larger magnetic field of the focusing structure to confine the electron beam of asmaller cross-sectional area (see section 4.2) at higher operating frequencies. Further, in order to restrict the value of the magnetic field to a reasonable value one needs to use an electron beam of a higher beam voltage V_0, that is, of a lower beam perveance $perv$ $(=I_0/V_0^{3/2})$ (defined preceding (4.10) in chapter 4, volume 1) (see section 4.2 for the magnetic focusing structure). Further, a higher value of V_0 is also sought at higher values of the device operating frequency ω for achieving a design-specific value of the parameter γa for a given value of the transverse dimension of the SWS, say, the helix radius a. This can be appreciated by examining the parameter $\gamma a \approx \beta a = (\omega/v_{\mathrm{ph}})a \approx (\omega/v_0)a = \omega/((2|\eta|V_0)^{1/2}a)$, where $\gamma = (\beta^2 - k^2)^{1/2}$ is the radial propagation constant of the SWS, which can be approximated as $\gamma \approx \beta$ under slow-wave assumption $\beta^2 >> k^2, k$ being the free-space propagation constant, $\beta = (\omega/v_{\mathrm{ph}})$ the axial phase propagation constant and $v_{\mathrm{ph}}(\approx v_0)$ (velocity synchronization) the phase velocity of the SWS, $v_0(=(2|\eta|V_0)^{1/2})$ being the DC beam velocity expressed in terms of V_0 and the magnitude of the charge-to-mass ratio of an electron $|\eta|$ (see sections 3.1 and 4.1). For an assigned value of $\gamma a \approx \omega/((2|\eta|V_0)^{1/2}a)$, one has to choose a higher V_0 and hence a lower beam perveance $perv$ for higher values of ω. However, the presence of thermal electrons in the beam formed by the low-perveance electron gun of the high-frequency, millimeter-wave tube, aggravates the problem of focusing. Further, it is obvious that the cathode of a millimeter-wave tube has to be operated with high current density loading which poses a reliability problem [23]. Moreover, thermal management becomes more critical with miniaturized parts of a TWT, more so if brazed helix technology is to be used to develop the device. In a millimeter-wave tube, heat dissipation can be improved by the use of II-A diamond as the helix support material and, alternatively, by plasma-sprayed beryllia over the outer surface of the helix [22, 24]. Structures such as the ridge-loaded helical waveguides [25] have been investigated for their large size, good heat dissipation capabilities, tightly controlled tolerances on the circuit pitch at a reasonable cost, and for their ability to mitigate the effect of the backward space harmonic [2].

6.1.7 RF input/output couplers

In a TWT, the design of the RF input/output couplers connected to the SWS should be commensurate with that of the SWS itself, say, with respect to its bandwidth. The shorter dimension of the waveguide, if it is used as the coupler, needs to be suitably tapered for a good impedance match, and, for wide bandwidths, a ridged-waveguide coupler can also be used. Also, RF windows need to be provided in the body of the

metal tube envelope through which to connect the input/output couplers. For a non-metallic tube envelope of a helix-TWT, the helical coupler in the form of a helix contra-wound with respect to the main helix SWS came into being [26–28]. In the conventional configuration of a helical coupler, called the synchronous coupler, the phase propagation constants on the two helices are the same. The parameters of such a coupler which need to be optimized for the best performance, say, with respect to its bandwidth, are the length of the coupler as well as its pitch and diameter relative to those of the main interaction helix [2, 26–28]. A non-synchronous coupler in which the propagation constant of the two helices are different has been found to be suitable for wideband coupling for a low-noise tube requiring a low beam voltage in which the main helix has a large number of turns and in a situation of loose coupling between the coupled helices [26]. In yet another type, called the tapered helical coupler, wideband coupling has been achieved by adjusting the pitch/diameter of the helices thereby tapering the relative propagation constants of the two helices [26]. Further, an innovative wideband elliptical-cavity coupler was suggested as the coupler of helical SWS [29]. In this coupler, a conical antenna is positioned at one of the foci of a right-elliptic cylindrical cavity so that the base of the conical antenna is fixed on one of the flat walls of the cavity and the cone-tip of the antenna is connected to the central conductor of the input/output coaxial connector through the remaining flat wall of the cavity. Power transfer takes place between the coaxial connector connected to the conical antenna at one of the foci of the cavity and the helix connected to a wire antenna positioned at the second focus of the cavity via reflection from the curved side wall of the elliptical cavity [29]. The coupler in the form of a coaxial line is simple but also the most extensively used type of coupler. In this type of coupler, the helix is directly connected to the central conductor of a coaxial connector. For impedance matching the pitch of the helix can be tapered. In a typical arrangement of a coaxial-cable coupler, the helix becomes an extension of a tapered-pitch slot on a metal cylinder while the latter in turn becomes an extension of the central conductor of the coaxial line; simultaneously with helix pitch tapering, the radius of the metal envelope can also be tapered [30]. The drawback of this arrangement is that it takes much of the interaction length of the tube. In another arrangement of the coaxial-coupler, impedance matching is done. The central conductor of the coaxial line is reduced as it approaches the helix. The arrangement, however, becomes fragile since a relatively long unsupported section of the central conductor of the coaxial line is subjected to mechanical shock and vibration; moreover, this section also needs to be properly cooled [30]. As an alternative to providing the arrangement for tapering the dimension such as the helix pitch or the envelope diameter in this type of arrangement, a simple multi-step quarter wavelength transformer can also be used for impedance matching [31].

6.1.8 Control of gain and phase variations

The impedance matching at the input/output couplers as well as that at each section end of a multi-severed TWT helps to reduce the gain and phase variation of the TWT with frequency. The gain and phase ripples of the TWT can also be minimized

by reducing the gain of each section as well as by increasing the cold distributed loss of the SWS [14, 32]. In a CC-TWT, the reduction of the gain and phase ripples can be implemented by adding small cavities loaded with lossy ceramic buttons and adjusting their protrusion or re-entrance to control the in-band loss that is tapered for a low mismatch [14, 32]. The power supply designer minimizes the phase pushing factor expressed in terms of degree per volt of the voltage of the relevant electrode (cathode, filament, anode, grid, etc) that controls the velocity of electron in beam and hence the phase of the RF output signal with respect to the input. The amplitude modulation (AM)-to-phase modulation (PM) conversion coefficient of a TWT measures the change in the phase difference between the input and output signals in terms of the change per dB of the input power level at a specified output power level. The AM-to-PM conversion coefficient maximizes at a point below the saturation of the output power, and it becomes higher at the high frequency end of the pass band of the tube [14]. Further, the SWS of a TWT needs to be designed for phase linearity which is a measure of the deviation of the tube from the linear phase-versus-frequency characteristics, which also manifests itself in a constant time of passage of a signal through the tube [33]. The phase compensation required for this purpose can be accomplished by adding a helix section of increased pitch which, as discussed earlier, on one hand provides the attenuation of the tube that stabilizes the tube against oscillation, and on the other hand degrades the efficiency of the tube by conflicting with the requirement to decrease the helix pitch for velocity re-synchronization. This calls for the use of a double-taper helix for simultaneous improvements in the device efficiency and linearity and, for more scope, requires dynamic velocity tapering that can be implemented by precise pitch profiling of the helix [34].

6.1.9 Requirement of space qualification

While discussing efficiency considerations in a TWT, we have already mentioned the requirement of long life and light weight along with high efficiency for space-TWTs. The efficiency enhancement by the method of velocity resynchronization in both helix- and CC-TWTs has already been discussed. The use of PPM reduces the weight of the magnetic focusing structure for beam confinement in a TWT. Therefore, lightweight magnetic materials such as samarium-cobalt ($SmCo_5$ and Sm_2Co_{17}) and ALNICO-5 for PPM, which have already been mentioned (section 4.2), need to be considered for space-TWTs. The life of a satellite is said to depend on the life of the TWT, which in turn depends on the life of the cathode of the tube. The following can lead to a longer life of the cathode (see section 3.1): a lighter loading of the cathode, that is, a lower cathode temperature operation for a lower emission current density; the use of a potted heater for an optimum heater-cathode heat exchange; the provision for the expansion and contraction of the heater wire during turn-on and turn-off cycles; the use of adequate emitter coating material if an oxide cathode is used; the provision for optimum porosity of the emitter if a dispenser cathode is used; a lower residual-pressure processing of the tube; the adequate thermal management of the tube; the use of an electronic power conditioner as an integral

part of the tube, which provides protective measures against alarming extremes such as high circuit intercept-current, voltage surge, load mismatch, system arc and inadequate cooling; and so on [2]. Over and above, a space-TWT should be rugged and able to withstand vibration and shock conditions, for example, during the launching of the satellite.

6.1.10 Dual-mode operation

A dual-mode TWT is a special purpose tube which can be selectively operated either in CW or pulsed mode [35]. For this purpose, in a typical arrangement, a dual-perveance electron gun is used in which the control grid of the gun is split into two electrically insulated sections flushing each other—the inner section being circular and the outer section annular. For a higher beam current and higher power of the tube, both the sections of the gun are operated at the same positive potential in the higher perveance-mode and, for a lower beam current and a lower power of the tube, the potential of the outer section is reduced to zero, or to some negative value in the lower perveance-mode. Thus, in this arrangement, an annular outer portion of the beam is removed in the lower perveance-mode reducing the beam current and the tube power. Interestingly, however, in this dual-perveance-mode operation of the gun, the beam's current and cross-sectional area are changed in the same proportion so that the beam current density remains the same in both modes of operation. This in turn allows the same focusing magnetic field to be used in both the modes as can be appreciated, say, with the help of (4.43) in chapter 4, volume 1 [36].

6.1.11 Performance improvement by external means

In order to attain high pulsed power over a wide band of frequencies and relax thermal management a number of pulsed TWTs can be combined in a system using 3-dB magic tees and phase shifters. Further, the operation of the system using such TWTs in combination can be operated in the condition of graceful output power degradation and with higher intrinsic reliability because of more redundancy in the system and the potential of operating each tube at a lower output power level in the system. Similarly, in order to reduce the harmonic content of the TWT that impairs the operation of a wideband TWT, particularly at the lower end of the operating frequency band and thus increase the electronic efficiency of the tube, one can inject another signal—along with the signal to be amplified—at the second harmonic frequency of the signal. The method involves the adjustment of the relative amplitude and phase of the harmonically related signals [14, 37, 38].

6.1.12 Backward-wave oscillator

The backward-wave oscillator (BWO), also known by its trade name 'carcinotron', belongs to the TWT family. They are available as sources of both O-type and M-type (see chapter 2, volume 1)—the latter using crossed electric and magnetic fields as in a magnetron (discussed in section 6.3). However, unlike a conventional TWT which is an amplifier, BWO is an oscillator that can be used as a voltage-tuned signal generator. Helix-type BWOs can be rapidly tuned in less than a microsecond

over an octave bandwidth. In view of the potential for being swept through the band fast enough—as if it delivers output over the entire band at the same time—BWO is suitable for jamming a radar in electronic warfare (electronic counter measure). BWOs are usually available at frequencies typically up to 50 GHz delivering tens of milliwatts of power [13]. Further, vacuum-microelectronic technology has extended the operating frequency of BWO to the terahertz regime (see chapter 8, volume 2). At high operating frequencies, typically, the O-type BWO can deliver powers ~50 mW at 200 GHz and ~1 mW at 1000 GHz. Also, relativistic BWOs have been built in the high power microwave (HPM) regime (see chapter 8, volume 2). Unlike in a TWT, where at the operating point the phase velocity (being the slope of the line joining the origin of the $\omega - \beta$ dispersion plot of the SWS to the operating point on the plot) and the group velocity (being the slope $d\omega/d\beta$ of the dispersion plot of the SWS at the operating point) are both positive (figure 6.2), in a BWO at the operating point, while the phase velocity is positive, the group velocity is negative (figure 6.4(a)). Consequently, in BWO, unlike in a TWT (figure 6.1), RF power is extracted at the output port located near the gun of BWO (figure 6.4(b)). The DC beam voltage of BWO can be changed to change the DC beam velocity, thereby changing the RF phase velocity to be synchronous with the beam velocity, and hence change the operating point of BWO over a wide negative group velocity region of the dispersion plot of the SWS (figure 6.4(a)).

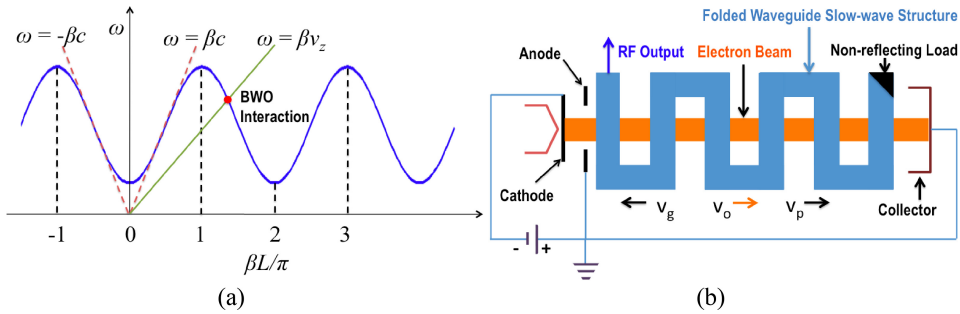

Figure 6.4. (a) The operating point of BWO where the line joining it to the origin has a positive slope representing a positive phase velocity and also where the slope of the tangent has a negative slope representing a negative group velocity and (b) a schematic of BWO using, typically, folded-waveguide SWS (see figure 5.1 (c) in chapter 5, volume 1).

6.2 Klystrons

The klystron may be classified as a linear beam/O/kinetic energy conversion/ localized interaction/ transition radiation type, etc. in the family of microwave tubes (see table 2.1 in chapter 2, volume 1). High power klystrons have applications in UHF television transmitters, satellite communication, radar transmitters as well as in particle accelerators. By providing a positive feedback from the output cavity to the input cavity the klystron can be made to work as a low-power oscillator in a microwave relay communication system. The klystron can also be used as a frequency multiplier [39]. Klystrons are available in two-cavity (figure 6.5(a)),

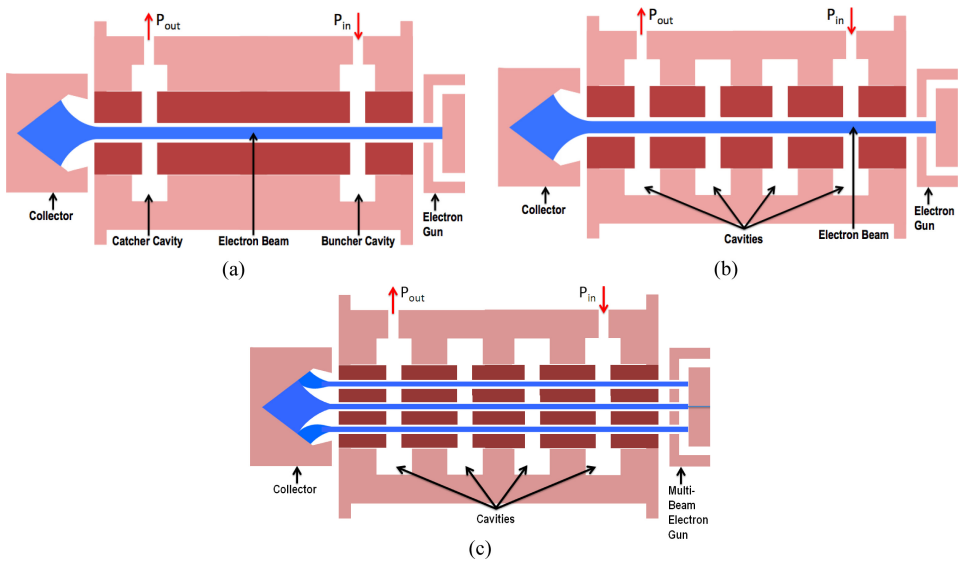

Figure 6.5. Schematic of klystrons in (a) two-cavity, (b) multi-cavity and (c) multi-beam configurations.

multi-cavity (figure 6.5(b)) and multi-beam (figure 6.5(c)) configurations. Power capabilities of typical high-power klystrons are given in table 9.3 of chapter 9, volume 2.

6.2.1 Two-cavity klystron

The two-cavity klystron configuration consists of (i) an electron gun (see section 4.1) similar to that of a TWT (section 6.1); (ii) two re-entrant cavities—one input cavity, also called the buncher cavity and the other output cavity, also called the catcher cavity, both tuned at the device operating frequency (a re-entrant cavity being one in which the metallic boundaries extend into the interior of the cavity); (iii) a drift region between the two cavities; and (iv) a collector (single-staged or multi-staged; see section 4.3) as in a TWT (section 6.1) (figure 6.5(a)). A magnet focusing structure (see section 4.2) confines the electron beam in the device.

An RF signal can be coupled into the input cavity of the klystron, for example, by a coaxial cable. A large RF electric field is created at the short gap of a re-entrant cavity through which the electron beam passes with a transit time much smaller than the RF time period $1/f$; where f is the operating frequency of the klystron which is also the cavity resonant frequency. RF energy fed into the input catcher cavity at or near the cavity resonant frequency creates standing waves and sets up an oscillating voltage across the gap of the cavity that acts on the electron beam thereby producing beam velocity modulation [39]. In the drift region where RF waves do not exist, the velocity modulation of the electron beam is converted into the density modulation of the beam so that the accelerated electrons catch up the retarded electrons to form a bunch of electrons as explained earlier using the Applegate diagram (see figure 3.2 in section 3.4 in chapter 3, volume 1). During the process of bunching, the fast and slow

electrons are respectively slowed down and speeded up to the DC beam velocity at an axial distance from the input cavity of the quarter of plasma wavelength (being the beam velocity per plasma frequency). At this axial distance, therefore, the beam current peaks where the output cavity is placed. At the output catcher cavity, a series of bunches of electrons arrive at an interval of time equal to the time period of the RF cycle to experience a decelerating RF electric field, thereby slowing down to transfer their kinetic energy to RF energy. As a result of this energy transfer, the oscillations induced in the cavity build up in amplitude, which are then coupled out through a coaxial line or a waveguide as an amplified version of the signal injected into the input cavity. After this energy exchange in the output catcher cavity the spent electron beam is captured by the collector of the device as in a TWT.

Unlike the TWT, which operates in the non-resonant mode, the klystron operates in the resonant mode. Therefore, the klystron has higher electronic conversion efficiency, though it is of narrower bandwidth—to a maximum ~10%—than the TWT which enjoys a multi-octave bandwidth. The gain of a two-cavity klystron which is ~10 dB can be increased by adding an intermediate cavity in a three-cavity klystron.

6.2.2 Multi-cavity klystron

In a three-cavity klystron, the third cavity, located where the first bunch of electrons appears beyond the first cavity, intensifies the beam density modulation and hence the current growth and therefore enhances the device gain and efficiency. The device gain can be increased by increasing the number of intermediate cavities (figure 6.5(b)) though to a limit imposed by the amplification of the shot noise. The RF beam current induces a signal at each intermediate cavity, which in turn produces a field that enhances the bunching in the beam. A gain as high as 60 dB and a limited bandwidth ~10% can be produced by the coupling of the intense RF beam current to the output cavity of the multi-cavity klystron. In order to achieve maximum device gain, all the cavities are synchronously tuned to the operating frequency. In order to maximize the device efficiency, the cavities are first synchronously tuned to the operating frequency and then the penultimate cavity is tuned upward in frequency to maximize the device power output. Tuning for maximum bandwidth is achieved by first synchronously tuning all the cavities to the operating frequency at a low power level and then adjusting the detuning of the intermediate cavities for the desired wide device bandwidth. Further, a high-perveance electron beam presenting low beam impedance in the output cavity can be used for wide bandwidths [13, 40]. Capable of delivering megawatts of output power at frequencies from 500 kHz to over 30 GHz, the multi-cavity klystrons have a variety of applications such as: radar, communication, charged-particle accelerator, plasma heating for tokomak, material processing, medical, industrial and scientific. Klystrons are not suitable for the amplification of low signal levels because of their shot noise. However, they can be cascaded in a number of stages to amplify a low-level signal to the desired level so that the last stage driven to saturation gives the desired high level of power [36]. An attempt has been made to develop klystrons for high frequencies with the help of

vacuum-microelectronic technology, such as the W-band klystrino (~3 mm wavelength), in which provision is made for separate beams, cavities and PPM stacks, but with a common collector (see chapter 8, volume 2).

6.2.3 Multi-beam klystron (MBK)

The use of a low-perveance, high-voltage beam to obtain high efficiency of a single-beam klystron entails the risk of voltage breakdown leading to the reduction of the reliability of the tube. On the contrary, a low-voltage beam is associated with a high perveance giving rise to space-charge repulsion thereby preventing the required bunching of the electrons in the tube to make it non-functional. The advent of MBK, which uses several electron linear beamlets, reportedly as low as six to as high as 94, each propagating in its own channel and then interacting with the field of a common interaction structure (figure 6.5(c)), is a breakthrough in the development of high power, light weight, compact klystrons. Even though the values of the current and perveance of the individual beams are not high in MBK, the values of the total current and perveance of the entire multi-beam stream can be high. Therefore, the space-charge effects and correspondingly the efficiency of MBK remain the same as those of a single-beam klystron, and by increasing the number of linear beamlets in MBK, its beam current, overall beam perveance and power can be increased. Thus, MBK can be designed to operate at a lower beam voltage, larger beam current and larger RF output power. Further, the reduction of the operating voltage also reduces the dimensions and weight of the device and its power supply and also saves the weight and size of the modulator. Also, the low perveance values of the individual linear beamlets relaxes the values of the magnetic field required to confine these beams and makes the design of the focusing structure less critical. The low beam perveance also gives the low beam impedance, which can support a low-Q operation of MBK leading to a wide device bandwidth. MBK also enjoys good spectrum purity and noise characteristics. However, the MBK has the disadvantage of the possibility of a reduction of the lifetime of the cathode due to its smaller size and higher loading. Issues such as the back scattering of electrons and the improvement of the device's average power by adequate thermal management need attention. The increased complexity of the design leads to a higher cost for the development of MBK. Technological challenges include the development of a multi-emitter cathode with higher emission density and longer life, the difficulty of focusing beamlets off the axis where a higher radial magnetic field is present, and the frequency tuning of cavities [13, 40].

The small size of MBK is attributed to the reduction of the plasma wavelength which determines the cavity-to-cavity distance. The required lower magnetic field in MBK attributable to the lower space charge field supported by the low-perveance beam makes it possible to design the device with PPM stacking, which lowers the weight of the device. Therefore, besides radars, particle accelerators, etc., MBKs also find applications in airborne systems. Typically, MBKs have delivered 1 GW power at 1.5 GHz frequency with 36 dB gain and 40% efficiency using 10 individual 500 kV, 500 A (1.5-microperv) beams (SLAC MBK); and 10 MW power at 1.3 GHz

frequency with 47 dB gain and 70% efficiency using 10 individual 115 kV, 13 A (1.6-microperv) beams (L-3 Communications Electron Devices MBK). The specifications of a typical Thales 7-beam MBK for a Tera-electron-volt energy superconducting linear accelerator (TESLA) programme in comparison with those shown in parenthesis of a single-beam klystron are frequency: 1.3 GHz (1.3 GHz), peak power: 10 MW (5 MW), pulse length: 1.5 ms (1.5 ms), prf: 10 Hz (5 Hz), efficiency 65% (45%), beam voltage: 117 kV (128 kV), beam current: 131÷7 = 18.71 A (89 A); number of klystrons per linac 600 (1200). In the preceding example, as compared to a single-beam klystron operating at the same frequency, the peak power and efficiency of MBK have both increased with lesser beam voltage and lesser beam current if they refer to individual linear beamlets, though with larger beam current, if it refers to the total beam current of the individual currents of the linear beamlets put together [13, 40].

6.3 Klystron variants

Oscillations can be excited at the resonant frequency, say, of a two-cavity klystron provided with high-Q cavities by the amplification of electronic noise in the cavity. In the device, a coaxial line or a waveguide provides a regenerative or positive feedback of the amplified noise from the output catcher cavity to the buncher cavity to be amplified again. The power from the oscillator can be coupled out from the output cavity. However, in a device called the reflex klystron that uses a single cavity, an internal positive feedback mechanism is provided [13, 40].

6.3.1 Reflex klystron

The reflex klystron is an oscillator tube which uses the same cavity, performing the function of the buncher and catcher cavities, providing internally a built-in feedback mechanism. In a reflex klystron, the electron beam from the electron gun (see section 4.1), the cathode and anode electrodes of which are shown in the schematic of the device (figure 6.6(a)), passes through the gap of a resonant re-entrant cavity to move towards the reflector or repeller electrode. The polarity of the repeller voltage V_r is reversed with respect to the anode voltage V_0 (figure 6.6(a)) so that the outgoing

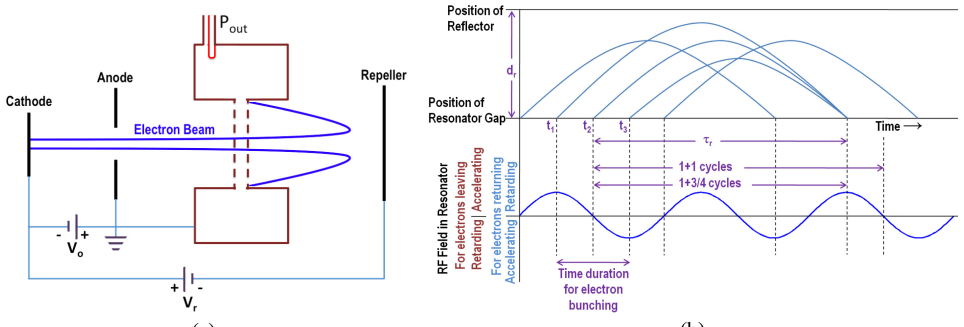

Figure 6.6. Reflex klystron —(a) schematic and (b) Applegate diagram for the explanation of electron bunching mechanism [39].

electrons from the cavity are repelled by the repller electrode to pass again through the cavity-gap where they are collected. The greater the V_0 and the less the V_r, the greater the distance will be for the outgoing electrons to penetrate into the cavity-gap-repeller region. The electrons are velocity-modulated in the cavity-gap before they move from the cavity-gap towards the repeller. The bunching of electrons takes place in the cavity-gap-repeller drift region that can be explained with the help of the Applegate diagram (figure 6.6(b)). The repeller voltage is adjusted so that the returning bunch of electrons should arrive at the cavity-gap at a time when the RF voltage becomes maximum in the accelerating phase of outgoing electrons, which corresponds to the retarding phase of the incoming bunch of electrons moving opposite to the outgoing electrons. Thus, the bunch of returning electrons in its second passage through the cavity gets retarded to transfer the kinetic energy of the bunch to the RF energy of the cavity. The understanding of this becomes further clear by referring to the trajectories of typically three electrons emanating from the resonator cavity at the instants of time t_1, t_2 and t_3 when the RF electric fields in the cavity are, respectively, at the three phases of outgoing electrons: (i) accelerating phase, (ii) neither accelerating nor decelerating phase and (iii) decelerating (or negative accelerating) phase of the RF cycle (figure 6.6(b)). The electrons, emanating at times t_1 and t_3, penetrate greater and less distances in the cavity-repeller region than the electron emanating at time t_2. When the repeller voltage V_r and the anode voltage V_0 are suitably adjusted, these three electrons, after completing their outgoing and returning flight in the cavity-gap-repeller region, arrive collectively at the cavity-gap to form a bunch around the electron that emanated from the cavity at the instant t_2, typically, after 1 + ¾ RF cycles (figure 6.6(b)). The phenomenon can be generalized by replacing the number of RF cycles 1 + 3/4, following which the bunch forms, with N + 3/4 N, where N is an integer typically between 1 and 10 [39].

The average transit time of travel of the outgoing and returning electrons in the cavity-gap-repeller region can be analytically appreciated starting from the equation of electronic motion

$$\frac{dv(t)}{dt} = -\frac{|e|}{m}\frac{V_0 + |V_r|}{d_{\text{gap-repeller}}}, \tag{6.7}$$

where $v(t)$ is the instantaneous velocity of the electron, and $|e|$ and m are, respectively, its charge magnitude and mass. $d_{\text{gap-repeller}}$ is the distance between the cavity-gap and the repeller, the electric field in the region being $(V_0 + |V_r|)/d$. Integrating (6.7) we obtain

$$v(t) = -\frac{|e|}{m}\frac{V_0 + |V_r|}{d_{\text{gap-repeller}}}t + v_i, \tag{6.8}$$

where v_i is the integration constant, being the initial velocity of the outgoing electron at time $t = 0$. The one-way drift time $t = t_{\text{one-way drift}}$ of the electron in the cavity-gap-repeller region before it comes to a stop can be found putting $v(t) = 0$ in (6.8) as

$$t_{\text{one-way drift}} = \frac{m v_i d_{\text{gap-repeller}}}{|e|(V_0 + |V_r|)}. \tag{6.9}$$

Therefore, with the help of (6.9) putting therein $v_i = v_0$, the DC beam velocity, the average electron transit time t_{average} in the cavity-gap-repeller region, taking into account both the outgoing and returning transit of the electron in the region, can be found as

$$t_{\text{average}} = 2t_{\text{one-way drift}}\Big|_{v_i=v_0} = \frac{2m v_0 d_{\text{gap-repeller}}}{|e|(V_0 + |V_r|)}. \tag{6.10}$$

Substituting $v_0 = \sqrt{2(|e|/m)V_0}$, where V_0 is the anode accelerating voltage of the electron gun (figure 6.6.(a))—the relation obtained by equating the beam kinetic and potential energies—in (6.10), we obtain

$$t_{\text{average}} = \frac{2d_{\text{gap-repeller}}}{V_0 + |V_r|}\sqrt{\frac{2mV_0}{|e|}}. \tag{6.11}$$

We can also find t_{average} as the time corresponding to $N + 3/4$ cycles of the accelerating field for outgoing electrons at the cavity-gap as

$$t_{\text{average}} = (N + 3/4)T = \frac{N + 3/4}{f}, \tag{6.12}$$

where T is the time period of a cycle and $f(=1/T)$ is the wave frequency which is also the cavity resonant frequency [39]. Therefore, equating (6.11) with (6.12) we get the condition for the energy transfer of the decelerated electron bunch at the cavity at its return passage as:

$$\frac{(N + 3/4)(V_0 + |V_r|)}{f} = 2d_{\text{gap-repeller}}\sqrt{\frac{2mV_0}{|e|}}. \tag{6.13}$$

It is clear from (6.13) that a series of the values of the repeller voltage $|V_r|$ exist for a fixed accelerating anode voltage V_0 for the device to oscillate at a constant frequency, for a given value of the $N + 3/4$ mode, the value of $|V_r|$ decreasing with the increase of the integer N. In other words, for example, the excitation at the mode $3 + 3/4$ will call for a lower value of the repeller voltage $|V_r|$ than that at the mode $1 + 3/4$. Further, the output power can be increased by increasing the beam power, which in turn can be done say by increasing the anode voltage V_0 for an increased beam voltage—which according to (6.13), will correspond to a lower value of N. Thus, for example, the out power of the mode $1 + 3/4$ will be greater than that of the mode $3 + 3/4$. It can be appreciated from (6.13) that the reflex klystron can be electronically tuned in frequency by adjusting the values of V_0 and $|V_r|$. Hence, the reflex klystron can be considered as a voltage-controlled oscillator that can serve as a local oscillator for radar equipment and microwave receivers. However, this electronic control of oscillation frequency of the reflex klystron is rather limited in view of the cavity having a high value of the Q factor, calling for mechanical tuning of the

operating frequency by changing the cavity dimensions. Even though the reflex klystron faces stiff competition from semiconductor devices developed by microelectronics technology, an attempt has been made to use the vacuum microelectronics technology itself to develop a monolithic terahertz reflex klystron capable of delivering ~mW of power at 1.2 THz (see chapter 8, volume 2).

6.3.2 Inductive output tube

The inductive output tube (IOT) or klystrode that finds use in radio and TV broadcasting in the UHF transmitter is emerging as a competitor to the klystron as an amplifying device, mainly because of its high efficiency and compactness. It also has potential application in a particle accelerator and a thermonuclear fusion reactor. The IOT (figure 6.7) is an integrated assembly of (i) a conventional electron tube like the triode and (ii) a klystron. The electron gun of the tube not only forms the electron beam but also becomes part of the interaction cavity where the bunching of electrons takes place simultaneously. In the IOT, the electron beam is density-modulated by applying the signal to be amplified to the grid of the electron gun (figure 6.7). Interestingly, in the TWT developed and patented by N E Lindenblad as early as 1949, the signal was applied to the grid, unlike in the present-day TWT in which the signal is coupled in the slow-wave structure at the input end of the tube (see table 1.1 in chapter 1, volume 1). In the IOT, a cavity, similar to the output or catcher cavity of the klystron (typically, a toroidal cavity), surrounding the electron beam extracts power from the beam without actually intercepting the beam (figure 6.7). A typical IOT (CPI-VKP-9050) can deliver 90 kW of power at 500 MHz with 70% efficiency.

6.3.3 Extended interaction klystron (EIK)

Notwithstanding the method available for broadbanding a conventional multi-cavity klystron by detuning the intermediate cavities of the device or by using a

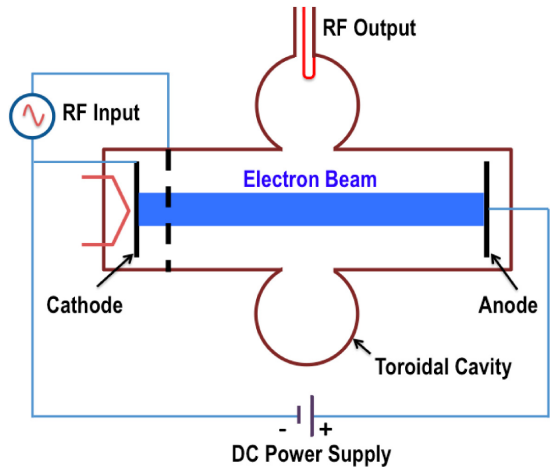

Figure 6.7. Schematic of an IOT.

high-perveance electron beam for low beam impedance in the output cavity, a variant of the device has come into being for wide bandwidths, namely, the extended interaction klystron (EIK). The EIK functions as an amplifying tube like a two-cavity klystron and CC-TWT and is, in fact, a mix of both of them, preserving the ruggedness as well as the high power capability of both while enjoying somewhat the bandwidth of the latter. In an EIK, one or more re-entrant cavities of the conventional klystron are replaced by the section(s) of the coupled-cavity SWS (see figure 5.1(b) in chapter 5, volume 1)—typically, here a ladder structure (figure 6.8). The ladder structure has alternate long slots and provides alternate accelerating or decelerating fields to the beam passing through the axis of the structure (figure 6.8). Each cavity (as in a CC-TWT) represents a short piece of the resonant SWS based on the ladder geometry. An electron beam with its DC velocity approximately synchronous with the RF phase velocity of the ladder SWS is velocity-modulated at each gap of the structure (figure 6.8). The electron bunch will form at a distance in the buncher section of the EIK where repeatedly accelerated electrons catch up with decelerated electrons. In the catcher section of the EIK the electron bunch crosses the gaps of the structure when the RF fields are retarding, so that the kinetic energy of the bunch is transferred to the RF energy for the bunch velocity, slightly greater than the RF phase velocity as in a CC-TWT, and the amplification RF signal takes place. The spent electron beam is captured by the collector which may be depressed for increased efficiency. The ladder SWS provides a higher interaction impedance K for a higher beam voltage V_0 and a lower beam current I_0 (that is, for a higher beam impedance V_0/I_0), which is required to realize a higher Pierce's gain parameter $C = (KI_0/4V_0)^{1/3}$ (see chapter 5, volume 1). A high gain per length of the device permits short-length SWS, which in turn enables a permanent magnet to confine the electron [13, 40] (figure 6.8). The number of periods of the structure determines the conditions of RF stability and efficient beam modulation. The short-length of the ladder helps to minimize parasitic modes. The device can be operated in the pulsed-power mode by switching the beam with the BFE potential of the electron gun (see section 4.1 in chapter 4, volume 1). In one of the modes of operation of the EIK, for a higher level of power, the fields in all cavities of

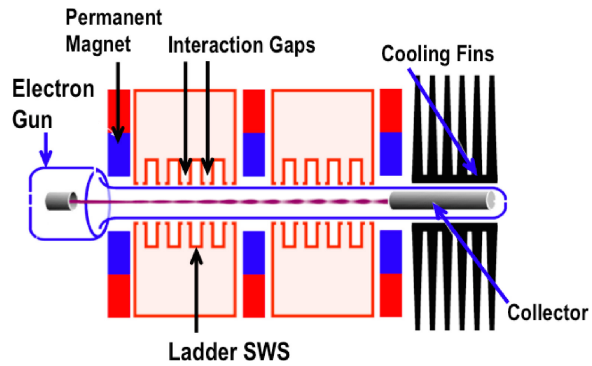

Figure 6.8. Schematic of the EIK showing the buncher and catcher sections comprising typically ladder SWS [41, 42].

the SWS are in phase while in another mode, for a medium level of power, the adjacent cavities are 180° out of phase, as in the fundamental backward-mode of a CC-TWT (chapter 5, volume 1). Further, the EIK provides increased power handling capability due to output voltage divided among the interaction gaps of the output cavities, which reduces each gap voltage thereby reducing the chances of breakdown and arcing [40] (figure 6.8). Considerations such as stability, however, limit the number of cavities.

EIK can be compact since the high gain per unit length of the extended interaction structure reduces the total length of the extended interaction structure, which also simplifies the design of the permanent magnet focusing system. The compactness enjoyed by the EIK makes it possible to fabricate the device by vacuum microelectronic technology (see chapter 8, volume 2) in the millimeter-wave and sub-millimeter-wave frequency regime from 18 to 280 GHz [43]. Typical EIKs developed by CPI, Canada, gave powers 3000 W (pulsed) and 400 W (average) at 95 GHz; 400 W (pulsed) and 50 W (average) at 140 GHz; 50 W (pulsed) and 10 W (average) at 183 GHz; 50 W (pulsed) and 6 W (average) at 220 GHz; and 50 W (pulsed) and 0.3 W (average) at 280 GHz [43].

6.3.4 Extended interaction oscillator (EIO)

An extended interaction oscillator (EIO) consists of a single resonator cavity containing a segmented drift tube in the form of a ladder-like coupled-cavity SWS, as in an EIK, through which the electron beam (formed by an electron gun) can pass. A collector captures the spent beam. Mechanical tuning of the resonator frequency with the help of a moving piston is provided in the device (figure 6.9).

The mechanism of electron bunching and energy transfer from the beam to RF is similar to that described for an EIK. The structure in the resonant mode provides strong cavity-to-cavity coupling and at sufficiently high beam currents, oscillations are sustained and significant RF power levels can be generated in an EIO. An EIO can operate at higher power levels than a reflex klystron or a magnetron since, unlike the latter, an EIO does not intercept the electron beam giving it, in particular, an

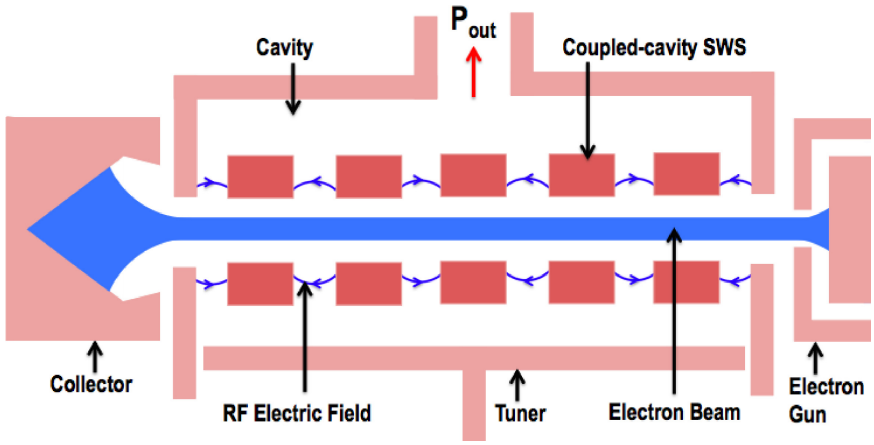

Figure 6.9. Schematic of an extended interaction oscillator (EIO).

edge at higher frequencies, say, in the millimeter-wave range where the tube sizes become reduced. The EIO output power depends on the beam voltage and it can give CW or pulsed power using a cutoff grid in the gun. Besides mechanical tuning by changing the position of the tuner piston (figure 6.9), it is possible to electronically tune the device by varying the beam voltage, which changes the rate at which the electron bunches pass the gaps in the segmented drift tube. Amplitude modulation can be implemented by controlling the beam current independently of the beam voltage, which can be done by isolating the electron gun from the body of the tube. Besides mechanically tuning the EIO by changing the position of the piston in the cavity, it is possible to vary its frequency without changing its output power level if the beam voltage and anode voltages are appropriately controlled. Power outputs of several kWs at 40 GHz and ~100 W down to 100 GHz are typical of the EIO [43].

6.3.5 Twystron

Twystron is an amplifying tube constituted by a klystron-like driver section and a TWT-like output section. In the gain-frequency response of the tube, the TWT section shows a single peak at the centre of the desired band. The klystron of the driver section is stagger-tuned to exhibit two gain peaks on the two sides of the centre of the band where it shows a gain sag in the response. The overall gain in dB of the tube, obtained by adding the gains in dB of the individual sections, shows a very wide gain-frequency response (figure 6.10). Typically, flat peak output powers of several MWs over a bandwidth up to 15% can be achieved by a twystron.

6.4 Crossed-field tubes

Crossed-field microwave tubes are basically electronic potential energy conversion devices. It has been appreciated earlier by a simple analysis that on average the kinetic energy of electrons remains unchanged in such a device (see section 3.7 in chapter 3, volume 1). In such a tube the electrons can be made to fall through a large electric potential for the conversion of their large potential energy into RF waves,

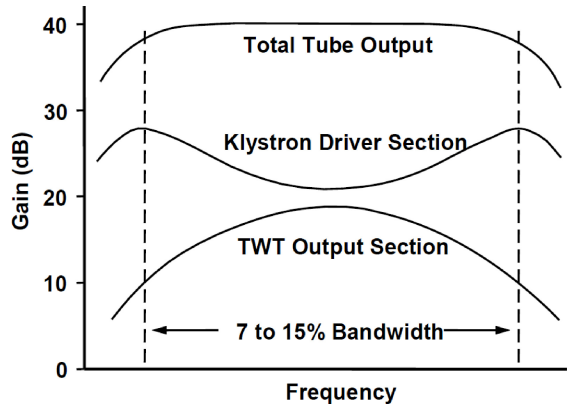

Figure 6.10. Gain-frequency response of a twystron [40, 44].

thereby making the tube highly efficient. Further, a crossed-field tube belongs to the M-type microwave tube category (see section 2.1 in chapter 2, volume 1) in which the electron flow is subject to crossed DC electric and magnetic fields. Crossed-field tubes are available as (i) sources, namely, the magnetron oscillator and the M-type backward-wave oscillator (M-BWO) or carcinotron and (ii) amplifiers such as the crossed-field amplifier (CFA) or amplitron.

6.4.1 Magnetron

Magnetrons came into being before the advent of TWTs (section 6.1), klystrons (section 6.2) and klystron variants (section 6.3) (see table 1.1 in chapter 1, volume 1) and continue to have applications as microwave devices even today in radar, diathermy, industrial heating, microwave ovens, etc. Large S-band magnetrons are capable of delivering MWs of peak power and kWs of CW power with efficiencies as high as 50%–80% [39]. Magnetrons of typical output pulsed peaks powers of 2 MW in the X-band and 8 kW in the W-band with a duty cycle of 0.01 are available [45]. Creating about 700 W of CW power at 2.45 GHz with an efficiency of around 65% with 1.1 kW input is typical of the magnetron of a microwave oven. Large magnetrons often requiring water-cooling have widespread applications where high power is needed without precise control over frequency and phase.

A magnetron is basically a diode in which one of the electrodes is a cylindrical cathode, typically, of an oxide-coated type (see section 3.1), while the other electrode is a coaxial anode, which at the same time is a cylindrical multi-cavity resonator. A DC electric field is applied in the radial direction from the cathode to the anode of the device. A permanent magnet provides an axial DC magnetic field in the direction of the length of the cathode perpendicular to the DC electric field. However, in this diode-type configuration of the magnetron, the DC magnetic field plays the role of the control grid of a triode. In the absence of a magnetic field, that is, for no magnetic field, the electron trajectory is straight from the cathode to the anode (figure 6.11). With the simultaneous application of the electric and magnetic fields and with the increase of the magnetic field, the electron trajectory bends and strikes the cathode—the bending increasing with magnitude the magnetic field. In a particular value of the increased magnetic field magnitude, the electron trajectory grazes azimuthally the surface of the cavity thereby ceasing the anode current flow. With further increase in magnetic field, in another extreme, the electrons in their trajectory strike back to the cathode and the cessation of the anode current continues. Moreover, some of the electrons of the magnetron which encounter the accelerating phase of the RF field of the cavity return to the cathode instead of reaching the anode [40, 45, 46].

Electrons sweeping past the slots of the cavity induce an RF field in each cavity of the SWS which, in turn, causes the electrons to bunch into groups more precisely in a spoke-like formation called the ‘space-charge wheel’ in view of its resemblance to the moving spokes of a wheel (figure 6.12).

The resonator of the magnetron may be of various types such as (a) slot-and-hole, (b) vane, (c) slot and (d) rising-sun (figure 6.13). In the slot-and-hole cavity resonator

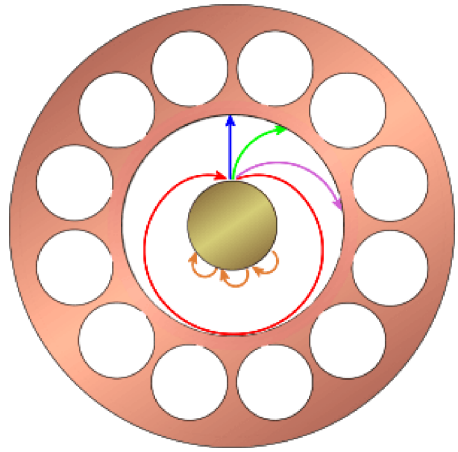

Figure 6.11. Electronic trajectories in crossed DC electric and magnetic fields for different values of their strengths relative to each other in a magnetron [42].

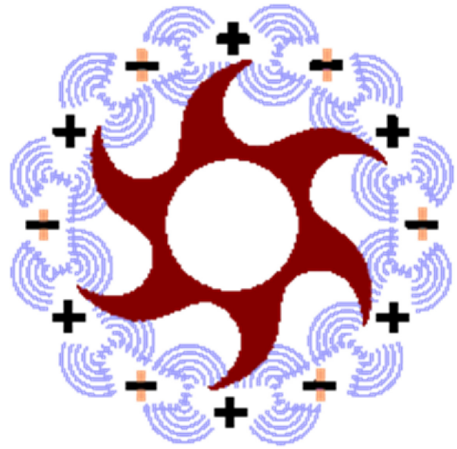

Figure 6.12. Rotating space-charge wheel past the π-mode-excited RF electric field of the coupled-cavity SWS of the magnetron [42].

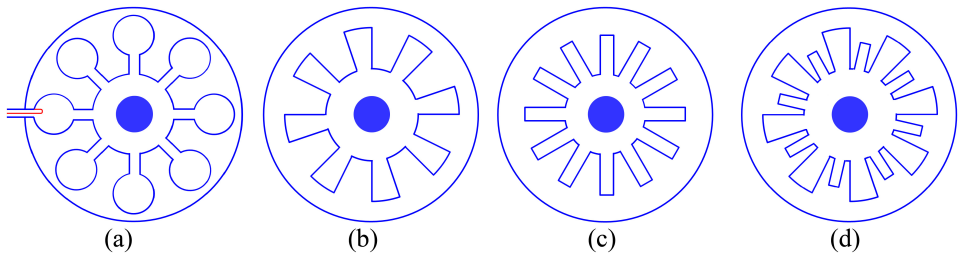

Figure 6.13. Schematic of a multi-cavity magnetron with anode-come-SWS cavity resonators of (a) slot-and-hole, (b) vane, (c) slot and (d) rising-sun types.

of the magnetron, the slots are cut along the length of the cavities that open into a central, common cavity space (figure 6.13(a)). In the π mode of excitation of the cavities of the slot-and-hole cavity resonator (figure 6.13(a)), the successive slots have a phase difference of π and the alternate slots have the same phase and thus the RF phase rotates.

If the spoke of the space-charge wheel circles about the cathode in synchronism with the rotating RF field pattern of the cavity resonator, then the spoke can arrive at each gap of the cavity at a time to induce a current in the cavity thereby reinforcing the oscillation. The condition corresponds to the rotation of the wheel of angular velocity of two slot segments per RF cycle for a π-mode-excited cavity. A well-defined threshold anode voltage—depending on the applied magnetic field and the cavity resonant frequency and hence on the cavity dimensions—must be applied before oscillations build up in the cavities. In the pulsed-power mode of the tube, care must be taken to adjust the anode voltage to coordinate with the build-up of oscillations to the full peak power level. The electrons returning to the cathode under the influence of the accelerating phase of the RF electric field can be taken advantage of in the self-heating of the cathode for secondary electron emission, thereby making it possible to switch off the heater of the cathode after the start-up of magnetrons using thermionic cathodes. Obviously, the phenomenon is of little relevance to field-emission cathodes of relativistic magnetrons (see chapter 8, volume 2).

The RF output sustained in the cavities at the desired frequency, being the resonant frequency of the cavity determined by its physical dimensions, is subsequently coupled out from one of the cavities. The coupler, in its simplest form, may be a loop of wire which magnetically couples a coaxial cable to the resonant structure of the cavity for extracting RF power from the tube to a load [40, 45, 46].

The undesirable resonant modes generated in a multi-cavity magnetron can be separated from the desired π mode by the method of 'mode strapping'. In this method, the alternate slots of the cavity are connected by a flat conducting ribbon strap and the remaining alternate slots, which are not connected by this ribbon strap, are connected by another concentric ribbon strap. Thus, in this mode-strapping arrangement for the π mode, there are two sets of alternate cavity slots such that the slots of the same set have identical phases, but these two sets of alternate cavity slots themselves have opposite phases. This in turn makes the two conducting straps connected to these two sets of slots have opposite polarities, thereby resulting in an additional large capacitance of the equivalent parallel resonant circuit of the cavity causing an appreciable change in the resonant frequency of the circuit. However, there would be no additional inductance introduced in the circuit in view of the current in a strap being nil since the length of the strap connected to alternate slots is held at the same potential in the π mode. On the contrary, in modes other than the π mode, the alternate slots connected to a strap do not have identical phases and there would be a current flow through the strap connecting these slots resulting in an inductance in addition to the capacitance of the equivalent parallel resonant circuit of the cavity. This will, therefore, separate the resonant frequencies of these modes from the resonant frequency of the π mode thereby separating the neighboring modes from the desired π mode. In this method of mode strapping the amount of

depression of the π mode resonant frequency of the cavity compared to the resonant frequencies of the undesirable modes of oscillation depends on the strap area and separation between the straps [40, 45, 46].

Further, the magnetron can be 'frequency-tuned' by (i) capacitive tuning in which a conducting ring is introduced in the region of high RF electric field and (ii) inductive tuning in which conducting rods are inserted in the hole of the slot-and-hole cavity. The combined capacitive and inductive tuning can bring about broad-band tuning over the extent of 1.5:1 using a bellow-type piston operated by a servo mechanism which can be microprocessor-controlled to be further useful in frequency agile or dither tuning of the magnetron for anti-jamming in electronic warfare [45].

A rising-sun magnetron is an alternative to using mode strapping to separate the desirable π mode from neighboring unwanted resonant modes in a multi-cavity magnetron. It has resonators with two different resonant frequencies arranged alternately for the purpose of mode separation. The resonators of the rising-sun magnetron appear as alternate long and short radial slots around the periphery of the anode block resembling the rays of the 'rising sun' (figure 6.11(d)). Such an anode block is easier to construct and has smaller RF losses than the strapped-slot cavity delivering high powers for wavelengths as long as 10 cm [46].

Coaxial magnetron is yet another alternative to mode strapping for alleviating the mode completion and stabilizing the π-mode operation. As the name suggests it has a circular coaxial cavity interaction structure, however, with its usual solid central conductor replaced by unstrapped slotted anode-come-multi-cavity resonator (figure 6.14(a)). The slots in the anode-come-resonator tightly couple the electric fields to the surrounding external cavity (figure 6.14(a)) from which the RF power is coupled out. In the π mode the electric fields in every other cavity are in phase and they couple in the same direction into the surrounding cavity. The structure in its outside region supports TE_{011}-mode electric field in circular form (circular electric mode) that decreases to nil at the conducting walls of the structure—the outer wall of the inner anode-come-resonator and the inner wall of the external cavity (figure 6.14(a)). The attenuators are provided at these walls to attenuate the unwanted modes other than the TE_{011} mode by dampening the currents due to non-zero electric field of the

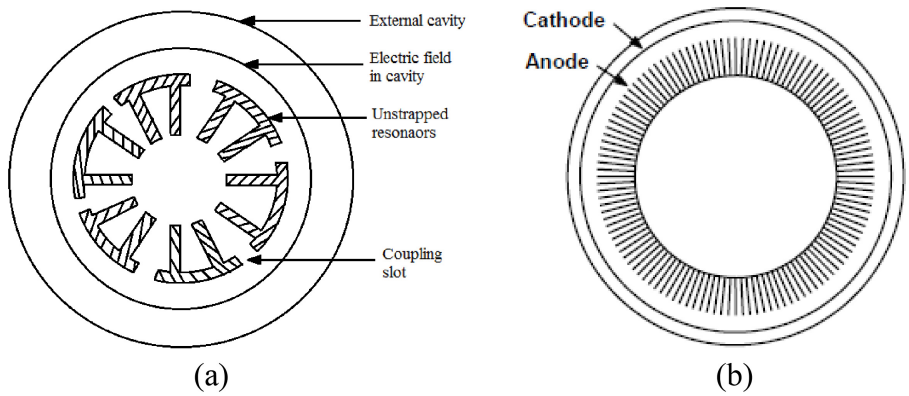

Figure 6.14. Interaction structures of (a) coaxial gyrotron and (b) inverted coaxial magnetron coaxial [40].

unwanted modes coupled to the attenuators, thereby providing mode suppression in this otherwise unstrapped device. The structure of the coaxial magnetron providing a high-Q stabilizing external cavity (figure 6.14(a)) besides being more stable in frequency can be larger and less complex even though it permits a larger number of resonators than the conventional strapped magnetron multi-cavity structure. Further, the confinement of maximum stored energy to the external cavity gives a lesser RF field at the tips of the anode resonating structure which in turn reduces the tendency of arcing in the tube. Frequency tuning of a coaxial magnetron can be done by moving a non-contacting plunger in the stabilizing external cavity. This method is much simpler than the capacitive or inductive loading of a conventional magnetron that involves perturbing the natural geometry of its resonators that in turn could lead to power variation, instability and arcing in the tube [40, 45, 46].

The inverted coaxial magnetron is the turned-inside-out form of the coaxial magnetron which can, typically, be a rising-sun magnetron (see figure 6.13(d)) in which the cathode surrounds the anode-come-resonator (figure 6.14(b)). The output waveguide can be in the circular electric mode that reduces the transmission loss. Comparatively, in an inverted configuration the cathode size is larger in the inverted configuration giving the advantage of a lesser cathode loading and a higher output power. This makes it easier to design a practical millimeter-wave magnetron. Further, the inverted configuration has potential application in a regime where the dimensions are small.

6.4.2 Crossed-field amplifier (CFA) and carcinotron

A crossed-field amplifier (CFA), also known as an amplitron, is a travelling-wave amplifier which can also be configured as an oscillator called a carcinotron. Compared to the O-type tubes, such as klystrons and TWTs, CFAs have a lower gain, less than 20 dB, but a higher efficiency, more than 70%, capable of delivering tens of megawatts of peak power and tens of kWs of average power. CFAs have found use in TV ground stations and deep-space telecommunication networks [13, 40, 47].

In a CFA, the electron bunches in the form of a space-charge wheel which circles about the cathode in velocity synchronism with the travelling RF waves supported by the neighboring circular anode-come-cavity SWS in which the signal is inputted (figure 6.15). The electron bunching is enhanced by the electric field of the cavity SWS and at the same time the electric field is enhanced by the currents induced in the cavity. CFAs can be grouped by (i) mode of interaction—forward-wave and backward-wave types and (ii) electron emission—injected-beam and emitting-sole types, both of which can be continuously emitting or pulsed. In an injected-beam device, the electron beam is formed by a separate gun and in a distributed emission device the electron beam is generated by a cathode adjacent to the full length of the SWS (figure 6.15(a) and (b)). In a typical initially developed CFA in the linear format, as in a linear-beam O-type TWT, a ribbon-shaped electron beam is injected into the interaction region between the anode-come-SWS supporting a forward-wave mode and the sole (figure 6.1(a)). (The conservation of beam kinetic energy has

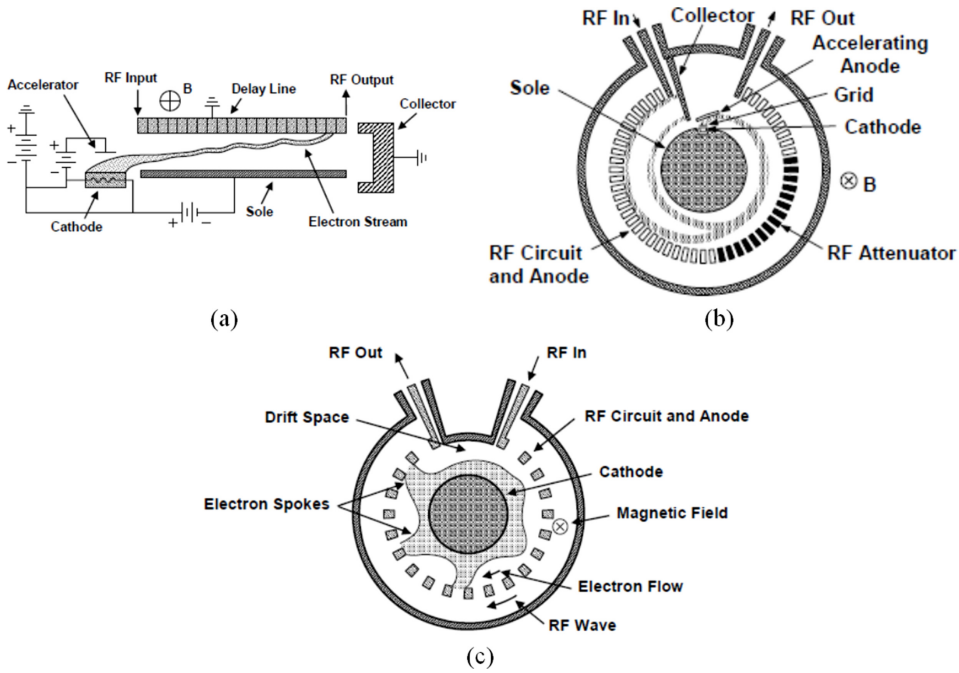

Figure 6.15. CFA schematic, typically, in (a) linear, injected-beam, forward-wave-mode (b) circular, injected-beam, backward-wave-mode and (c) circular, distributed emission, forward-wave-mode [13, 40, 47].

already been analytically appreciated with reference to the linear format of the device (see section 3.7 in chapter 3, volume 1).) In an emitting-sole CFA, the current emanates by field emission from the cathode. In the forward-wave configuration of the device, the directions of beam-spoke motion, RF phase velocity and RF group velocity and hence RF power flow, are the same (figure 6.15(a) and (c)) while, in the backward-wave configuration of the device, though the directions of beam-spoke motion and RF phase velocity are the same, the RF group velocity and hence RF power flow are opposite to the former (figure 6.15(b)).

Some of the CFA interaction structures in the forward-wave category are meander-line, ceramic-mounted serpentine-line and helix-coupled vane structures, and some in the backward-wave category are generalized vane-strap SWS and parallel-plate SWS [13, 40, 47]. These CFA structures are selected trading off their potentials for dispersion-free characteristics for wide device bandwidths and thermal management for a greater device power-handling capability.

In a CFA the input power can reach the output even when the device is cold, that is, its DC power supply is turned off. This makes it possible to use a transmitter to operate at a reduced power level, if so desired, by turning off the CFAs in the final stages of the transmitter. Further, the system in which two CFAs are connected sequentially enjoys a built-in redundancy in that if one of them fails accidentally its DC power could be removed and applied to the other to keep the system

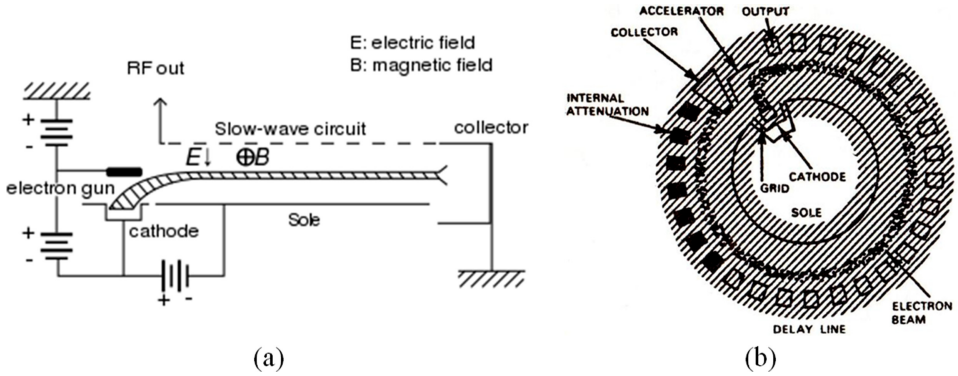

Figure 6.16. Schematic of a M-BWO (carcinotron) in (a) linear [48] and (b) circular [39] configurations.

operational. In fact, such a redundancy was provided in the downlink transmitter of the Apollo Lunar Module where high efficiency and reliability were needed.

A linear M-BWO (carcinotron) (figure 6.16(a)) is similar in configuration to a linear, injected-beam CFA (figure 6.15(a)), however, operating now in the backward-wave instead of forward-wave-mode. Therefore, in this device the RF output is taken from the gun end. The device also exists in its circular configuration in which the interaction structure is broken electrically to provide the RF input and output couplers with uninterrupted continuity of the electron beam (figure 6.16(b)). The carcinoron can be electronically frequency-tuned over a wide band by with respect to the anode-sole voltage. Hence, carcinorons can be used for electronic counter measure applications. Moreover, they find use as illuminators in terahertz imaging due to the quality wavefront they can produce.

References

[1] Falce L R 1966 Improved technique for producing pyrolytic graphite attenuator film for microwave tubes *IEEE Conf. Rec. 8th Conf. Tube Tech.* pp 157–62

[2] Basu B N 1996 *Electromagnetic Theory and Applications in Beam-wave Electronics* (Singapore: World Scientific)

[3] Agarawala SSS and Dattatreyan C 1965 Development of helical couplers and coupled helix attenuators for an S-band TWA tube *IETE J. Res.* **11** 5029

[4] Chu L J 1951 A kinetic power theorem *IRE-PGED Electron Tube Research Conf.* (Durham: New Hampshire)

[5] Kliiver J W 1958 Small-signal power conservation theorem for irrotational electron beams *J. Appl. Phys.* **29** 618–22

[6] Jain P K and Basu B N 2000 Electromagnetic wave propagation through helical structures *Electromagnetic Fields in Unconventional Materials and Structures* ed O N Singh and A Lakhtakia (New York: Wiley) 433–55

[7] Ghosh S, Jain P K and Basu B N 1996 Modified field analysis of inhomogeneously-loaded helical slow-wave structures for TWTs *Int. J. Electron.* **81** 101–12

[8] Ghosh S, Jain P K and Basu B N 1997 Rigorous tape analysis of inhomogeneously loaded helical slow-wave structures *IEEE Trans. Electron Dev* **44** 1158–68

[9] Kesari V and Basu B N 2017 Analysis of some periodic structures of microwave tubes: part 1: analysis of helical slow-wave structures of traveling-wave tubes *J. Electromagn. Waves Appl* **37** 1–37
[10] Putz P L and Cascone M J 1979 Effective use of dispersion shaping in broadband helix TWT circuit *Tech. Dig. Int. Electron Dev. Meeting* (New York: IEEE)) pp 422–4
[11] Rymer J P and Cascone M J 1982 Three octaves with one TWT *Tech. Dig. IEEE Int. Electron Dev. Meeting* pp 30–1
[12] Scott A and Cascone M J 1978 What is new in helix TWTs *Tech. Dig. IEEE Int. Electron Dev. Meeting* pp 526–9
[13] Gilmour A S Jr 1986 *Microwave Tubes* (Norwood: Artech House)
[14] Hughes 1975 *TWT and TWTA handbook* (Electron Dynamics Division, Hughes Aircraft Company)
[15] Mendel J T 1973 Helix and coupled-cavity traveling-tube waves *Proc. IEEE* **61** 280–98
[16] Fleury G, Kuntzmann J C and Lafuma P 1977 High power brazed-helix telecommunication TWTs *Tech. Dig. IEEE Int. Electron Dev. Meeting* pp 116–9
[17] Gosset P and Maloney E D 1979 Brazed-helix TWTs for TV-broadcasting and high-power telecommunication satellites *IEEE Conf. Rec. Nat. Telecomm. Conf.* (*Washington*) vol 1 2.10.1–2.10.5
[18] Hobrecht C E 1979 Study of resonant loss for helix TWTs *Tech. Report* (*Rome Air Dev. Centre, New York*) RADC-TR-79-35
[19] Haus H A and Bobroff D 1957 Small-signal power theorem for electron beams *J. Appl. Phys.* **28** 694–703
[20] Ezura E and Kano T 1975 Measured and theoretical nonlinear phase distortion in traveling-wave tubes *IEEE Trans. Electron Dev.* **22** 890–7
[21] Bremenson C, Palazo M and Neger R 1980 Linearising TWTAs in satellite transponders *Conf. Proc. AIAA 8th Commun. Satellite Conf,* (Orlando)
[22] Epsztein B 1984 Slow-wave structures in microwave tubes *Tech. Dig. IEEE Int. Electron Dev. Meeting* pp 486–9
[23] Campbell R 1975 Recent developments in low noise mm-wave TWTAs *Microw J.* **18** 45–6
[24] Sauseng O, Manoly A E and Hall A 1978 Thermal properties and power capability of helix structures for millimeter waves *Tech. Dig. IEEE Int. Electron Dev. Meeting* pp 534–7
[25] Liss C, Harper R and Puri M P 1988 Helical waveguide millimeter wave TWT *Tech. Dig. IEEE Int. Electron Dev. Meeting* pp 374–7
[26] Cook J S, Rompfner R and Quate C F 1956 Coupled helices *Bell Syst. Tech. J.* **35** 127–78
[27] Chen T S 1959 Design and performance of coupled-helix transducer for traveling-wave tubes *J. Electron. Control* **6** 289–306
[28] Singh V N, Basu B N, Pal B B and Vaidya N C 1983 Equivalent circuit analysis of a system of coupled helical transmission lines in a complex environment *J. Appl. Phys.* **54** 4141–6
[29] Konrad G T and Cho S K 1963 Elliptical-cavity coupler for travelling-wave tubes *IEEE Trans. Electron Dev.* **10** 85–9
[30] Gittins J F 1965 *Power Traveling-Wave Tubes* (New York: Elsevier)
[31] Belohoubek E F 1965 Helix support structures for ultra-wideband travelling-wave tube *Radio Corp. Am. Rev* **26** 106–17
[32] Limburg H C, Davis J A, Tammaru I, Vaszari J P and Wilson J 1988 Reducing the gain and phase variation in high power MMW TWTs *Tech. Dig. IEEE Int. Electron Dev. Meeting* pp 381–4

[33] Gilmour A S Jr 1994 *Principles of Traveling Wave Tubes* (Norwood: Artech House)
[34] Kosmahl H G and Paterson J C 1984 TWT amplifier exhibits linear power transfer characteristics and improved efficiency *Proc. 10th Commun. Satellite Syst. Conf.* (Orlando)
[35] Yarrington L I and Maynard E D 1973 The status of dual-mode tubes *Microw J.* **16** 15–20
[36] Soohoo S F 1971 *Microwave Electronics* (Reading, MA: Addison-Wesley)
[37] Dionne N J 1970 Harmonic generation in octave bandwidth traveling-wave tubes *IEEE Trans. Electron Dev.* **17** 365–72
[38] Sauseng O and Garrigus W E 1975 Reduction of intermodulation distortion with harmonic injection for wideband traveling wave tubes *Tech. Dig. IEEE Int. Electron Dev. Meeting* pp 411–4
[39] Gandhi O P 1981 *Microwave Engineering and Applications* (New York: Pergamon Press)
[40] Gilmour A S 2011 Klystrons, Traveling Wave Tubes, Magnetrons *Crossed-Field Amplifiers, and Gyrotrons* (Boston: Artech House)
[41] Barker R J, Luhmann N C, Booske J H and Nusinovich GS (ed) 2005 *Modern Microwave and Millimeter-wave Power Electronics* (Piscataway: Wiley-IEEE Press)
[42] www.radartutorial.eu
[43] Steer B, Roitman A, Horoyski P, Hyttinen M, Dobbs R and Berry D 2007 Advantages of extended interaction klystron technology at millimeter and sub-millimeter frequencies *Proc. 16th IEEE Int. Pulsed Power Conf.* vol 2 pp 1049–53
[44] Varian Associates 1979 *Microwave Tube Manual* Air Force Publication No. T. O. 00-25-251,
[45] Kar S 2016 *Microwave Engineering Fundamentals, Design and Applications* (Hyderabad: Universities Press)
[46] Millman S and Nordsieck A T 1948 The rising sun magnetron *J. Appl. Phys.* **19** 156
[47] Eppley K, Feinstein J, Ko K, Kroll N, Lee T and Nelson E 1991 A high power cross-field amplifier at X-band *Proc. SPIE IEEE Particle Accelerator Conf.* (San Francisco) pp 1–3
[48] Khan A S 2014 *Microwave Engineering: Concepts and Fundamentals* (London: CRC Press)

IOP Concise Physics

High Power Microwave Tubes: Basics and Trends

Volume 2

Vishal Kesari and B N Basu

Chapter 7

Fast-wave tubes

There exists a technology gap in the generation and amplification of RF waves in the mm-wave band. This is because, if the operating frequency of conventional microwave tubes (MWTs) such as the TWT were increased to the mm-wave band, the sizes of the interaction structures would reduce, thereby limiting the device's output power capability. Alternatively, if the operating frequency of quantum mechanical devices, such as the laser, were decreased to the mm-wave band, the energy of each quantum and hence the device's output power would reduce and the retention of population inversion would also become difficult. This gap in mm-wave technology is alleviated with the advent of fast-wave MWTs such as gyrotrons, gyro-klystrons and gyro-TWTs, since with the increase of the operating frequency the sizes of the interaction structures of these devices do not reduce as much as the sizes of conventional MWTs. Consequently, this has intensified the effort in the development of fast-wave MWTs and opened up many of their applications.

Operating point of fast-wave tubes

In a fast-wave tube, interaction between an electron beam and an RF wave with phase velocity greater than the speed of light takes place where the azimuthal kinetic energy of the electron beam is transferred to RF waves. The fast-wave tubes are mostly gyro-devices such as gyro-monotron or gyrotron, gyro-klystron, gyro-TWT and gyro-BWO, which are the fast-wave counterparts of conventional slow-wave devices, namely, monotron, klystron, TWT and BWO, respectively; each operating at the intersection between the beam-mode and the waveguide-mode dispersion characteristics (figure 7.1), which are obtainable from their respective dispersion relations. The waveguide-mode dispersion relation is given by [1–4]

$$\omega^2 - \beta^2 c^2 - \omega_{\text{cut}}^2 = 0, \tag{7.1}$$

where ω is the wave angular frequency, and β is the phase propagation constant of RF waves supported by the waveguide, which is a resonant structure of a gyrotron

doi:10.1088/978-1-6817-4704-0ch7

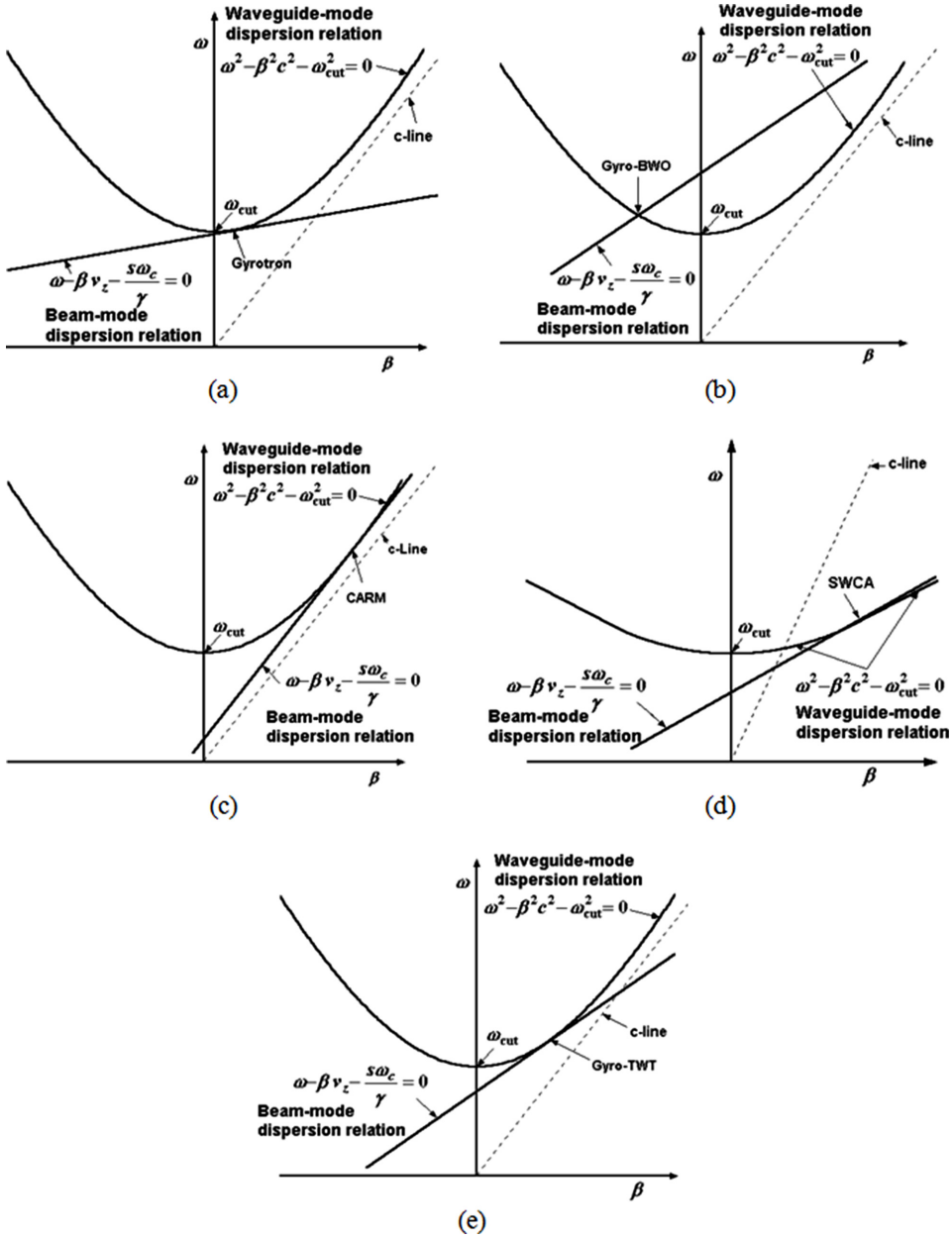

Figure 7.1. Plots of the $\omega - \beta$ beam-mode and waveguide-mode dispersion characteristics showing the operating point as the intersection between these plots, for the (a) gyrotron, (b) gyro-BWO, (c) CARM, (d) SWCA and (e) gyro-TWT [3].

and a propagating structure of a gyro-TWT. ω_{cut} is the cutoff angular frequency of the waveguide and c is the velocity of the electromagnetic waves in free-space. The beam-mode dispersion relation of such a gyro-device is essentially the dispersion

relation of the fast cyclotron wave on a beam of electrons in motion transverse to a DC magnetic field, and is given by (see section 3.3):

$$\omega - \beta v_z - \frac{s\omega_c}{\gamma} = 0, \tag{7.2}$$

where ω_c is the non-relativistic angular cyclotron frequency, and γ is the relativistic mass factor, so that ω_c/γ represents the relativistic angular cyclotron frequency. v_z is the axial beam velocity of the gyrating electrons. s is the beam-harmonic mode number, it being assumed that the device operates at the sth harmonic $\omega \approx s\omega_c/\gamma$, considering βv_z, which is the Doppler-shift frequency, to be small in (7.2). Further, ω_c may be expressed, in terms of the axial magnetic flux density B_0 in the device, as:

$$\omega_c = \frac{|\, e \,|\, B_0}{m_{e\,0}} \tag{7.3}$$

where e and $m_{e\,0}$ are the electronic charge and rest mass, respectively. It may be easily appreciated, with the help of the relation (7.3) and the near-cyclotron harmonic resonance: $\omega \approx s\omega_c/\gamma$, that the required magnetic flux density for a given operating frequency would be reduced by a factor s for the operation of the device at the sth beam harmonic. The plot of the waveguide-mode $\omega - \beta$ dispersion characteristics, obtainable from (7.1), is a hyperbola with the ω-intercept equal to ω_{cut}. Similarly, the plot of the beam-mode $\omega - \beta$ dispersion characteristics, obtainable from (7.2), is a straight line of slope equal to the axial beam velocity v_z, with the ω-intercept equal to $s\omega_c/\gamma$ (figure 7.1). The relativistic mass factor γ is given, in terms of the axial and the azimuthal components of the beam velocities, v_z and v_t, as

$$\gamma = \left(1 - \left(v_z^2 + v_t^2\right)/c^2\right)^{-1/2}. \tag{7.4}$$

Alternatively, in terms of the beam potential V_0, one may express γ, by equating the beam's potential energy $|e|\ V_0$ with the relativistic kinetic energy $\gamma\, m_{e\,0}c^2 - m_{e\,0}c^2$, as

$$\gamma = 1 + \frac{|e|\ V_0}{m_{e0}c^2}. \tag{7.5}$$

7.1 Cyclotron resonance maser (CRM) and Weibel instabilities

In a gyro-device, the exchange of energy between the electron beam and RF waves causes a change in the relativistic mass of gyrating electrons and thus azimuthal electron bunching (as discussed in section 3.4). This change in the relativistic mass factor of an electron is also responsible for the cyclotron resonance maser (CRM) instability in a gyro-device. The electrons in oscillatory motion radiate coherent waves when the Doppler-shifted frequency of the wave supported by a waveguide excited in TE mode coincides with the frequency of oscillation of electrons or with one of its harmonics. In another class of gyro-devices such as the slow-wave cyclotron amplifier (SWCA), a change in the axial electron velocity, caused by the Lorentz force due to the transverse component of the RF magnetic field and the transverse component of electron velocity, causes what is termed the Weibel

instability in the device. In the Weibel-instability-based device, axial and non-relativistic bunching takes place, and a slow waveguide-mode is destabilized in the waveguide, unlike in a conventional gyro-device, such as the gyrotron, in which the bunching is essentially azimuthal and relativistic and in which a fast waveguide-mode is destabilized. There is yet another gyro-device, namely the cyclotron auto-resonance maser (CARM), in which the CRM and Weibel instabilities are present in equal proportions and a mildly fast waveguide-mode is destabilized [2–4].

The Doppler-shifted cyclotron angular frequency ω_D, say, with the help of (7.2), may be written as

$$\omega = \omega_D = \beta v_z + s\omega_c/\gamma. \tag{7.6}$$

Therefore, taking the differential of (7.6) one can express the incremental change in ω_D as:

$$\Delta\omega_D = \beta\Delta v_z - \frac{s\,\omega_c}{\gamma^2}\Delta\gamma. \tag{7.7}$$

The two terms in the right-hand side of (7.7) tend to cancel each other thereby making $\Delta\omega_D \to 0$, which points towards the phenomenon of 'auto-resonance' in the device.

The change in the axial electron velocity Δv_z is caused by Weibel instability due to the Lorentz force on electrons in transverse motion in the transverse RF magnetic field, which can be described by the equation of motion:

$$\gamma\, m\frac{dv_z}{dt}\vec{a}_z = e(\vec{v}_\perp \times \vec{B}_\perp),$$

the subscript $\perp$ representing the perpendicular or transverse component, whence, with the help of Maxwell equations, we can obtain:

$$\Delta v_z = \frac{e}{\gamma\, m}\frac{\beta}{\omega}(\vec{v}_\perp \,.\, \vec{E}_\perp)\Delta t \quad \text{(relevant to Weibel instability)}. \tag{7.8}$$

The change in the relativistic mass factor $\Delta\gamma$ is caused by the energy exchange between the electrons in transverse motion and in the transverse RF electric field described by the following equation of motion:

$$\frac{d}{dt}(\gamma mc^2) = e(\vec{v}_\perp \cdot \vec{E}_\perp)$$

whence we obtain

$$\Delta\gamma = \frac{e}{mc^2}\frac{\beta}{\omega}(\vec{v}_\perp .\, \vec{E}_\perp)\Delta t \quad \text{(relevant to CRM instability)}. \tag{7.9}$$

Substituting Δv_z and $\Delta\gamma$ from (7.8) and (7.9), respectively, into (7.7), one may write

$$\Delta\omega_D = \frac{e}{m}\left[\frac{\beta^2}{\omega\,\gamma} - \frac{s\omega_c}{\gamma^2 c^2}\right](\vec{v}_\perp .\, \vec{E}_\perp)\Delta t\ . \tag{7.10}$$

The auto-resonance condition $\Delta\omega_D \to 0$ (mentioned following (7.7)), in (7.10) then leads to

$$\frac{\beta^2}{\omega\,\gamma} - \frac{s\omega_c}{\gamma^2 c^2} = 0 \quad \text{(auto-resonance)}. \tag{7.11}$$

The first and the second terms in the left-hand side of (7.11) originating from Weibel and CRM instabilities, respectively, cancel each other suggesting that at auto-resonance ($\Delta\omega_D \to 0$), these two instabilities are present in equal proportions.

Further, in view of the near-synchronization condition $s\omega_c/\gamma \lesssim \omega$ required for the electron bunch to remain in the decelerating RF electric field (see section 3.4), the condition (7.11) will lead to $\omega/\beta \gtrsim c$, which corresponds to the destabilization of the mildly fast waveguide mode in a CARM (see section 7.6), ω/β being the RF phase velocity. However, if the first term dominates over the second term in (7.11), then we get $\omega/\beta < c$, which in other words means that Weibel instability dominates over CRM instability and the slow-wave is destabilized, as in a SWCA (see section 7.7). On the other hand, if in (7.11) the second term dominates over the first term, then we get $\omega/\beta > c$, which represents that CRM instability dominates over Weibel instability and the fast-wave is destabilized, as in a gyro-TWT (see section 7.5).

7.2 Gyrotron

The gyrotron is a high-power fast-wave MWT which is capable of delivering RF output powers ranging from tens of kilowatts to megawatts in the mm-wave frequency range and even higher up to the edge of terahertz. The high power handling capability of the gyrotron is due to the dimensions of its fast-wave interaction structure not reducing as much as those of interaction structures of slow-wave tubes with the increase of operating frequencies. It belongs to the type of MWTs: bremsstrahlung in magnetic-field radiation (table 2.1) in which CRM instability dominates over Weibel instability (see section 7.1). In this device, high-frequency electromagnetic radiation is generated by cyclotron resonance stimulated when electrons move through a strong axial magnetic field that could be generated with the help of a superconducting magnet around the tube. Further, here the electron beam is made periodic in the form of a helical beam rather than the interaction structure unlike in a conventional TWT in which the interaction structure, say, helix is made periodic rather than the beam [2, 4].

The device is a fixed-frequency oscillator that is operated close to the waveguide cutoff frequency at near-zero group velocity (figure 7.1(a)) that makes the axial phase propagation constant β of the RF wave rather small to mitigate the effect of electron beam velocity spread on inhomogeneous broadening of the cyclotron resonance band. Moreover, at the operating point, the energy velocity also becomes slow to keep electromagnetic energy in the waveguide resonator cavity long enough that makes beam-wave interaction more effective in the device. A small mismatch in the beam-mode (7.2): $\omega - \beta v_z - s\omega_c/\gamma \lesssim 0$, and correspondingly a small frequency mismatch $\omega_c \lesssim s\omega/\gamma$ for a small value of the Doppler shift βv_z, ensures the

achievement of coherent phasing to keep the electron bunches in the retarding phase of the waveguide resonator mode so that the transverse kinetic energy of the gyrating bunch of beam electrons gets transferred to RF waves (see section 3.4 for relativistic bunching in a gyrotron).

The major subassemblies of a typical small-orbit gyrotron are: (i) magnetron injection gun (MIG), (ii) beam tunnel, (iii) interaction cavity, (iv) nonlinear taper, (v) focusing structure (super conducting magnet) (vi) mode launcher and mirror section, (vii) window and (viii) collector (figure 7.2). The annular electron beam comprising helical beamlets of a small-orbit gyrotron and the axis-circling electron beam of a large-orbit gyrotron (LOG) are formed by a MIG and cusp gun, respectively (see section 4.1). A large part of the axial energy of the beam is converted into its rotational energy in the beam tunnel or adiabatic compression region of the slowly increasing magnetic field of the MIG (see section 4.1) such that the rotational velocity of the electrons becomes 1.5 to 2 times (known as the beam pitch factor), their axial beam velocity. The electron beam is azimuthally bunched (section 3.4) and made to take part in CRM interaction with the chosen TE waveguide mode of the open-ended circular cavity resonator. The required DC magnetic field in which the cavity is immersed for this interaction is provided by a solenoid made of a superconducting coil. A small down-tapering of the waveguide resonator radius at the entrance on the cathode side makes the cutoff frequency in the tapered region larger than the operating frequency thereby preventing electromagnetic radiation from entering the cathode region from the interaction region and implementing mode confinement. Similarly, an up-taper at the exit of the resonator facilitates the

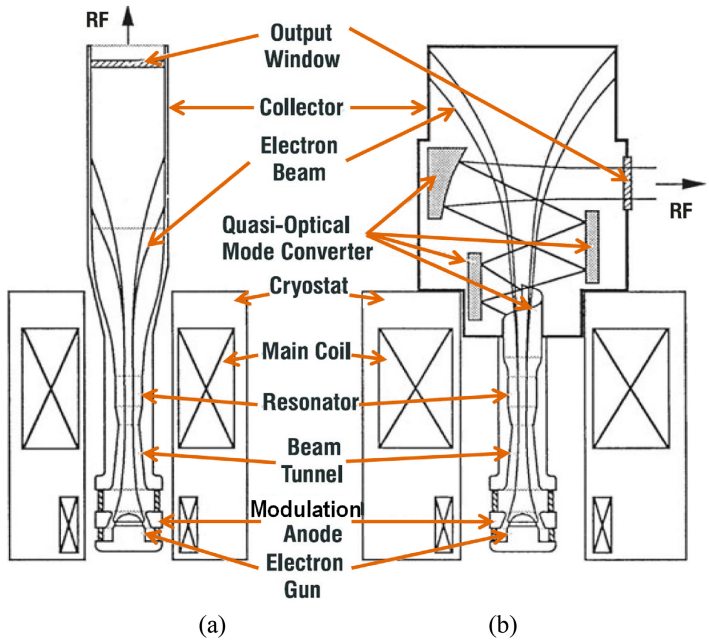

Figure 7.2. Schematics of (a) axial-output and (b) transverse-output gyrotrons [10].

output coupling. Also, a diameter taper region is provided in the device that connects the interaction region with the main waveguide system. The region is called the nonlinear taper which can have various designs such as raised-cosine, exponential, triangular and Chebyshev tapers to provide a good match between the input and output sections of the taper without generating many spurious modes [2].

The spent beam in the gyrotron diverges off the axis to settle on the collector surrounding the beam (figure 7.2). Also, in general, a mode converter is to be provided, since the interaction waveguide mode could be different from the mode of the output waveguide system. Based on the output configurations, the gyrotrons are categorized in (i) axial-output and (ii) transverse-output types (figure 7.2). The former uses an axial-output window, which is generally placed at the end of the collector (figure 7.2(a)). In this type, the RF output mode can be the same as the oscillation mode, and no internal mode conversion is required. As the collector is a high heat zone, it is essential to handle the thermal issues of the window. However, the transverse-output gyrotron uses a transverse-output window, which is generally positioned before the collector, and needs an internal mode converter to convert the mode of interaction to the Gaussian mode (figure 7.2(b)). It also needs a quasi-optical mode launcher and a mirror assembly to separate the RF beam from electron beam and to transmit the RF beam in a transverse direction. Such a transverse-output configuration also makes the transverse-output window see less thermal severity than the window of the axial-output gyrotron [2, 4, 5].

There are three types of waveguide modes in vogue in a gyrotron: TE_{1p} mode, $TE_{\nu p}$ mode with $\nu \gg p$ (whispering-gallery), and TE_{0p} mode. The fields in the waveguide reduce approximately as $1/r^{1/2}$, due to the asymptotic behavior of the Bessel function, and hence the power loss density decreases approximately as $1/r$. Thus, the structure in such a device is made oversized to reduce the power loss density of the waveguide wall. This, however, makes the waveguide rather over-moded, which makes it important to address the problem of mode competition. For instance, a gyrotron cavity of 5λ diameter and 6λ length can support as many as 30 modes in 1% frequency intervals (λ being the wavelength in free space) [6]. Splitting the waveguide along the sides alleviates the mode competition in the waveguide excited in the TE_{1p} mode. Hence, the electron beam in such a device needs to be placed near the axis of the waveguide, away from the waveguide wall, to experience the maximum mode field. This, however, causes a space-charge depression of the beam potential and the related beam velocity spread. The space-charge depression also reduces the beam current transport. Further, the modes TE_{1p} for $p \gg 1$ degenerate in frequency. The whispering-gallery mode $TE_{\nu p}$ ($\nu \gg p$) has larger fields nearer the waveguide wall, where an electron beam could be placed for interaction, and provides a lesser space-charge depression, a lesser beam velocity spread, and a larger beam current transport than the TE_{1p} mode [7]. Also, it encounters less mode competition because of poorer coupling of the beam, placed nearer the wall, to the volume modes, and also provides a larger frequency separation between the competing modes. However, since the electron beam is to be placed nearer the wall, the beam confinement has to be stricter. The TE_{0p} mode

Table 7.1. Some representative gyrotrons [4].

Frequency (GHz)	Power (MW)	Pulse length (s, ms, μs)	Efficiency (%)	Institution
1300	0.0005	40 μs	0.6	IAP
164.98	2.2	100 ms	28	KIT (FZK)
170	2.3	1 ms	30	EGYC
84	0.1	CW	14	CPI, NIFS Toki
75	0.8	100 ms	70	GYCOM, IAP Nizhny Novgorod

enjoys the lowest wall loss of these three types of waveguide modes; the wall power loss density decreasing with frequency, though it encounters mode competition from the TE_{2p} mode that impairs high powers in the device [7–9].

The gyrotrons (see table 7.1 and also tables 9.4 and 9.5 in chapter 9, volume 2 for their specifications) find application as high-power mm-wave sources, for instance, in industrial heating, plasma heating for controlled thermonuclear reactors (nuclear fusion), electron spin resonance (ESR) and nuclear magnetic resonance (NMR) spectroscopy, plasma diagnostics and plasma chemistry, active denial system (ADS), directed energy weaponry, early detection of ballistic missiles, high resolution imaging radar, space surveillance radar for LEO satellites, weather radar, high-temperature processing of materials—glass, composites, and ceramics, annealing of semiconductors, sintering of special nanomaterials, and so on (see section 2.2 in chapter 2, volume 1).

7.2.1 Higher beam-harmonic operation

In a simplified picture considering the axial electron velocity $v_z = 0$ (see section 3.4) we obtain from (7.2) the fundamental and sth harmonic resonance relations for an electron rotating in a circular orbit in a transverse RF electric field of the waveguide resonator, respectively, as

$$\begin{aligned} \omega &= \omega_c \quad \text{(fundamental resonance)} \\ \omega &= s\omega_c \quad \text{(sth harmonic resonance)}, \end{aligned} \tag{7.12}$$

where ω is the wave frequency, and ω_c is the 'relativistic' angular cyclotron frequency (choosing to change the terminology of (7.2) where ω_c and ω_c/γ were non-relativistic and relativistic angular cyclotron frequencies, respectively). For the fundamental resonance ($s = 1$), then from (7.12) we get $\omega(= 2\pi/T) = \omega_c(= 2\pi/T_c)$, which gives $T = T_c$, where T is the time period of an RF cycle and T_c is the time of one orbital rotation of an electron of the annular or hollow beam. We have considered, here for the fundamental resonance, the beam to be located nearly midway between the axis and the wall of the waveguide resonator where the transverse RF electric field of the waveguide excited typically in the TE_{01} mode becomes maximum (figure 7.3(a)). Under this fundamental resonance condition, if an electron is decelerated (or

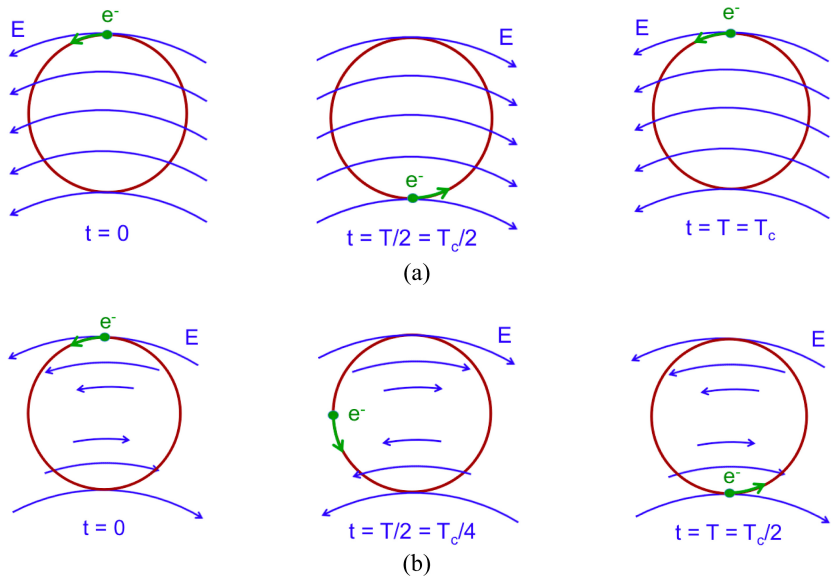

Figure 7.3. Rotational picture of an orbiting electron over a period of cycles of RF electric field in (a) TE_{01} waveguide mode under fundamental and (b) TE_{02} waveguide mode under second harmonic resonance conditions.

accelerated) by the RF electric field at $t = 0$ (thereby its kinetic energy being converted into RF energy) (figure 7.3(a)), the electron will continue to be decelerated (or accelerated) at (i) $t = T/2 = T_c/2$, that is, when the electron makes half an orbital rotation and the RF field reverses its sign of cycle at the same time, and also (ii) at $t = T = T_c$ when the electron makes one complete orbital rotation and, at the same time, the RF electric field completes one cycle (figure 7.3(a)).

Similarly, for the beam-harmonic resonance, say, second harmonic resonance ($s = 2$), from (7.12) we get $\omega(= 2\pi/T) = 2\omega_c(= 2 \times 2\pi/T_c)$, which gives $T = T_c/2$. We consider the annular beam to be the beam located nearly midway between the axis and the wall of the waveguide resonator excited typically in the TE_{02} mode such that the RF electric field reverses at the centre of the electron orbital rotation (figure 7.3(b)). Under this second beam-harmonic condition, if an electron is decelerated (or accelerated) at $t = 0$, it remains unaffected by the RF electric field that acts perpendicular to its motion at $t = T/2 = T_c/4$, when the electron makes a quarter of one orbital rotation and, at the same time, the RF electric field reverses its sign (figure 7.3(b)). The same electron, which was decelerated (or accelerated) at $t = 0$, will find itself in the decelerating (or accelerating) RF electric field at $t = T = T_c/2$, that is, when the electron makes half an orbital rotation and, at the same time, the RF electric field completes one cycle (figure 7.3(b)). Thus, as can be appreciated with the help of (7.12) and (3.10) (see chapter 3, volume 1), that the beam harmonic resonance reduces the required magnetic flux density by a factor of the beam harmonic number s compared to the fundamental resonance ($s = 1$).

7.2.2 Mode selectivity

An azimuthally periodic vane-loaded cavity—magnetron-like structure—for a large-orbit gyrotron operating at a higher beam harmonic can not only relax the required background magnetic field of the gyrotron, but also call for lower electron beam energies and provide superior mode selectivity of the device [11–13]. Such azimuthal periodicity can also be extended to a coaxial gyrotron that uses a coaxial insert in a circular cavity interaction structure to enhance the space-charge limiting current thereby increasing the electron beam power available for conversion to RF waves for a large output power of the gyrotron. Further, the radius of the coaxial insert of the coaxial cavity needs to be appropriately tapered to select the desired mode for interaction in the device out of the competing modes which would be generated when the cavity is oversized to reduce ohmic wall losses of the cavity within the acceptable limit of 2–3 W cm^{-2} that permits the usual cooling techniques for the thermal management of the device. For this purpose, the radius of the coaxial insert is down-tapered—and hence the ratio of the outer-to-inner radii of the coaxial waveguide resonator is increased—towards the output end [14–16]. If such a tapered coaxial cavity is so designed that the plot of the eigenvalue versus outer-to-inner radii of the coaxial waveguide has a more positive slope, or in other words, the eigenvalue increases more toward the output end, for the desired mode than for the competing modes, then the desired mode would move closer to the cutoff frequency and, thus, have a lower group velocity than the competing modes. This would reduce the group velocity of the desired mode and hence increase its diffractive quality factor as compared to the competing modes. Consequently, this would increase the total quality factor and in turn reduce the start oscillation current of the desired mode for the gyrotron as compared to that of the competing modes [17–29]. Further, as in a vane-loaded gyrotron, the azimuthal periodicity could be introduced in a coaxial-cavity gyrotron by corrugating the coaxial insert with azimuthally periodic axial slots and optimizing the dimensions of the slots to enhance the effectiveness of down-tapering the radius of the insert in the mode selection [18]. The potential of a coaxial-cavity structure in the mode selection has also been illustrated in the sub-millimetre-wave, high-power regime, typically for 100 kW (CW) at 340 GHz under second beam-harmonic operation [27].

There is yet another method of increasing the mode selectivity in which the cylindrical wall of the circular waveguide resonator is replaced with a triangular lattice or an array of metal rods parallel to the axis of the gyrotron and the direction of the magnetic field of the gyrotron [2]. This structure is called the photonic band-gap (PBG) structure named after the PBG structure with a lattice defect in semiconductors proposed by Yablonovitch [30] to suppress spontaneous emission in semiconductors. The analogous defect in the PBG structure for the gyrotron is implemented by removing a number of rods from the centre of the array of rods to form a 'defect' to support a defect mode in the band-gap or stop-band of the ω–β dispersion diagram of the structure. The array of metal rods of the structure is held in position by being inserted through a matching array of holes in two conducting end plates which make the PBG gyrotron cavity (figure 7.4). The band-gap of the

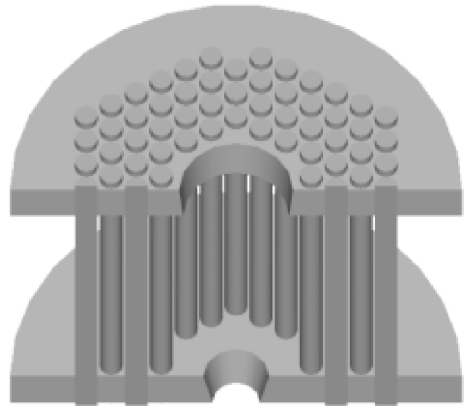

Figure 7.4. Schematic of a section of the PBG resonator [32].

PBG cavity structure is so adjusted that the resonant frequency of the desired mode lays in the stop-band of the PBG structure and the resonant frequencies of all other competing modes in neighborhood lay in the propagating pass-band of the structure. Thus, the competing modes leak through the array that acts like a transparent wall to them and can be absorbed at the periphery of the array and the desired mode in the stop-band could take part in the interaction with the electron beam. Thus, the PBG cavity gives a single-mode performance—typically, TE_{041} in a gyrotron and TM_{010} in a linear accelerator. In an initial experiment, J Sirigiri Rao [31] took, typically, 102 copper rods, each of 1.59 mm diameter held in a triangular array with 2.03 mm centre-to-centre spacing between the rods to form the PBG structure (figure 7.4).

7.3 Gyro-backward-wave oscillator

The gyro-backward-wave oscillator (gyro-BWO) (figure 7.5) is a frequency tunable device, in which the frequency is tuned by tuning the magnetic field or beam energy (figure 7.1(b)). It finds applications in high-resolution radars, electron spin resonance (ESR), plasma diagnostics, high-energy accelerators, etc. The gyro-BWO operates in backward-wave mode at a point corresponding to the negative values of both the phase and group velocities of the RF waves (figure 7.1(b)). However, by providing an artificial mismatch reflector at the gun end, it is possible to take power from the beam dump or collector end (figure 7.5). The device is frequency tunable over a wide range of frequencies by changing the beam voltage or magnetic field. By changing the beam voltage one can change the axial beam velocity which in turn would change the slope of the beam-mode dispersion characteristics thereby changing the operating point of the device to change (figure 7.1(b)). Similarly, by changing the magnetic flux density one can move the beam-mode dispersion line parallel to itself, thereby changing the ω-intercept of the beam-mode dispersion characteristics, and hence again the operating point of the device. However, since here for the gyro-BWO, β is negative, one may read (7.2) as $s\omega_c/\gamma = \omega - \beta v_z = \omega + |\beta| v_z$, which, in view of the relation (7.3), indicates that a

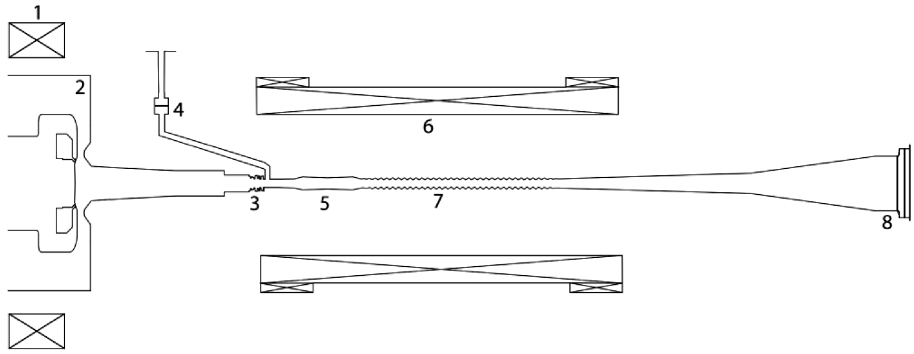

Figure 7.5. A schematic view of the CW gyro-BWO: (1: gun coil, 2: gun, 3: Bragg reflector, 4: output coupler, 5: circular to linear wave converter, 6: main coil, 7: helically corrugated interaction structure, and 8: far field output window) [32].

Table 7.2. Some representative gyro-BWOs [4].

Frequency (GHz)	Power (kW)	Bandwidth (%)	Efficiency (%)	Institution
140	2	3	9	MIT, Cambridge
10	200 000		22	IAP, N Novgorod
8.6	65	17	16.5	Univ. Strathclyde, IAP, N Novgorod
33.5	164	1	41	NTHU, Hsinchu

relatively large magnetic flux density is called for in the operation of a gyro-BWO ($s\omega_c/\gamma > \omega$). Several institutions have developed gyro-BWOs of various output specifications (table 7.2).

7.4 Gyro-klystron

A gyro-klystron (figure 7.6) is the fast-wave counterpart of a klystron (see section 6.2) in which, however, the electron bunching is relativistic and azimuthal, unlike in the klystron, in which the bunching is non-relativistic and axial. In its simplest form, as in a two-cavity klystron, the gyro-klystron has input and output cavities with a drift region between them (figure 7.6). Although predominant emphasis has been given to the development of gyrotron oscillators, gyro-amplifiers, namely, gyro-klystrons and gyro-TWTs, have also received attention for their potential applications as RF drivers for linear colliders/accelerators and high-resolution radars. These radar applications include precision tracking of targets, imaging of space objects, such as missiles, asteroids, space debris, and satellites, etc (see section 2.2). In addition, for applications in which coherent power combining is required, say, for phased-array radar, a gyro-amplifier would be preferred to a source like the gyrotron. For example, gyro-klystrons are used as RF drivers for linear colliders/accelerators and low-bandwidth radars. However, the gyro-klystron employing

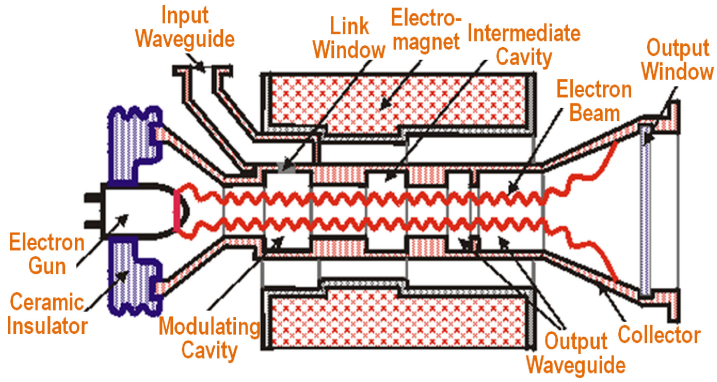

Figure 7.6. Schematic of a gyro-klystron [33].

Table 7.3. Some representative gyro-klystrons [4].

Frequency (GHz)	Power (kW)	Gain (dB)	Bandwidth (%)	Efficiency (%)	Institution
94.2	10.2	33	0.75	31	CPI, Litton, NRL, Univ. Maryland
8.57	75 000	30	0.2	32	Univ. Maryland
34.9	208	53	0.5	30	NRL Washington
9.17	0.7	22	0.3	70	IAP, N Novgorod

resonant cavities has a lesser bandwidth than the gyro-TWT, as does the klystron in comparison with the TWT. Several institutions have developed gyro-klystrons of various output specifications (table 7.3).

7.5 Gyro-travelling-wave tube

The gyro-travelling-wave tube (gyro-TWT) (figure 7.7) differs from a gyrotron in that it uses a propagating waveguide interaction structure instead of an open-ended waveguide resonator. Besides, an RF input coupler is provided with the waveguide. The waveguide is coated with a lossy material to suppress backward-wave oscillations. If the device bandwidth is the requirement, a gyro-TWT which uses a non-resonant waveguide is preferred to a gyro-klystron which employs resonant cavities [2, 3]. Gyro-TWTs are suitable for application in high information density communication systems and high-resolution radars in the high power, mm-wave frequency regime (see table 7.4 for a list of some of the gyro-TWTs developed).

In a gyro-TWT, the mismatch $\omega - \beta v_z - s\omega_c/\gamma \gtrsim 0$ ensures that the axial phase synchronism takes place between the electrons gyrating in helical paths and co-propagating travelling RF waves over an appreciable interaction length. As a result, an electron bunch forms that twists around the helix system with a pitch substantially greater than the electron pitch. The spatial positions where the

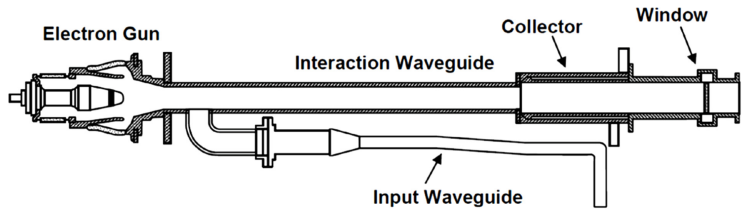

Figure 7.7. Schematic of a gyro-TWT [34].

Table 7.4. Some representative gyro-TWTs [4].

Frequency (GHz)	Power (MW)	Gain (dB)	Bandwidth (%)	Efficiency (%)	Institution
36.5	3	33	20	27	Univ. Strathclyde, IAP, N. Novgorod
35	20	30		11	NRL, Washington
9.4	1.3	47	3	27	Univ. Strathclyde
9.4	1.1	37	21	29	Univ. Strathclyde, IAP, N. Novgorod

electrons in the bunch are decelerated advances with a phase velocity approximately equal to the RF phase velocity that gives continuous interaction over a relatively larger length in the device [7–10]. Further, for wideband performance of the device, one has to ensure wideband coalescence or a grazing intersection between the beam-mode and waveguide-mode dispersion characteristics (figure 7.1(e)).

7.5.1 Grazing intersection

The condition for a grazing intersection or coalescence between the beam-mode and waveguide-mode dispersion characteristics for a gyro-TWT (figure 7.1(e)) may be easily developed with the help of the waveguide-mode and the beam-mode dispersion relations (7.1) and (7.2), respectively. At the grazing point of intersection (coalescence), one may equate the slopes of the dispersion plots, obtained from (7.1) and (7.2), respectively, as

$$v_z = v_g, \tag{7.13}$$

where $v_g(= \partial\omega/\partial\beta)$ is the group velocity of the waveguide mode or the slope $(\partial\omega/\partial\beta)$ of the $\omega - \beta$ waveguide-mode dispersion characteristics, at the point of intersection between the beam-mode and waveguide-mode dispersion plots (figure 7.1(e)). One may obtain differentiating (7.1):

$$v_g = \frac{\partial\omega}{\partial\beta} = \frac{\beta c^2}{\omega},$$

Table 7.5. Some representative CARMs [4].

Frequency (GHz)	Power (MW)	Gain (dB)	Efficiency (%)	Institution
220	50		2.5	LLNL Livermore
6.2	0.02	53	10	NRL, Washington
9.4	1.3	47	27	Univ. Niigata, NIFS, Univ. Maryland

which, with the help of (7.13), may be written as:

$$v_z = \beta c^2/\omega. \tag{7.14}$$

Further, one may easily obtain, with the help of (7.2) and (7.14),

$$\omega = s\omega_c \gamma_z{}^2/\gamma, \tag{7.15}$$

where

$$\gamma_z = (1 - v_z{}^2/c^2)^{-1/2} \tag{7.16}$$

is the relativistic mass factor corresponding to the axial beam velocity v_z.

Similarly, with the help of (7.1) and (7.14), one may easily obtain

$$\omega = \omega_{\text{cut}} \ \gamma_z. \tag{7.17}$$

Equating the right-hand sides of (7.15) and (7.17), one may then write

$$\frac{s\omega_c}{\gamma}\gamma_z{}^2 = \omega_{\text{cut}} \gamma_z,$$

which may be rearranged to be read as

$$\omega_c = \gamma\frac{\omega_{\text{cut}}}{s\gamma_z}. \tag{7.18}$$

The following expression for the grazing-point magnetic flux density is then obtained, with the help of (7.18) and (7.3):

$$B_0 = \frac{\gamma}{\gamma_z}\frac{m_{e\,0}}{|e|}\frac{1}{s}\omega_{\text{cut}} \quad \text{(grazing)}, \tag{7.19}$$

where γ and γ_z are obtainable from (7.5) and (7.16), respectively. The grazing-point operation of a gyro-TWT can be chosen by adjusting the magnetic flux density in the interaction region at or around the value given by (7.19).

It is obvious that, in order to achieve wideband performance of a gyro-TWT, one has to realize the grazing intersection between the beam-mode and waveguide-mode $\omega - \beta$ dispersion characteristics over a wide range of frequencies. One of the methods of broadbanding a gyro-TWT is to taper the cross section of the waveguide and synchronously profile the magnetic flux density. This method gives wide bandwidths but at the cost of the gain of the device [3, 35–38]. This is because different smaller length portions of the interaction length of different cross sections

become effective for different operating frequency ranges over the amplification band of the device. Alternatively, one may load the wall of a non-tapered waveguide either by dielectric lining of its wall or by placing a dielectric rod at the axis of the guide to straighten the waveguide-mode dispersion characteristics over a wider frequency range for the wideband grazing intersection between the waveguide-mode and beam-mode dispersion plots [3, 39, 40]. Consequently, this results in a wideband gain-frequency response of the gyro-TWT. However, this method of widening the bandwidth of the device entails loss due to dielectric charging. The problem can be alleviated by the method of all-metal loading of the waveguide by axially periodic metal discs and dispersion-shaping the structure by optimizing the disc dimensions for wideband coalescence between the waveguide-mode and beam-mode dispersion characteristics, which gives an improved wideband device performance [3, 39, 40].

The gyro-TWT with a conventional unloaded waveguide interaction structure has a bandwidth ~5%, while with dielectric loading the bandwidth improves to ~11%, however with disc loading it reaches ~20% [40]. A cylindrical waveguide provided with vanes—referred to in the literature as a magnetron-like structure—can be tried out as an interaction structure of a gyro-TWT. However, such vane loading does not provide the required dispersion control for a broadband coalescence between the beam-mode and waveguide-mode dispersion characteristics for wide bandwidths of a gyro-TWT [38, 41], though it enhances the device gain. Furthermore, though vane loading does not widen the bandwidth of a gyro-TWT by controlling the waveguide dispersion, it enhances the device gain. Therefore, such vane loading has been suggested to compensate for the gain of a gyro-TWT that would deteriorate in an attempt to widen the device bandwidth by tapering the waveguide cross section [38, 41].

7.6 Cyclotron auto-resonance maser (CARM)

A CARM (figure 7.8) uses highly relativistic electron beams with beam voltage V_0~1 MV or more supporting moderate transverse momentum with a beam-velocity pitch factor less than 0.7. The waveguide interaction structure of a CARM supports RF waves with a phase velocity close to the speed of light (figure 7.1(c)). CRM and Weibel instabilities are present in equal proportions in a CARM (section 7.1) that causes the so-called 'auto-resonance' so that once the electron beam is phase-bunched a large amount of energy can be extracted without losing synchronism. This auto-resonance is made possible since, as can be appreciated from (7.2), an increase in the third term of the left-hand side of (7.2), caused by a decrease in the relativistic mass factor γ of an electron due to the extraction of beam transverse energy, is compensated by a decrease in the second term caused by a decrease in the axial electron velocity since the beam axial energy is also tapped in the CARM. Unlike the gyrotron, the CARM operates at a large value of the Doppler shift βv_z. This would call for a rather less magnetic flux density B_0 for the device operation, which can be appreciated with the help of (7.3) and (7.2)—the latter to be read as $s\omega_c/\gamma = \omega - \beta v_z$. Further, the CARM operates at a lower pitch factor, higher beam voltage, hence at a higher power level, and at a higher frequency. The device also

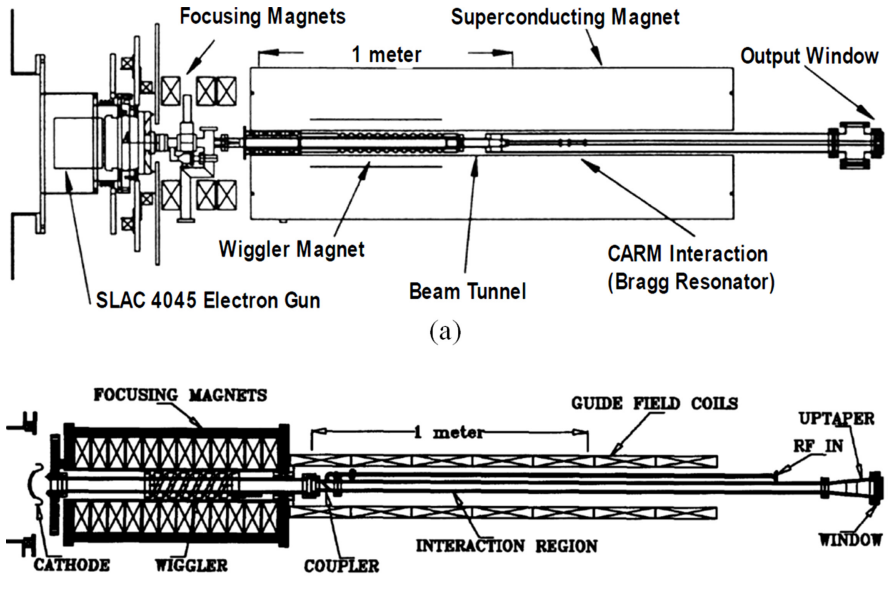

Figure 7.8. Schematic of a (a) CARM oscillator [42] and (b) CARM amplifier [43].

enjoys increased stability as it operates with higher axial electron velocities; an increased efficiency as it taps the beam axial kinetic energy of the beam over and above the beam azimuthal kinetic energy, though at the cost of the device gain caused by the offsetting of the azimuthal bunching by the axial bunching. Further, the CARM is inherently a wideband device since it operates with wideband coalescence between the beam-mode and waveguide-mode dispersion characteristics (figure 7.1(c)). However, since the CARM is essentially a Doppler-shift device (and incidentally, so is the gyro-BWO) operating at a large value of β (figure 7.1(c)), corresponding to a larger value of βv_z, the device is prone to inhomogeneous broadening of the cyclotron resonance band due to beam velocity spread unlike the gyrotron (figure 7.1(a)).

7.7 Slow-wave cyclotron amplifier (SWCA)

A SWCA is a gyro-device in which, unlike in conventional gyro-devices, the axial rather than the azimuthal kinetic energy is converted into electromagnetic energy. Moreover, in this device the axial non-relativistic, rather than the azimuthal relativistic, electron bunching takes place in the waveguide interaction structure and the slow rather than the fast waveguide-mode is destabilized in the structure. The slow-wave mode is realized by dielectric lining on the waveguide wall such that the waveguide-mode dispersion characteristics is depressed below the beam-mode dispersion characteristics of the device (figure 7.1(d)). Also, the SWCA provides (as does the CARM (see section 7.6)), wideband coalescence between the beam-mode and waveguide-mode dispersion characteristics (figure 7.1(d)) that makes SWCA

inherently a wideband device. However, SWCA operates at relatively lower frequencies. It also operates at relatively lower beam voltages or beam powers, and hence it delivers lesser RF output powers as well. However, the presence of a dielectric in the waveguide to slow down the RF waves makes the device prone to heating by the charging of the dielectric if it is lossy. Thus, the device needs to be provided with a good beam alignment in the device to avoid the dielectric charging. A thin layer of metal coating on the dielectric surface has also been suggested to drain out the charge developed, if any, on the surface. Further, SWCA is a Doppler-shift device, as are the CARM and gyro-BWO, both operating at a large value of β (figure 7.1) making SWCA prone to inhomogeneous broadening of the cyclotron resonance band due to beam velocity spread [3, 4].

7.8 Hybrid gyro-tubes

Some hybrid gyro-tubes are: gyro-twystron, harmonic multiplying gyro-TWT, triplet gyrotron amplifier (gyro-triotron) and phigtron. Gyro-twystron (figure 7.9) with extended length of the drift section and a slightly tapered waveguide output section is the fast-wave counterpart of the slow-wave hybrid twystron tube (see section 6.3). The device has been developed by several institutions with various output specifications (table 7.6).

The harmonic multiplying gyro-TWT (figure 7.10) is a two-stage nonlinear device in which electrons are pre-bunched for better harmonic content. The first stage operates at the fundamental wave frequency and the second stage at a chosen harmonic q of the wave frequency of the first stage. However, both the stages are operated at the same magnetic field and hence have the same cyclotron frequency. In order to make this happen the beam harmonic mode number s_2, say of the second stage, is chosen as the frequency harmonic (q) times the beam harmonic mode number s_1, say of the first stage such that the relation $s_2 = qs_1$, holds good. The device requires a lesser magnetic field due to beam harmonic operation and also has a less expensive input drive at a lower frequency [44].

The triplet gyrotron amplifier—gyro-triotron—was developed by combining the advantages of the clustered-cavity gyro-klystron and the harmonic multiplying gyro-TWT at the University of Maryland, USA (figure 7.10). The gyro-triotron yields high gain, high efficiency, and wide bandwidth. This device, with its advantages of

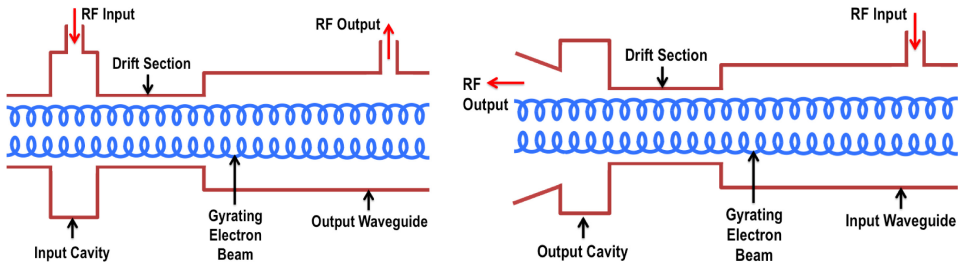

Figure 7.9. Schematic of a (a) gyro-twystron and (b) inverted gyro-twystron.

Table 7.6. Some representative gyro-twystrons [4].

Frequency (GHz)	Power (MW)	Gain (dB)	Bandwidth (%)	Efficiency (%)	Institution
94	59	35	1.6	14.9	CPI, NRL, Washington
31.5	160	30	1.3	25	NRL, Washington
4.5	73	37	1.5	22.5	NRL, Washington
9.2	4.4	18	1.6	27.5	IAP, N. Novgorod, NRL, Washington

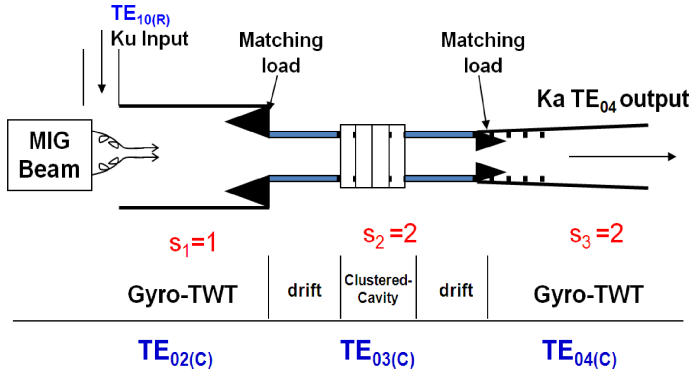

Figure 7.10. Schematic of a frequency-doubling gyro-TWT also called a gyro-triotron. s_1, s_2 and s_3 are the beam harmonic mode numbers of the input gyro-TWT, the clustered cavity gyro-klystron and the output gyro-TWT stages, respectively [44].

multistage mode selective interaction and over-moded operation with TE_{04} output, results in high operation stability and high power capability (figure 7.10) [44].

The phigtron is the harmonic multiplying inverted gyro-twystron (figure 7.11). In the interaction structure of a slow-wave twystron tube described earlier (see section 6.3), the first stage is an input cavity (klystron) and the second stage is an output waveguide (TWT). In contrast, in an inverted twystron, the first and the second stages are the input waveguide (TWT) and the output cavity (klystron), respectively. A 2 kW Ku-band helix TWT was used as the driving tube of Ku-to-Ka band (16.85–33.7 GHz) phigtron developed at the University of Maryland, USA. The power delivered by this tube was 720 kW, with 34% efficiency, 33 dB gain and 0.3% bandwidth, in a higher power category, while it was 400 kW, with 35% efficiency, 30 dB gain and 0.7% bandwidth, in a wider bandwidth category [45].

7.9 Peniotron

The peniotron ('penio' meaning spool or reel in Greek invented by S Ono and K Yamanouchi in 1963) belongs to the family of fast-wave gyro-devices [46–49]. However, unlike a conventional fast-wave gyro-device such as the gyrotron, the

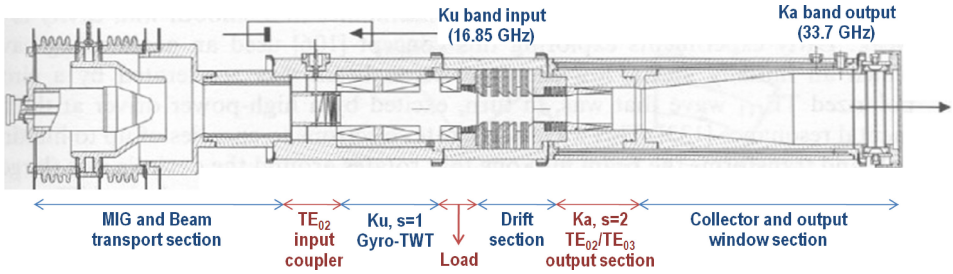

Figure 7.11. Schematic of a phigtron (University of Maryland, USA). *s* represents the beam harmonic mode number [45].

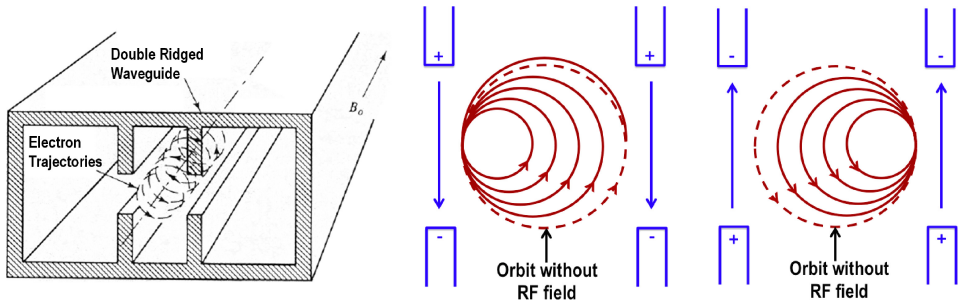

Figure 7.12. (a) Helical electron trajectory in a double-ridged peniotron in an axial magnetic field of flux density magnitude B_0, showing also the cross section of the shrinking of the electron orbits to the region of stronger decelerating RF electric field for both (b) initially decelerated and (c) initially accelerated electrons [6, 47–49].

peniotron does not require relativistic bunching of electrons for its operation. In a peniotron, both initially accelerated and initially decelerated electrons are made to deliver their kinetic energy to the RF waves thereby making the device highly efficient (figure 7.12) [46–49]. It operates with an axis-circling electron helical beam configuration (figure 7.12(a)) in a higher beam-harmonic mode thereby requiring a lesser magnetic field [46–49].

Taking, typically, a double-ridged peniotron, an initially accelerated electron in an RF electric field has its radius enlarged after half an orbital rotation to encounter a stronger though now a decelerating RF electric field. The orbital radius of the initially accelerated electron now shrinks under the influence of the decelerating RF electric field and this shrinking of the radius continues in subsequent orbital rotations of the electron with the movement of the electron in a stronger decelerating field (figure 7.12(b)). As a result, an initially accelerated electron when averaged over an orbital period delivers its net energy to the RF field. Similarly, the orbital radius of an initially decelerated electron in an RF electric field shrinks after half an orbital rotation to encounter a stronger decelerating RF electric field (figure 7.12(c)). For this electron, too, the shrinking of its radius continues in subsequent orbital rotations with the movement of the electron in a stronger decelerating field causing a net

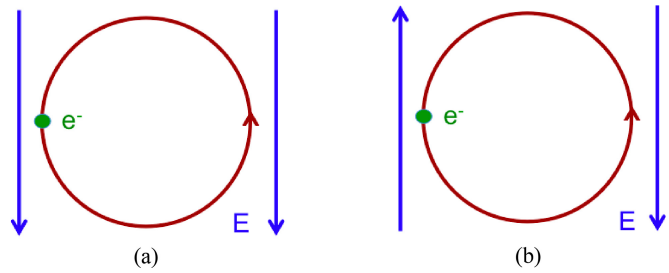

Figure 7.13. Cross-sectional view of an electron in orbital rotation in a decelerating RF electric field of a (a) double-ridged peniotron and (b) gyro-peniotron in TE_{02} mode.

delivery of energy to the RF field when averaged over an orbital period. Thus, irrespective of their initial RF phase distribution, all electrons of a peniotron are found to be 'good' to render the device highly efficient.

For beam-harmonic operation of a double-ridged peniotron, an initially accelerated electron is decelerated after half rotation, if the field changes by a cycle or a number of cycles (figure 7.13(a)). The condition may be stated as $T_c/2 = T,\ 2T,\ 3T, \ldots = pT$, which may be alternatively expressed as $\omega = 2p\omega_c$, where p is an integer; T and $\omega = (2\pi/T)$ are the wave time period and angular frequency, respectively; and T_c and $\omega_c = (2\pi/T_c)$ are the cyclotron time period and angular cyclotron frequency, respectively. Thus, the double-ridged peniotron operates under even beam-harmonic conditions ($\omega = 2p\omega_c$). Similarly, for beam-harmonic operation of a gyro-peniotron operating, typically, in TE_{02} mode, an initially accelerated electron is decelerated after half a rotation, if the field reverses its phase (figure 7.13(b)). The corresponding condition is: $T_c/2 = T/2,\ 3T/2, \ldots = (2p-1)T/2$ or $\omega = (2p-1)\omega_c$. Thus, in these examples, the double-ridged peniotron and gyro-peniotron operate under even beam-harmonic ($\omega = 2p\omega_c$) and odd beam-harmonic ($\omega = (2p-1)\omega_c$) conditions, respectively. Thus, for beam-harmonic operation of a gyro-peniotron excited typically in the whispering-gallery mode TE_{m1}, the beam mode dispersion relation $\omega - \beta v_z - (m-1)\omega_c = 0$ needs to be implemented relating the beam-mode number m with the waveguide-mode number s as $s = m - 1$ in (7.2) (while remembering relativistic mass $\gamma = 1$ in a gyro-peniotron). A typical peniotron excited in the TE_{41} mode under third beam-harmonic operation has delivered 6.9 kW of power in TE_{01} output mode at 30.3 GHz with 75% electronic efficiency at Tohoku University [4].

References

[1] Basu B N 1996 *Electromagnetic Theory and Applications in Beam-wave Electronics* (Singapore: World Scientific)

[2] Edgecombe C F (ed) 1993 *Gyrotron Oscillators - Their Principles and Practice* (London: Taylor and Francis)

[3] Kesari V 2009 *Analysis of Disc-loaded Circular Waveguides for Wideband Gyro-TWTs* (Germany: Lambert Academic Publishing AG & Co)

[4] Thumm M 2017 State-of-the-art of high power gyro-devices and free electron masers update 2016 *KIT Scientific Reports* 7735

[5] Shahana K, Kesari V, Karmakar S and Seshadri R 2017 Simulation of $TE_{6,2}$-to-Gaussian mode launcher for a millimeter-wave gyrotron *J. Electromagn. Waves Appl.* **31** 1959–70
[6] Smith L and Carpentier M (ed) 1993 *The Microwave Engineering Handbook: Microwave Components*vol 1 (London: Chapman and Hall)
[7] Thumm M K and Kasparek W 2002 Passive high-power microwave components *IEEE Trans. Plasma Sci.* **30** 755–86
[8] Symons R S and Jory H R 1986 Cyclotron resonance devices *Adv. Electron Phys.* **55** 1–75
[9] Chu K R 2004 The electron cyclotron maser *Rev. Mod. Phys.* **76** 489–540
[10] Thumm M 2003 MW gyrotron for fusion plasma applications *Plasma Phys. Control. Fusion* **45** A141–63
[11] Chu L J 1951 A kinetic power theorem *IRE-PGED Electron Tube Research Conf.* (Durham, New Hampshire)
[12] Haus H A and Bobroff D 1957 Small-signal power theorem for electron beams *J. Appl. Phys.* **28** 694–703
[13] Gould R W and Trivelpiece A W 1958 A new mode of wave propagation on electron beams *Proc. Symp. Electronic Waveguides* (Brooklyn: Polytechnic Press)
[14] Collin R E 1992 *Foundations for Microwave Engineering* 2nd edn (New York: Wiley-IEEE Press)
[15] Kluver J W 1958 Small-signal power conservation theorem for irrotational electron beams *J. Appl. Phys.* **29** 618–22
[16] Tonks L and Langmuir I 1929 Oscillations in ionised gases *Phys. Rev.* **33** 195–210
[17] Gaponov-Grekhov A V and Granatstein V L (ed) 1994 *Applications of High-Power Microwaves* (Boston: Artech House)
[18] Singh K, Jain P K and Basu B N 2005 Analysis of a corrugated coaxial waveguide resonator for mode rarefaction in a gyrotron *IEEE Trans. Plasma Sci.* **33** 1024–30
[19] Kreischer K E, Danly B G, Schutkerer J B and Temkin R J 1985 The design of megawatt gyrotrons *IEEE Trans. Plasma Sci.* **13** 364–73
[20] Flyagin V A, Gaponov A V, Petelin M I and Yulpatov V K 1977 The gyrotron *IEEE Trans. Microw. Theory Tech.* **25** 514–21
[21] Dumbrajs O and Zaginaylov G I 2004 Ohmic losses in coaxial gyrotron cavities with corrugated insert *IEEE Trans. Plasma Sci.* **32** 861–6
[22] Vlasov S N, Zagryadskaya L I and Orlova I M 1976 Open coaxial resonators for gyrotrons *Radio Eng. Electron. Phys.* **21** 96–102
[23] Flyagin V A and Nusinovich G S 1988 Gyrotron oscillations *Proc. IEEE* **76** 644
[24] Nusinovich G S, Read M E, Dumbrajs O and Kreischer K E 1994 Theory of gyrotrons with coaxial resonators *IEEE Trans. Electron Dev* **41** 433–8
[25] Iatrou C T, Kern S and Pavelyev A B 1996 Coaxial cavities with corrugated inner conductor for gyrotrons *IEEE Trans. Microw. Theory Tech.* **44** 56–64
[26] Barroso J J, Corrêa R A and de Castro P J 1998 Gyrotron coaxial cylindrical resonators with corrugated inner conductor: Theory and experiment *IEEE Trans. Microw. Theory Tech* **46** 1221–30
[27] Avramides K A, Iatrou C T and Vomvoridis J L 2004 Design considerations for powerful continuous-wave second-cyclotron-harmonic coaxial-cavity gyrotrons *IEEE Trans. Plasma Sci.* **32** 917–28
[28] Dumbrajs O and Nusinovich G S 2004 Coaxial gyrotrons: Past, present and future *IEEE Trans. Plasma Sci.* **32** 934–46

[29] Piosczyk B, Dammertz G, Dumbrajs O, Kartikeyan M V, Thumm M K and Yang X 2004 165-GHz coaxial cavity gyrotron *IEEE Trans. Plasma Sci.* **32** 853–60
[30] Yablonovitch E 1987 Inhibited spontaneous emission in solid-state physics and electronics *Phys. Rev. Lett.* **58** 2059–62
[31] Sirigiri J R, Kreischer K E, Machuzak J, Mastovsky I, Shapiro M A and Temkin R J 2001 Photonic-band-gap resonator gyrotron *Phys. Rev. Lett.* **86** 5628–31
[32] He W, Donaldson C R, Zhang L, Ronald K, McElhinney P and Cross A W 2013 High power wideband gyrotron backward wave oscillator operating towards the terahertz region *Phys. Rev. Lett.* **110** 165101
[33] https://sites.google.com/site/girokurayev/gyroklystron-theory-and-experiment
[34] Ferguson P and Symons R 1980 A C-band gyro-TWT *Tech. Dig. IEEE Int. Electron Dev. Meeting* pp 310–3
[35] Kesari V, Jain P K and Basu B N 2006 Exploration of a double-tapered disc-loaded circular waveguide for a wideband gyro-TWT *IEEE Electron Dev. Lett.* **27** 194–7
[36] Kesari V, Jain P K and Basu B N 2006 Analysis of a tapered disc-loaded waveguide for a wideband Gyro-TWT *IEEE Trans. Plasma Sci.* **34** 541–6
[37] Kesari V, Jain P K and Basu B N 2007 Parameters to define the electron beam trajectory of a double-tapered disc-loaded wideband gyro-TWT in profiled magnetic field *Int. J. Infrared Millim. Waves* **28** 443–9
[38] Agrawal M, Singh G, Jain P K and Basu B N 2001 Analysis of tapered vane-loaded structures for broadband gyro-TWTs *IEEE Trans. Plasma Sci.* **29** 439–44
[39] Choe J Y and Uhm H S 1981 Analysis of wide-band gyrotron amplifiers in a dielectric loaded waveguide *J. Appl. Phys.* **52** 4506–16
[40] Leou K C, McDermott D B and Luhmann N C Jr 1996 Large-signal characteristics of a wide-band dielectric-loaded gyro-TWT amplifier *IEEE Trans. Plasma Sci.* **24** 718–26
[41] Singh G, Ravi Chandra S M S, Bhaskar P V, Jain P K and Basu B N 1999 Analysis of dispersion and interaction impedance characteristics of an azimuthally-periodic vane-loaded cylindrical waveguide for a gyro-TWT *Int. J. Electron.* **86** 1463–79
[42] Pendergast K D, Danly B G and Temkin R J 1991 Operation of a long-pulse CARM oscillator *Nucl. Instrum. Methods Phys. Res. A* **304** 121–6
[43] Menninger W L, Danly B G, Alberti S, Chen C, Giguet E, Rullier J L and Temkin R J 1993 CARM and harmonic gyro-amplifier experiments at 17 GHz *Proc. Int. Conf. Particle Accelerators* vol 4, pp 2656–8
[44] Rodgers J, Antonsen T Jr, Guo H and Granatstein V 2003 Harmonic gain and noise in frequency-multiplying gyro-amplifiers *AIP Conf. Proc.* **691** 1
[45] Rodgers J, Guo H, Nusinovich G S and Granatstein V L 2001 Experimental study of phase deviation and pushing in a frequency doubling, second harmonic gyro-amplifier *IEEE Trans. Electron Dev* **vol 48** 2434–41
[46] Gilmour A S Jr 1986 *Microwave Tubes* (Norwood: Artech House)
[47] Ono S, Tsutaki K and Kageynama T 1984 Proposal of a high efficiency tube for high power millimeter or submillimeter wave generation: the gyro-peniotron *Int. J. Electron.* **56** 507–19
[48] Dohler G, Gallagher D, Richards J and Scaffuri F 1993 Harmonic high power 95 GHz peniotron *Tech. Dig. IEEE Int. Electron Dev. Meeting* pp 363–6
[49] Yamanouchi K, Ono S and Shibata Y 1964 Cyclotron fast wave tube, the double ridge traveling wave peniotron *Proc. 5th Int. Conf. Microwave Tubes (Paris)* pp 96–102

IOP Concise Physics

High Power Microwave Tubes: Basics and Trends
Volume 2
Vishal Kesari and B N Basu

Chapter 8

Vacuum microelectronic, plasma-filled and high power microwave (HPM) tubes

In the preceding two chapters we have discussed the various aspects of conventional (chapter 6, volume 2) and fast-wave (chapter 7, volume 2) microwave tubes (MWTs). In the present chapter, let us discuss three kinds of MWTs: (i) vacuum microelectronic microwave tubes (VME-MWTs) which can operate at higher frequencies in the terahertz (THz) (300–3000 GHz) region of the electromagnetic spectrum (section 8.1), (ii) plasma-filled MWTs with high beam current transport which can deliver large power (section 8.2), and (iii) HPM MWTs which can be used in directed energy weapons (DEW) (section 8.3).

8.1 Vacuum microelectronic (VME) MWTs

MWTs, which are essentially vacuum tubes, continue to have extensive applications despite competitive incursion from solid-state devices (SSDs) (see chapters 1 and 2, volume 1). The reach of MWTs in the THz regime has opened up several applications in scientific, medical, communication (high data rate), high security protection, etc (table 8.1). The applications of MWTs in the THz regime also extend to the field of imaging (table 8.2), say, of biological tissues, which have relatively large specific absorption rates (SARs) requiring high powers.

8.1.1 Vacuum microelectronic (VME) technology

The advent of vacuum microelectronic (VME) technology, which is a fusion of MWT and SSD technologies while accruing the advantages of both, has made it possible to fabricate VME-MWTs for the implementation of these applications. However, the challenge to meet the demand of applications in the THz regime (tables 8.1 and 8.2) is to develop reliable coherent radiation THz sources which can deliver 0.01–10.0 W CW of power with greater than 1% efficiency and frequency agility of instantaneous tunability with a bandwidth over 1%. Unfortunately, neither

doi:10.1088/978-1-6817-4704-0ch8

Table 8.1. Present and futuristic applications of THz tubes other than imaging [1–5].

Area	Application
Security	Hazardous-gas detection Screening of people Non-contact postal screening Standoff suicide bomber detection
Communication and information technology	High data rate wireless communication and instant data transmission (>10–40 Gbit s^{-1}) Communication between two satellites High attenuation in the atmosphere (huge absorption by water vapor of air; for water content 7.5 g m^{-3}, atmospheric attenuation ~10 dB Km^{-1} at 0.3 THz)
Medical	Detection of skin cancer Hardness measurement of drugs
Semiconductor and industrial	Material evaluations (e.g. inspection of silicon solar cells, nano-composites, polymer films, dielectric films, etc) Fault analysis in the development of sophisticated next-generation LSI circuit Control of food and agricultural products (e.g. evaluation of damage to fruit, water content in vegetables, etc)
Earth and space science	Environmental monitoring of the Earth Monitoring of the new born galaxies including new solar system, and invisible dark universe
Basic science	THz spectroscopy Study of the nature of light by THz pulses Development of electromagnetic meta-materials in THz regime

Table 8.2. Applications of THz tubes in imaging [1–5].

Civilian/public sector	All-weather navigation Biomedical imaging Medical diagnosis: DNP for NMR Quality control (semiconductor, manufacturing and food industries) Product and packaging control Plasma diagnostics for fusion research
Military/defence sector/security and law enforcement	Higher resolution radar/passive imaging Target structure characterization on sub-mm scale Identification of Sarin and Soman in chemical warfare Detection of personnel or weapons through thin foliage/camouflage Spectral fingerprinting THz spectrum of materials (fingerprint) Identification of biological weapons through phonon excitation Detection of chemical and biological substances and hidden weapons

SSDs, such as IMPATT diodes, nor microwave tubes, such as gyrotrons (see section 7.2 in chapter 7, volume 2), can meet this demand. IMPATT diode sources have fairly narrow instantaneous bandwidths and very low efficiencies (<0.01%), while gyrotrons become rather bulky and expensive. However, this demand can be met by VME tubes with field-emission cathodes based on carbon nanotubes (CNTs) and precision-dimensioned micro-machined interaction structures. The micro-fabrication techniques which can be used to fabricate VME-MWTs are: (i) electric discharge machining (EDM), (ii) deep reactive ion etching (DRIE) and (iii) lithographie (lithography), galvanoformung (electroforming) abformung (moulding) (LIGA). Thus, for example, a serpentine trench can be etched in silicon with a DRIE tool and then gold-plated and then two such trenches can bond together to form a folded waveguide (FW) slow-wave structure of a FW-TWT (figure 8.1). Typically, FW-TWTs have delivered 100 W at 83 GHz with 5% efficiency and 5 W at 180 GHz with 3% efficiency using 12.8 kV, 0.156 A and 12.8 kV, 0.013 A electron beams, respectively [2].

LIGA, which is a combination of deep-etch high-energy x-ray lithography and electroforming, is capable of fabricating precision high frequency, high aspect ratio structures that are much taller than wide with lateral precision below one micrometer of vertical dimensions from hundreds of microns to millimeters and horizontal dimensions as small as microns. LIGA typically involves four steps. In the first step called 'exposure', a gold-plated chrome mask partly covered with a strong x-ray absorbing material—which is placed, typically, over a polymethyl metahacrylate (PMMA) x-ray sensitive photo-resist and which is bonded to an electrically conductive substrate, say, of aluminium (low atomic number to reduce back scattering)—is exposed to synchrotron x-ray radiation. In the second step called 'development', a structured resist is formed on the substrate. In the third step called 'electroplating', metal is deposited in the resist. In the fourth step called 'resist stripping', the resist is chemically stripped off to leave the desired structure formed behind. Similarly, field emission cold cathodes of CNTs, which are essentially allotropes of carbon with a cylindrical nanostructure, are called for in the successful

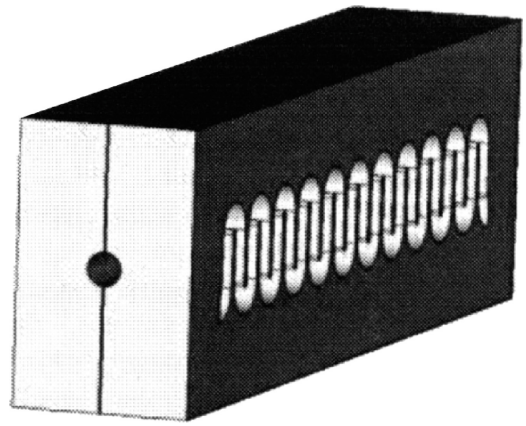

Figure 8.1. An FW-TWT slow-wave structure with a hole to pass an electron beam through [3].

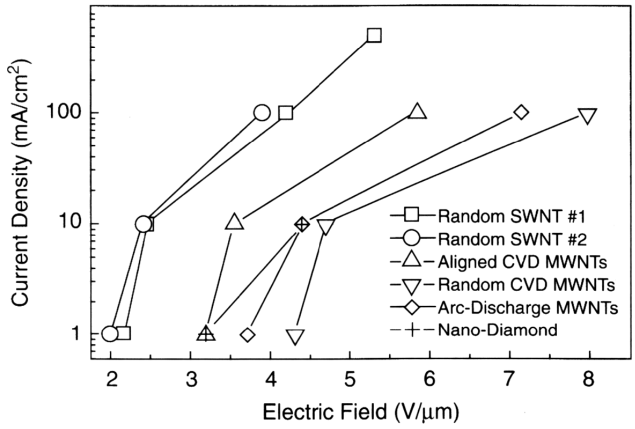

Figure 8.2. Current density versus typical CNT cathodes [4,6].

development of VME-MWTs. CNT fibers each of 1–50 nm diameter derived from single-wall and multi-wall strands—with an aspect ratio of up to 1000, yielding more than 1 μA stable current per fiber at fields of only a few MV m^{-1}—make single-wall nanotube (SWNT) and multi-wall nanotube (MWNT) field-emission CNT cathodes, respectively (figure 8.2) [4]. Typically, a CNT-based field emission cathode is fabricated first by preparing CNT materials and then by depositing them on to the cathode substrate so that the desired surface morphology, CNT density and adhesion between the CNT deposition and the substrates are achieved [4]. Thus, VME technology has led to global efforts in practically developing VME-MMTs and characterizing them (table 8.3).

8.1.2 Typical vacuum-microelectronic (VME) MWTs

In chapter 6, we discussed klystrons including muti-cavity, multi-cavity klystron, MBK (see section 6.2 in chapter 6, volume 2) and klystron variants, namely, reflex klystron, IOT, EIK, EIO and twystron. Here, let us mention another member of this family, namely, the 'klystrino' module which can operate at high frequencies in the W band (~3 mm wavelength) and can be fabricated using VME technology. A typical module consists of 6 klystrinos in parallel, with separate electron guns, 0.6 μperv each, cavities and PPM stacks, but a common vacuum and beam dump or collector. The cavities of the module can be fabricated using LIGA technology featuring 2–3 μm tolerances and an excellent surface finish. A typical W-band klystrino module of 6 inch diameter and 12 inch length and less than 20 lb in weight with 120 kV, 15 A beam, has yielded 0.5 MW peak and 5 kW average powers. Also, a monolithic terahertz reflex klystron, called the nanoklystron, has been developed (figure 8.3). The device uses the CNT field-emission cold cathode. The cavity structure of the device is formed monolithically from two thermo-compression-bonded silicon wafers which are processed using DRIE VME technology. The device typically delivers ~mW of power at 1.2 THz [5].

Table 8.3. Global efforts in the development of VME-MWTs [5–10].

Agency, country	Device	Frequency	Power output	Gain	Efficiency	Bandwidth
Samsung, Korea, CCR, USA	BWO	0.1 THz	6 W		1%	
CPI, Canada	EIO	0.214 THz	6 W			2%
CPI, Canada	EIK	0.218 THz	7 W	23.6 dB		0.14%
NRL, CPI, DARPA	FW-TWT amplifier	0.218 THz	64 W	14 dB	4%	6.8%
NGES, Teledyne, DARPA	Power FW-TWT amplifier	0.214 THz	54.2 W	38.5 dB	2.1%	2.3%
NGFS, Teledyne, DARPA	FW-TWT SSPA power module	0.65 THz	108 mW	21.5 dB	0.44%	6.8%
Lancaster Univ, Thales	Backward-wave amplifier	1 THz	2.5 mW (target)	10 dB	0.001%	
JPL, NASA	Nano-klystron	1.2 THz	3 mW (target)		0.02%	

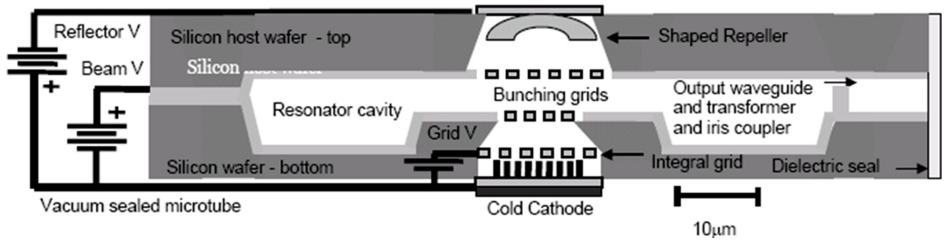

Figure 8.3. Schematic of the nanoklystron [5].

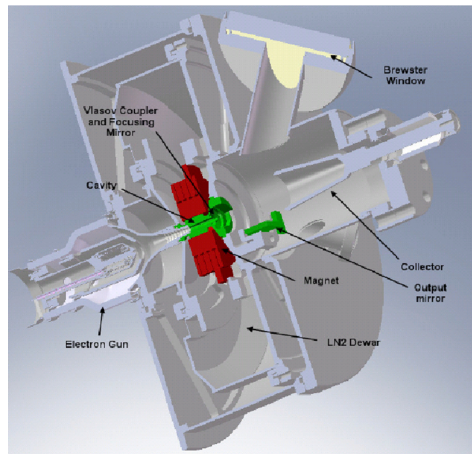

Figure 8.4. Cut-view model of the THz gyrotron developed by Calabazas Creek Research Inc. [8].

Calabazas Creek Research Inc. has developed a THz gyrotron both at the fundamental (650 GHz–1 THz) and second (1–2 THz) beam-harmonic frequencies (figure 8.4). They have used a repetitive pulsed magnetic field provided by a pulsed solenoid producing up to 37 T (PRF ~ 1 Hz). A 5 kW output power in 10 μs pulses has been obtained [7]. In addition to the global effort in the development of VME-MWTs (table 8.3), it is worth noting the scenario of the state-of-the-art achievement of power versus frequency capability of some of these devices in the terahertz regime (figure 8.5).

The clinotron—so far not introduced in the preceding chapters (including chapter 6, volume 2)—mentioned in the state-of-the-art scenario (figure 8.5), is basically a BWO with an inclined electron beam impinging on a grating interaction structure (figure 8.6) [9]. The angle of inclination of the beam can be changed to optimize the interaction length of the device without changing the geometry of the tube. As compared to a conventional BWO, the beam thickness of the clinotron is larger, which allows each layer of the inclined beam to take part in beam-wave interaction effectively. Further, even though the device has a resonant structure, it enjoys large tunability by the successive excitation of the resonator modes obtained by varying the beam voltage. The output power level, several watts at frequencies around

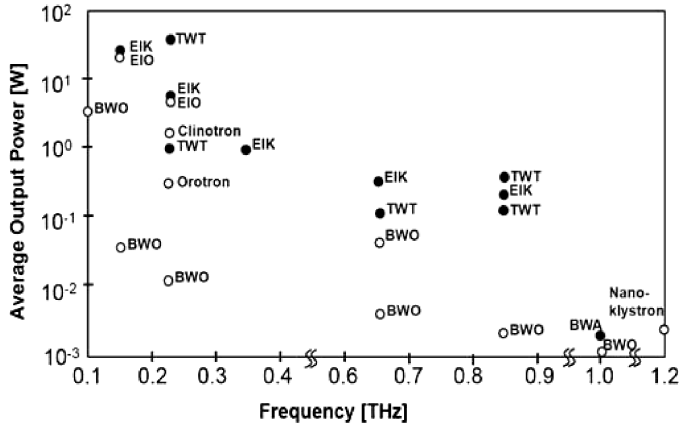

Figure 8.5. Scenario of state-of-the-art achievements of power versus frequency of terahertz VME-MWTs [5, 9].

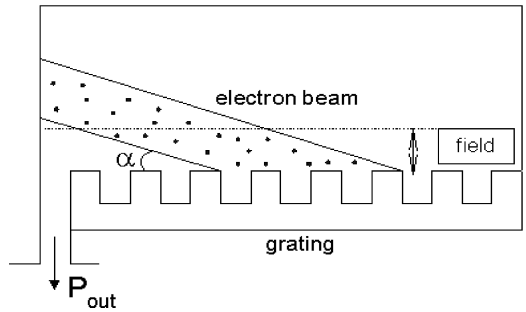

Figure 8.6. Schematic of the clinotron. α is the angle of beam inclination [9].

100 GHz and ~100 mW at frequencies around 500 GHz, have been achieved at Radio Astronomy of the National Academy of Sciences of Ukraine [9].

8.2 Plasma-filled MWTs

The space-charge limiting current of an electron beam transporting through the axis of a conducting circular envelope is imposed by the potential depression caused by the negative electronic space-charge. This limit can be increased by increasing the number density of positive ions relative to that of electrons, which can be easily appreciated by inspecting the expressions (3.23) and (3.27) (see section 3.6 in chapter 3, volume 1). This is one of the reasons prompting the MWT developers to fill MWTs such as the TWT, BWO and gyrotron with plasma, with a view to improving their performance, say, with respect to RF output power by increasing the beam current. Furthermore, ions partially compensate for beam space-charge forces enabling the beam to pinch (ion-channel) resulting in the 'self focusing' of the beam known as the Bennett effect. The plasma-assistance of an MWT giving larger beam currents provides the azimuthal magnetic field, which in turn arouses a

radially inward magnetic confining force on the beam thereby relaxing the requirement of an external magnetic field. This also helps in negating the effect of misalignment of the magnetic field if applied externally for beam confinement. Further, the phase velocity of the electromagnetic waves is higher in plasma than in vacuum. Therefore, the wave frequency (which is phase velocity divided by wavelength) is also higher in plasma than in vacuum for a given tube size, that is, for a given wavelength since the tube size is of the order of wavelength. Hence, another advantage of plasma-assistance of MWTs is that it can enhance their operating frequencies [10].

Further, there is an issue arising from the placement of the electron beam far from the metal envelope in a MWT—a requirement for the beam to experience a larger interaction area. However, such requirement of beam placement makes the envelope radius much larger than the beam radius thereby reducing the space-charge limiting current, which again can be appreciated with the help of (3.23) and (3.27). However, this reduction of space-charge limiting current could be compensated for by increasing the number density of positive ions relative to that of electrons by plasma assistance. Yet there are other advantages of plasma-filling MWTs such as the frequency tunability of the device by controlling the plasma electron number density as well as the long-pulse, high-PRF, high-efficiency and wideband device performance. Moreover, plasma-filled MWTs, in view of the nonlinearity of the plasma medium and the presence of abundant eigenmodes in plasma, have the potential for being used as noise sources. However, the noise generated could be a disadvantage as well for a plasma-filled MWT to be used as an amplifier or an oscillator. Thus, fluctuations in ion density in the device also cause the output frequency and power of the device to fluctuate. The other difficult areas of plasma-filled MWTs are the coupling of the RF power in and out of the device and the creation of a stable quiet plasma column with a plasma density of the order of 10^{12}–10^{15} cm^{-3} required for the centimeter-to-millimeter-wave band region.

8.2.1 Plasma-cathode electron (PCE) gun

In order to prevent a material cathode from being damaged by the bombardment of high-energy ions, a material cathode is replaced by a 'plasma-cathode' in a plasma-cathode electron (PCE) gun, making the latter suitable for a plasma-filled MWT. A PCE-gun provides large current densities (50–1000 A cm^{-2}) and long pulse-widths (>100 μs). Such high-level performance cannot be provided by either a usual thermionic cathode that has low current densities or a field-emission cathode that has short pulse-widths (<1 μs). A low-pressure (5–50 mTorr of helium or hydrogen) plasma discharge between a hollow cold cathode and a discharge anode becomes the source of electrons in a PCE gun; a beam anode is also provided to throw the beam into the interaction region of the device beyond the gun (figure 8.7) [11]. For single-pulse or low-PRF operation, a gas-puff PCE-gun has been used (figure 8.7(a)). However, for high-PRF operation over 10–50 Hz, in another version of the PCE-gun a static gas-fill has been employed besides a thermionic cathode to increase the ionization efficiency. In this gun, a permanent magnet array surrounding the plasma

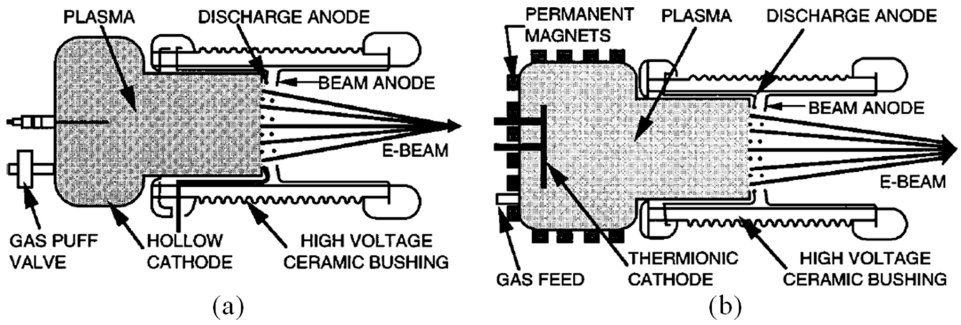

Figure 8.7. A PCE gun for (a) low-PRF or single-pulse and (b) high-PRF operations [11].

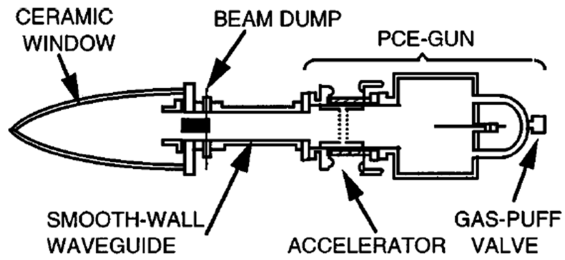

Figure 8.8. Schematic of the plasma wave tube (PWT) [12].

provides the confinement of the primary electrons emitted from the cathode (figure 8.7(b)) [11]. The neutral gas can be present in the gun either due to the gas leakage from a puff (figure 8.6(a)) or due to the presence of a background gas feed (figure 8.7(b)). A PCE-gun can be used to develop plasma-filled MWTs such as a plasma-wave tube (PWT), plasma-assisted slow-wave oscillator (PASOTRON) and plasma-filled TWTs.

8.2.2 Typical plasma-filled MWTs

A PWT is a microwave/mm-wave source that employs a PCE-gun (figure 8.8) [12]. A typical PWT, in a hydrogen plasma-fill and a smooth-wall circular waveguide, has used $\leqslant$40 kV, $\geqslant$200 A, 5–20 μs-pulse-width beam for the beam-plasma-wave interaction. A getter, typically Zr–Al, can take care to control the background gas pressure of the tube and pump out the other gasses evolved in the tube with time. The energy in the electron plasma waves couples to an electromagnetic TM_{01} mode at twice the plasma frequency generated due to nonlinear effects in the beam-plasma interaction. The radiation can be coupled out of the waveguide and radiated through a ceramic radome by a broadband antenna and the spent beam collected by a beam dump (figure 8.8) [11]. The beam transport in the device can be accomplished without an external magnetic field since the background plasma cancels the beam space charge in this plasma-filled MWT. The device has generated typically ~10 kW of radiated power with $\geqslant$0.4% conversion efficiency and wide instantaneous spectrum (1–10 GHz, typical) in the frequency range of 6–60 GHz. However, the

centre frequency of the device is likely to change with the change of plasma density and hence the plasma frequency with time. The device power can be increased by increasing the beam current, which unfortunately changes the centre frequency, which in turn causes the power level to fall. A power level up to 10 kW with 1% efficiency has been reported obtained across the X-band in a typical PWT [11].

A PASOTRON is essentially a backward-wave oscillator (BWO) capable of producing high-power, long-pulse microwave energy, which can be used as a directed energy source (see section 8.3) (figure 8.9). Being a plasma-filled MWT it enjoys (like the PWT) the advantage of self-focusing and thus does not require any external magnetic field for confining the electron beam. Therefore, it can be constructed to be smaller and lighter than other vacuum high power MWT sources, thereby making it attractive for airborne and mobile applications. PASOTRONs have been developed in xenon, helium and hydrogen plasmas delivering 1–5 MW of power of pulse duration >100 μs with 15–20% efficiency in L, C, S and X bands, using a plasma cathode current density of PCE guns up to 50–1000 A cm^{-2} and 30 A–1 kA beam current and 30–220 kV accelerating voltage. Also, PASOTRONs are capable of a repetitively fired operation with reproducible shot-to-shot characteristics. The output can be taken either downstream from the collector end (figure 8.9(a)) or upstream from the gun end (figure 8.8(b)). Since the device operates in the BWO-mode, for downstream collection from the collector end an iris has been placed at the gun end reflecting backward waves towards the collector end (figure 8.9(a)). A helix PASOTRON has been configured with an upstream high power load and a downstream sliding short to control the phase of the reflected signal (figure 8.9(b)). A helix-waveguide coupling structure converts helix modes to the TE_{10} mode for RF output coupling and facilitates a flow of cooling liquid through the helix to remove heat generated during high-power operation (figure 8.9(b)).

Typically, the rippled-wall waveguide (figure 8.9(a)), for example, with 3.25 cm average radius, 0.715 cm ripple-depth, and 2.4 cm periodicity in the L band, and the helix (figure 8.9(b)), have been used as slow-wave structures. A typical L-band 200 kV PASOTRON produced 20 MW peak power with 1 kJ per pulse [11, 13–15]. There is an issue in the PASOTRON related to increasing the pulse duration for applications requiring ~1 kJ pulse energy. It is likely that such a long pulse duration

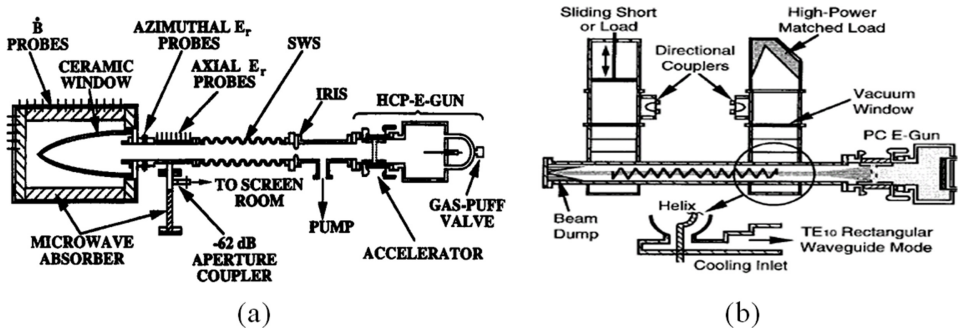

Figure 8.9. (a) Rippled-wall [13] and (b) helix PASOTRONs [16]. In (a), the HCP-E-gun is the abbreviation of a hollow-cathode plasma electron gun representing the PCE-gun [13].

would allow the high-density gas front to reach the interaction region causing a microwave breakdown. This calls for a strong gas pressure gradient, to be maintained in the duration of pulse, between the gun and the interaction regions where the pressures ought to be 10^{-3}–10^{-2} Torr and $<5\times10^{-5}$ Torr, respectively. This can be achieved by first activating a He puff valve and then energizing the plasma gun after a suitable delay [15].

Plasma filling has also improved the performance of TWTs with different kinds of slow-wave structures such as the rippled-wall waveguide, helix and coupled-cavity (CC) structure. In a typical plasma-filled rippled-wall TWT, the space-charge waves on the beam formed by a PCE gun resonantly couple to RF modes of the rippled-wall waveguide and the energy transferred from the beam to the RF waves is coupled to space through an output horn antenna [17]. The plasma filling has reportedly enhanced the output power and widened the bandwidth of a CC-TWT [18] (figure 8.10). In a typical example of a plasma-filled CC-TWT the slow-wave structure used is a chain-of-coupled-cavity abbreviated as CCC, the structure using an array of 10 alternating-slot cavities [18]. This plasma-filled CCC-TWT, however, has not accrued the advantage of self focusing of plasma filling and used instead an external magnetic field of flux density of 0.25–0.30 T for beam confinement (figure 8.9(a)). An electron beam of 2–4 A of energy up to 25 keV formed by LaB_6 or a W thermionic gun transporting through a narrow drift channel in the magnetic field

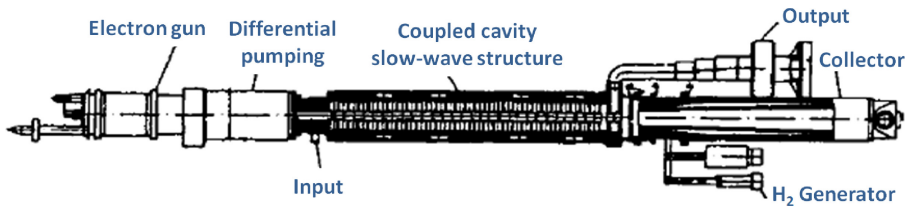

(a)

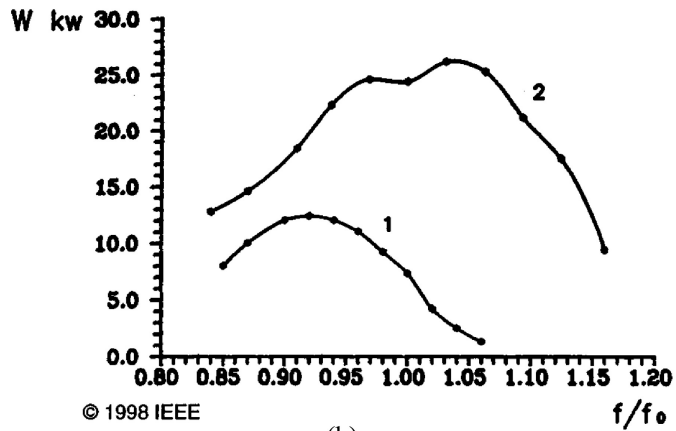

(b)

Figure 8.10. (a) Schematic of a typical CCC-TWT and (b) its output power versus frequency characteristics under vacuum ($\sim1\times10^{-6}$ Torr) (1) and plasma-filled ($\sim1\times10^{-3}$ Torr) (2) of conditions showing power in kW on the ordinate and operating frequency f normalized with respect to the resonant centre frequency f_0 [18].

Table 8.4. Pulsed power and energy per pulse obtainable from typical HPM tubes [22–24].

HPM MWT (typical)	Pulsed power (GW)	Energy per pulse (J)
RELTRON	0.5	300
MILO	1.5	330
Relativistic klystron	10	1000
PASOTRON	0.005	500
MWCG	15	900

generates a cylindrical hydrogen plasma column of density up to 10^{12} cm^{-3} at a pressure of 1×10^{-3} Torr [18]. An arrangement of the titanium-hydride reservoir and getter provides the hydrogen gas fill with a differential pumping system between the interaction region and the gun region (figure 8.9(a)). The plasma-filled ($\sim 1 \times 10^{-3}$ Torr) CCC-TWT has delivered wideband power ~25 kW—two and a half times that of a corresponding vacuum ($\sim 1 \times 10^{-6}$ Torr) in centimeter wavelength range (figure 8.10(b)). Furthermore, the device is said to have operated continuously for >5000 h with a life estimate of 20 000 h based on the storage and pumping capacities of the hydrogen gas handling system [18].

The power of a gyrotron can also be enhanced by plasma filling (table 8.4). For this purpose, typically, an annular beam is formed by an array of plasma guns derived from field-emission cathodes and injected into the cavity excited in the $TE_{6,2}$ waveguide mode at 35 GHz. A beam current in excess of 10 kA can be attained in such space-charge neutralizing background plasma. The beam creates plasma filling of density $\sim 10^{13}$ cm^{-3} in the gyrotron. The power ~1 GW has been obtained from such as a plasma-filled gyrotron which is much larger than 100–200 MW of power of the corresponding plasma-free gyrotron with a beam of lesser current of 1–3 kA at beam voltage 0.6–1.35 kV obtained in the space-charge limited background [19–21].

8.3 High power microwave (HPM) MWTs

Generation of HPM using MWTs has expanded the domain of the applications of these devices from the radar, communication and EW to information warfare (IW); the latter involving DEW—both lethal and non-lethal [22–24]. HPM has a frequency range, usually, of 300 MHz to 300 GHz and it refers to powers characterized by

(i) long pulse duration, high-PRF, or CW and
(ii) high-peak, short pulse duration, low-PRF or single-shot.

The narrow-band (<10% of carrier frequency) HPM spans a 1–100 GHz frequency range and it is generated at the expense of the electron beam energy by driving the beam with pulses of duration from tens to hundreds of ns. The ultra-wideband (>10% of carrier frequency) HPM spans over many decades in frequency

Table 8.5. Representative parameters for some Cerenkov devices [24].

Source parameter	BWO	MWCG	MWDG, RDG or Orotron
Frequency range	3–10 GHz	10–35 GHz	13–60 GHz
Peak power	3 GW	15 GW	4.5 GW
Efficiency	20%	48%	10%–20%
Pulse width	~20 ns	~100 ns	Up to 700 ns
Tunable range	300 MHz	150 MHz	NA
Repetition rate	200 Hz	NA	
Output mode	TM_{01}	TM_{01}	Complex
Bandwidth	~1%		
Voltage 1–2 MV	0.5–1 MV	1–2 MV	1–2 MV
Magnetic field	3–4 T	~2.5 T	~2.8 T

from tens of MHz to tens of GHz and is driven by a high voltage spike with as short a rise time as possible, ideally by a δ-function generator, without an electron beam.

HPM weapons can radiate hundreds of megawatts to gigawatts of power with hundreds of joules of energy per pulse (table 8.5). They use electromagnetic power rather than explosives as ammunition and can attack at nearly the speed of light. Moreover, HPM weapons need not be pointed, unlike in laser warfare, since microwaves can spread by diffraction and thus can accommodate a lack of precision in tracking. HPM attack could also be effective in adverse weather conditions. They can be of hard-kill causing large-scale physical destruction of targets and soft-kill or smart HPM type disabling mission-critical components. (For instance, the energy density $\sim 10^{-7}$ Jcm^{-2} is good enough to cause bit error in computers and computer-aided equipment and cause disaster in air-traffic control.) The effects that can cause damage or disruption are joule heating, RF breakdown and/or Fermi-level inversion due to large electric fields, and RF induction by eddy-current heating. Large or relatively small power densities on target are required for HPM-DEW accordingly as the requirement is to cause burnout/lethal damage to electronic systems or deception/spoofing of the enemy system to mission failure [22]. An intense relativistic electron beam (IREB) drives HPM-MWTs. The required power density on target increases as the need ascends from (i) deceptive jamming by spoofing of the system into mission failure to (ii) brutal jamming causing blinding of RF receivers or radar to (iii) upset causing temporary disruption of memory or logics in electronic systems to (iv) burnout causing physical damage to electronic systems [24].

Both explosive and non-explosive types of field-emission cathodes (see section 3.1 in chapter 3, volume 1) can be used in HPM-MWTs. Pulsed power is used to form IREB, which in turn drives an HPM-MWT in an HPM system (figure 8.11).

Pulsed power can be typically generated by a Marx generator which is an assembly of capacitors that are charged in parallel and then quickly discharged in series (figure 8.12). This enhances the pulse voltage by a factor of n to nV_0, where V_0 is the voltage across each charged capacitor and n is the number of capacitors in the

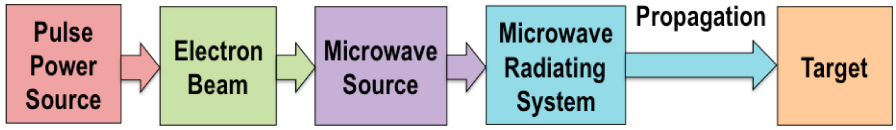

Figure 8.11. HPM system configuration showing a pulsed power source driving an electron beam into a microwave source (HPM-MWT).

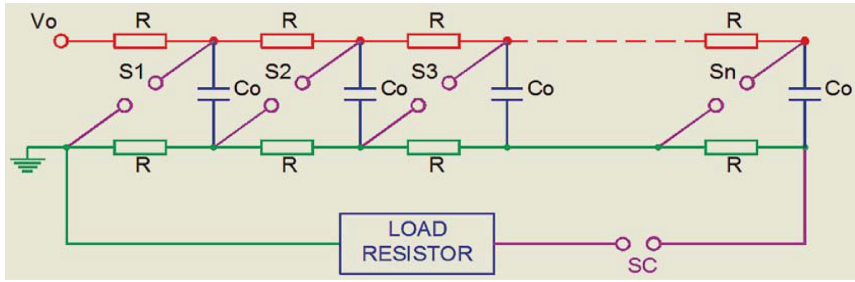

Figure 8.12. Bank of n number of capacitors in a Marx generator. A spark gap 'SC' is used to reduce the charging current though the external load, while the front and tail resistors 'R' and the number of stages adjust the pulse duration [26].

generator. For this purpose, the individual capacitors, each charged to the capacitance C_0, are discharged through spark gaps S1–Sn. An external source triggers the first one or more spark gaps. Consequently, the remaining gaps get overloaded and their self-breakdown takes place. Spark gap SC reduces the charging current though an external load (figure 8.12). (In a typical pulsed power system, a Marx generator can be inputted to a further stage of pulse compression, such as a pulse forming network [24].) A typical Marx generator with a 20-stage Marx generator has delivered 230 kV, 1500 ns duration voltage pulse to a matched load of 90–100 Ω, and subsequently tested in a typical diode of 7.5 mm cathode-anode gap using a brass/aluminium explosive-emission cathode to obtain 230 kV, 150 ns voltage pulse [25].

Some examples of IREB-driven HPM-MWTs are: the 'relativistic' versions of conventional MWTs such as the magnetron, klystron, TWT and BWO, RELTRON (being a kind of relativistic klystron). The other IREB-driven devices are a magnetically insulated line oscillator (MILO), PASOTRON (see section 8.2), virtual cathode oscillator (vircator), surface-wave oscillator (SWO), orotron or radiation diffraction generator (RDG), multiple-wave Cerenkov generator (MWCG), multi-wave diffraction generator (MWDG), etc. These tubes can generate several hundreds of gigawatts of power and nearly a thousand joules of energy per pulse (see table 8.4 for some typical representative parameters) [22–24].

8.3.1 Relativistic MWTs

MWTs can deliver high power if the beam power is increased by increasing the beam current. Large beam currents can be obtained with the help of electron guns of high

perveance (see section 4.1). However, it becomes somewhat difficult to design electron guns of perveance $>2\times10^{-6}$ perv. Alternatively, in order to obtain high powers from MWTs the beam current can be increased by making the accelerating potential of the gun greater than 80 kV. In the gigawatt class of HPM-MWTs usually one may need 500–700 kV accelerating potential. Such an enhanced accelerating potential, however, renders $>c/2$ electron velocities, which in turn makes relativistic effects of relevance in HPM-MWTs whenever several megawatts need to be generated by them. HPM-MWTs with such high accelerating potentials are referred to as relativistic MWTs.

One of the advantages of relativistic MWTs is that they have large transverse dimensions. This can be appreciated with reference to a TWT. In the design of a TWT, the value of $\gamma a(\approx(\omega/v_0)a)$ is considered to be an important parameter, where $\gamma(\approx\omega/v_0)$ is the radial propagation constant of the RF supported by the slow-wave structure, a is the radius of the interaction structure of the device, and $v_0(=2\mid\eta\mid V_0^{1/2})$ is the DC electron velocity, V_0 being the beam voltage and η the charge-to-mass ratio of an electron. Therefore, a *relativistic TWT* operating with high values of V_0 and hence with high values of v_0 for an assigned value of $\gamma a(\approx(\omega/v_0)a)$ enjoys large values of a, that is, large transverse interaction structure dimensions, which allows a flow of large beam currents and also mitigates the problem of electric breakdown in the interaction region. An added advantage in a *relativistic TWT* is that velocity synchronization between the beam and RF waves is maintained even if the beam's kinetic energy is significantly reduced due to the transfer of energy from the beam to RF waves.

However, for a *relativistic TWT* (figure 8.13), the Pierce's growth parameter, which is inversely proportional $V_0^{1/3}$ [27, 28], decreases with the increase in V_0. Further, the axial electric field at a radial coordinate r in the slow-wave structure of the TWT for beam-wave interaction is a function of $\gamma r(\approx(\omega/v_0)r)$ and, in fact, it increases with γr, that is, it decreases with the increase in the value of $v_0(=2\mid\eta\mid V_0^{1/2})$ and hence that of V_0. Therefore, the reduction of the axial electric field with the increase in the value of V_0 poses difficulty in the development of a *relativistic TWT*. Moreover, the force on an electron due to electric fields diminishing due to the relativistic increase in mass with velocity of the electron, as V_0 is increased, adds to this difficulty. Furthermore, the advantage of large transverse dimensions of a *relativistic TWT* is associated with the risk of generating backward-wave modes in

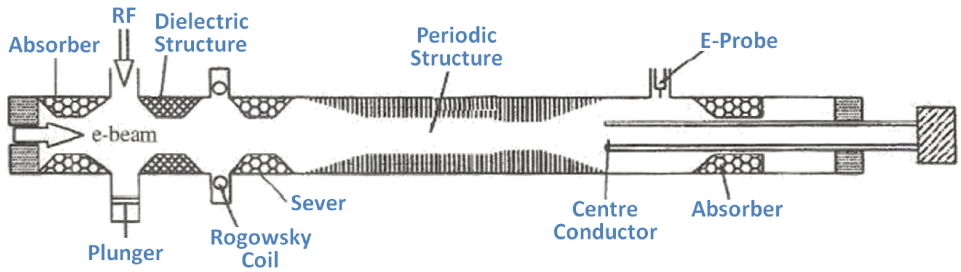

Figure 8.13. Schematic of a relativistic TWT showing two sections of amplifier stages with a break between them [29].

the structure. Also, the properties of the driving electron beams make the system break into oscillation [24].

Relativistic TWTs in the X band have been developed by Cornell University, delivering hundreds of megawatts of power with 45% efficiency, and by the Institute of Applied Physics (Nizhny Novgorod) collaborating with the University of New Mexico, delivering 1.1 GW of power with 45 dB gain. A typical *relativistic TWT* has been severed in two sections to prevent the device from oscillating due to the reflection caused by a mismatch at the output end and backward-wave modes generated (figure 8.13) [29].

The *relativistic BWO*, supposed to be the first true HPM source, was developed with the advent of IREB technology by the Lebedev Institute in Moscow and the Institute of Applied Physics in Nizhny Novgorod producing 10 ns, 400 MW pulses in the X band. The *relativistic BWO* with power raised to 500 MW was also developed about a year later by Cornell University [24]. In the 1980s *relativistic BWOs* were built delivering powers of 1 GW and 2 GW and above with accelerating voltages below and above 1 MV, respectively, with pulses of several tens of nanoseconds [24]. A typical Russian X-band *relativistic BWO* in a rippled-wall circular waveguide has used 500 kV, 10 kA electron beam derived from a cold cathode to produce 1 GW of power with 20% efficiency in 30 ns pulses while using a cryogenic magnetic field for focusing if a constant rather than pulsed magnetic flux density is used [30] (figure 8.14).

In a typical Indian *relativistic BWO* delivering 2 MW of power in the X band, a 230 keV, 2 kA, 150 ns duration electron beam was used. For this purpose, the beam was generated with the help of a Marx generator and injected into a rippled-wall circular waveguide excited in TM_{01} mode. The beam was confined by 1 T peak pulsed magnet of 1 ms duration using a solenoid coil through which current was sent by discharging a capacitor bank while ensuring that the electron beam is generated at the instant when the axial magnetic field attains its peak value [25].

The *RELTRON* is another member of the family of relativistic MWTs, which is basically a state-of-the-art variant of a relativistic klystron—a reliable, flexible, cost-effective, compact, high-power source (see section 6.2 for a conventional klystron).

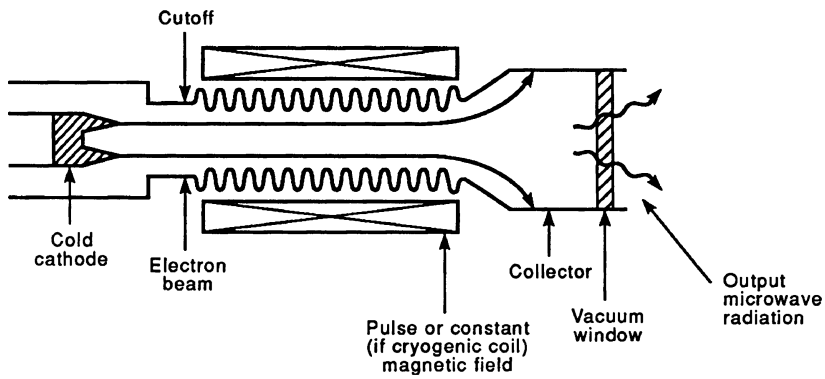

Figure 8.14. Schematic of a typical Russian relativistic BWO [30].

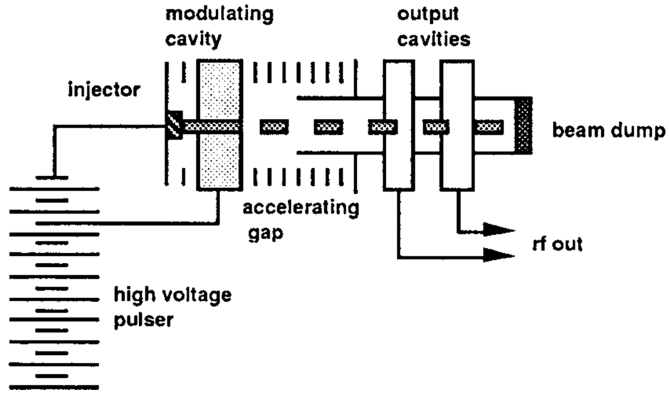

Figure 8.15. Schematic of a typical RELTRON [31].

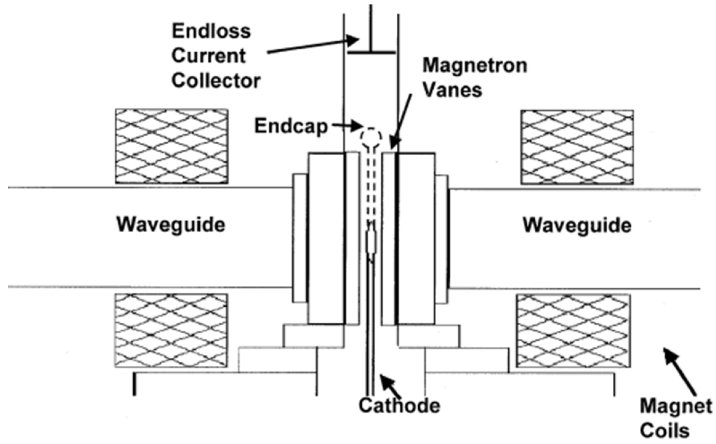

Figure 8.16. Cross section of a typical relativistic magnetron [38].

It enjoys advantages in terms of the powers per unit size and unit weight. The basic parts of a typical *RELTRON* are: a voltage injector to produce high current beam, modulating cavity, accelerating gap, low-Q output cavities and beam dump (figure 8.15). The device can provide straightforward output coupling to deliver power directly through the fundamental TE_{10} mode in a standard rectangular waveguide. The *RELTRON* requires no external magnetic field for high peak power while it requires small permanent magnets for high average powers. A typical device (figure 8.15) in the L band delivers 400–500 MW (rms) of power, 1 GW peak power driven by a 1.5 MV voltage pulse, hundreds of Joules of energy per pulse (with flat-top pulse duration of a few nanoseconds), >40% electronic efficiency, >15% frequency tuning. For this purpose, the beam parameters used are a 1.1 kA beam current, 800 kV beam injector voltage and 800 kV post-acceleration voltage.

The *relativistic magnetron* is yet another relativistic MWT (see section 6.4 for a conventional magnetron) which is relatively compact while being capable of delivering >100 MW power (figure 8.16). It is of interest to compare the parameters

of *relativistic magnetrons* with those of conventional magnetrons. Typically, in conventional and relativistic magnetrons the beam parameters are $\leqslant$100 kV and $\geqslant$500 kV, respectively; the cathode processes are thermionic/secondary and explosive emission types, respectively; the pulse durations are ~1 ms and ~100 ns, respectively; the output powers are $\leqslant$10 MW and ~1 GW, respectively; the efficiencies are 50% and ~20%–40%, respectively; and the tunable range ~5% and ~30%, respectively [22]. Further, despite enjoying the high-efficiency potential of an M-type tube (see chapter 2, volume 1), a *relativistic magnetron* is somewhat restricted with respect to efficiency, power, frequency and pulse duration as compared to a conventional magnetron. This restriction is caused by the deterioration of the anode surface of the device due to large beam power and microwave breakdown due to high intensity electric fields generated in the cavity.

In some initial experiments on *relativistic magnetrons* (figure 8.16) below 50 ns pulse duration, devices were developed delivering 1.7 GW power with 35% efficiency at 3 GHz [32]; 2 GW power with 40% efficiency at 2.3 GHz [33]; 4.5 GW power with 30% efficiency at 3.9 GHz [34]; 6.9 GW power with 30% efficiency at 4.5 GHz [35]; and so on [23]. In some experiments with higher pulse duration, devices were developed delivering 0.8 GW power with 30% efficiency at 2.4 GHz with 300 ns pulse duration [35]; 90 MW power with 12% efficiency at 4.1 GHz with 250 ns [36]; and so on. Furthermore, using a train of bursts of short pulses, peak power of 360 MW and average power of 0.5 kW with 3 GHz repetition rate in a 3-short burst experiment [37]; peak power of 1 GW and average power of 4.4 kW with 1.1 GHz repetition rate in a 50-short burst experiment; and so on [23].

In a typical *relativistic magnetron* (figure 8.16), the magnet coils encircle the cylindrical axis that runs along the cathode stalk [38] and if pulsed field coils are not used, then water-cooled or superconducting magnets need to be used, for instance, in repetitively fired operation at high average powers. The explosive emission cathodes (see section 3.1) may be built out of materials such as velvet covered by a stainless steel mesh, carbon fabric, stainless steel, etc, with due care in its design to maximize the ratio of radial to axial current flow with a view to reducing the axial electron flow that does not contribute to microwave generation [24]. The cathode end cap—with a rounded surface to reduce the electric field at the surface and coated with material such as glyptal that inhibits electron emission—is provided to reduce the axial end loss from the cathode. As a result the efficiency of the device increases [24].

Furthermore, the concept of a magnetron with diffraction output (MDO) has improved the performance of *relativistic magnetrons*. In the MDO, radiation is extracted axially along the vanes of the anode block which are tapered and extended to the inside of a conical horn antenna [39]. The MDO has made a r*elativistic magnetron* much more immune to microwave breakdown while multi-gigawatts of radiated output. The MDO also makes the device require a smaller volume for the magnetic field compared with a device with Helmholtz coils. The concept allows any eigenmode of MDO to be chosen as the operating mode. It can also function as a mode converter by extending only those vanes to the horn antenna that correspond to the symmetry of the desired radiated wave mode pattern [24, 40].

8.3.2 Some other high power Cerenkov tubes

Cerenkov HPM sources have produced several gigawatts of power at frequencies ranging from one to ten GHz in pulse durations ranging from tens of seconds to a few hundreds of nanoseconds (tables 8.4 and 8.5). Some high power Cerenkov devices, other than the relativistic TWT and BWO discussed earlier, are: the SWO, RDG or orotron, MWCG and MWDG (mentioned in the beginning of this section following figure 8.12).

The operating points of the BWO, TWT, RDG or orotron and SWO can be represented as the points of intersection between the ω versus axial propagation constant k_z dispersion characteristics of the rippled-wall waveguide/grating slow-wave structures (SWSs) and the beam-mode dispersion lines of these devices of different slopes corresponding to the different beam velocities (figure 8.17).

The *SWO* operates at the upper-edge frequency of the lowest order mode, located at point 4 of the intersection between the dispersion curve of the SWS and the beam-mode line of slope v_{z3} (figure 8.17). At operating point 4 of the *SWO*, the slope of the dispersion curve, that is, the group velocity $\partial w/\partial k_z = v_g \cong 0$ and $k_z = h_0/2 = \pi/z_0$, where $h_0 = 2\pi/z_0$, z_0 is the axial periodicity of waveguide ripples (figure 8.16). The ripple amplitude of the SWS is required to be made sufficiently large to depress the peak of the lowest dispersion curve below the light line or c-line in order to achieve SWO operation [22]. The device power can be increased by increasing the diameter D relative to the wavelength λ of the rippled waveguide thereby increasing the size of the device. However, a compromise would be to operate the device at a reduced voltage which would in turn reduce the size of the pulsed power. Using this approach, a typical *SWO* has delivered ~1 GW of power with a voltage of 500 kV at 8.3 GHz with $D = 9.8$ cm (corresponding to $D/\lambda \sim 2.7$) [22, 41].

The *RDG or orotron* operates at the lower-edge frequency of a higher order mode, and at a higher frequency ω as well as at a higher phase propagation constant k_z than SWO, located at point 3 of the intersection between the dispersion curve of the SWS and the beam-mode line of slope v_{z2} (figure 8.17). At operating point 3 of the *RDG or orotron*, the slope of the dispersion curve, that is, the group velocity $\partial w/\partial k_z = v_g \cong 0$ and $k_z = h_0 = 2\pi/z_0$ (figure 8.17). A sheet beam transports through a pair of mirrors one of which has a planar grating surface while the other has a curved surface (figure 8.18). The pair of mirrors forms an open resonator. The sheet beam is close to the grating-surface plane mirror. Radiation takes place perpendicular to the axis in view of the operation of the device corresponding to $v_g \cong 0$ at the operating point 3 (figure 8.17). The output of the device is taken through a hole on the curved-surface mirror (figure 8.18). The *RDG or orotron* is capable of delivering ~4.5 GW of power at 13–60 GHz with 10%–20% efficiency (table 8.5). The typical *RDG or orotron* output parameters of 100 MW power at 8.6 mm wavelength with 10% efficiency and 50 MW power at 5.5 mm wavelength with 5% efficiency have also been reported. Further specifications of the *RDG or orotron* in a two-section configuration are: 3.5 GW of power at 46 GHz and 1 GW of power at 60 GHz RDG [24, 42].

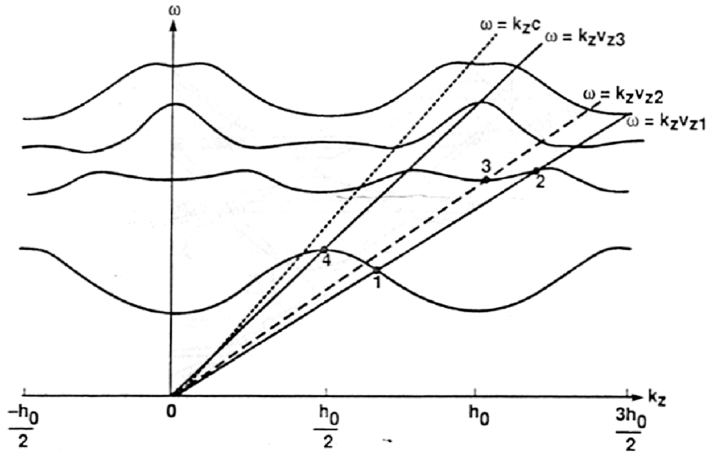

Figure 8.17. Dispersion (ω versus axial propagation constant k_z) characteristics indicating the operating points 1, 2, 3 and 4 of the BWO, TWT, RDG or orotron and SWO, respectively. The typical beam-mode lines with increasing slopes correspond to the beam velocities $v_{z3} > v_{z2} > v_{z1}$. The dotted line represents the c-line [22].

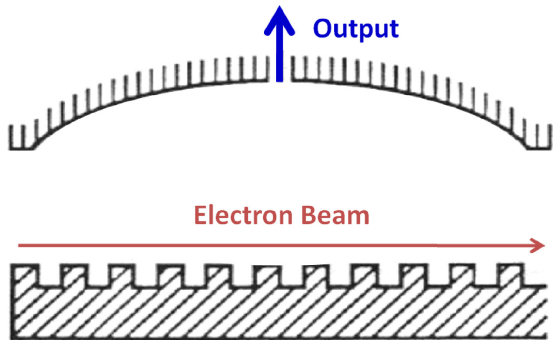

Figure 8.18. Schematic of the RDG or orotron [23].

The *MWCG* is a high power, over-sized ($D/\lambda \gg 1$), which makes it an over-moded device. It is a multi-wave device in the sense that the interaction structure of the device supports several normal modes oscillating at the same frequency. Sectioning or severing of the SWS aids in the mode selection in the device. In a three-section tube, the first and the third sections have identical corrugation geometry and periodicity each operating as the the SWS of a SWO. The second section is a drift section which, however, unlike the drift region of a klystron, is operated above the waveguide cutoff thereby allowing radiation to flow between the first and the third sections. Moreover, the drift section allows feedback between these two sections thereby helping the output mode of the device to stabilize. *MWCGs* are capable of delivering ~15 GW of power at 10–35 GHz with 48% efficiency (table 8.5) [24, 43]. The output parameters of the *MWCG* depend on the size of the interaction structure as well. Thus, it has delivered output power 3–5 GW

at 9.4 GHz with $D/\lambda \cong 5$ and 1.5 GW at 35 GHz with $D/\lambda \cong 13$ [22, 44], and 15 GW of power with 50% efficiency in the X-band and 3 GW of power with 20% efficiency in the Ka band [45]. 3 GW of power at 31 GHz from an MWCG operating in a super-radiant TWT-like mode has also been reported [22, 44].

The *MWDG*, like MWCG, is a multi-wave device and has three sections. Its first section operates as the SWS of the BWO; its second section operates as the drift section above cutoff as in the MWCG; and its third section operates as the RDG or orotron. Moreover, its first and the third sections have different corrugation geometries and periodicities. The MWDG has delivered 0.5–1 GW at 17 GHz in an MWDG [24, 46].

8.3.3 Vircator—bremsstrahlung radiation HPM tube

Previously, we discussed fast-wave high power MWTs, which are essentially based on bremsstrahlung in the magnetic field (chapter 7, volume 2), such as the gyrotron (section 7.2), gyro-BWO (section 7.3), gyro-klystron (section 7.4), gyro-TWT (section 7.5), CARM (section 7.6), etc. Let us now examine a high power tube, namely, a *vircator* (figure 8.19) in the class of HPM-MWTs based on bremsstrahlung radiation in an electrostatic field realized in a waveguide resonator, instead of choosing to describe it under the category of relativistic MWTs described earlier, even though it involves relativistic electrons. It is a simple, low-cost, single-shot device. The device can operate with somewhat low requirements of quality electron beams and with lower operating voltages. It requires no external magnetic field and enjoys frequency tunability controlled by the space-charge density. However, there are some problems, too. For instance, the device is very sensitive to the problem of gap closure causing an increase in the diode current and consequent shifting of the frequency upward, thereby upsetting the cavity resonance together with a drop in the output power [24].

The phenomenon of the formation of the virtual cathode that restricts the transport of high beam currents due to the potential depression caused by the negative space-charge in a conventional tube is taken as a phenomenon of advantage in a *vircator*. It follows from (3.23) and (3.27) (chapter 3, volume 1) that the space-charge-limiting current of a tube could be increased by placing the electron beam closer to its metal surrounding in the interaction structure of the tube. In contrast to this, in a *vircator*, in order to enhance potential depression and reduce the space-charge limiting current, the beam is placed far from the metal surrounding that would favor the formation of a virtual cathode. In the device the electrons of the beam, which are emitted typically by an explosive field-emission graphite cathode, oscillate back and forth in a microwave cavity while passing through an anode made of thin aluminium or titanium foil (figure 8.19(a)) or alternatively through a thick metal anode with large holes (figure 8.19(b)). The virtual cathode oscillation takes place at approximately the relative plasma frequency f_p, which may be written with the proper interpretation of (3.6) (given in chapter 3, volume 1) as

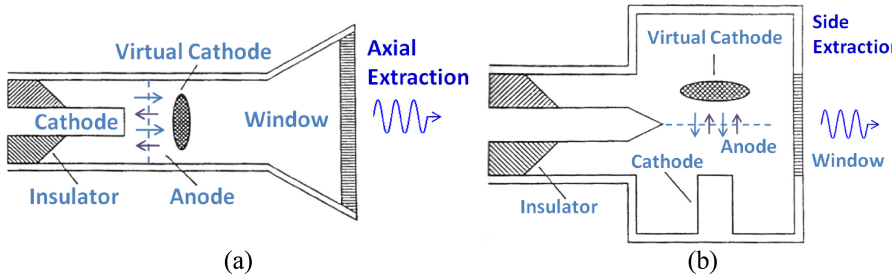

Figure 8.19. Schematic of a vircator in (a) axial and (b) transverse extraction configurations in basic reflex triode geometry [23, 24, 47].

$$f_p = \frac{1}{2\pi}\left(\frac{n|e|^2}{\varepsilon_0 m\gamma}\right) = 8.98 \times 10^3\left(\frac{n(\mathrm{cm}^{-3})}{\gamma}\right)\mathrm{Hz} = 4.10\left(\frac{J(\mathrm{kA/cm}^2)}{\beta\gamma}\right)\mathrm{GHz}$$

with $v_b/c = (1-1/\gamma^2)^{1/2}$, n being the electron number density of electrons in the beam, γ being the relativistic mass factor of the electron with velocity v_b, and e and m being the charge and non-relativistic mass of an electron, respectively [24].

Power can be fed to the device through the centre conductor of a transmission line attached to either the cathode (figure 8.19(a)) or the anode (figure 8.19(b)). The cavity is held at the anode potential. The frequency of the oscillating electrons tuned to a cavity mode defines the frequency of microwave bremsstrahlung radiation. Power can be taken out of the device through either of the axial (figure 8.19(a)) TM-mode extraction and transverse (figure 8.19(b)) TE-mode extraction. The *vircator* provided with an additional electrode is known as the triode *vircator* or reflex triode. In the typical configuration of the Barkhausen–Kurtz oscillator [23, 48], the device provides an additional electrode, taking the role of an anode, kept at a potential close or equal to the cathode potential, and a foil, taking the role of a triode grid placed between, and kept at a potential higher than the potentials of the cathode and the anode. Electrons reflected from the additional electrode of the reflex triode oscillate (reflexing back and forth) around the middle grid-foil in the same manner as in the diode vircator causing bremsstrahlung radiation [23, 24].

Vircator experiments demonstrated GW power levels at a frequency range covering hundreds of MHz to approximately 20 GHz with tens of nanoseconds of pulse duration in single shots, though with somewhat lower efficiencies less than a few percent [49]. Several gigawatts of power with 0.3% efficiency have been obtained with 6.5 MV, 0.3 MA beam pulses with pulse duration of 100–200 ns [23, 50]. In other experiments with low voltage (<100 kV), long pulse (600 ns) operation, 87 MW power could be delivered by the triode version (reflex triode) with 46% efficiency at 2–3 GHz frequency range, while in experiments with 250 keV beam, power could be enhanced to 550 MW in the same frequency range with 37% efficiency [23, 51]. In general, the reflex oscillation frequency is different from the virtual cathode oscillation frequency. In order to enhance the device frequency, the transit time that determines the reflex oscillation frequency is lengthened using a *double-anode vircator* with a view to lengthening the transit time, thereby making the

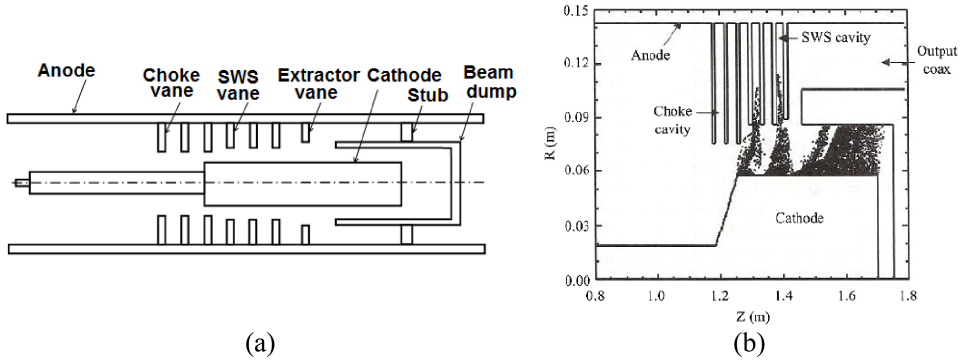

Figure 8.20. (a) Schematic of the MILO and (b) simulated electron spoke formation [24, 58].

reflex oscillation frequency equal to the virtual cathode oscillation frequency [24, 52]. Similarly, there are other related concepts such as the alleviation of the problem of competition between the virtual cathode and reflexing oscillations in a device called the *reditron*, which stands for 'reflected electron discrimination'. In a *reditron*, a thin annular beam emanating from an annular cathode and being guided by an external magnetic field is made to pass through a thin annular cutout in a thick anode block. The part of the beam that reflects from the virtual cathode expands radially and no longer passes through the annular slot and gets absorbed in the anode, thereby completely eliminating reflexing electrons and allowing only the virtual cathode oscillations to produce radiation [53–56]. There is yet another innovative configuration, namely, the *cavity vircator*, to combat the problem of the excitation of the waveguide modes due to the changes in the characteristics of the vircator due to variations in voltage or gap—out of a large number of modes present in the downstream region which is rather large in dimension compared to the wavelength. A mechanism in the *cavity vircator* by means of a cavity allows the field induced by the oscillating virtual cathode in the cavity to provide a feedback on the virtual cathode. As a result of this feedback, the oscillating electrons of the virtual cathode are forced to oscillate at the resonant frequency of the desired cavity mode [57].

8.3.4 MILO—M-type HPM tube requiring no external magnetic field

The *MILO*, invented in 1987 by Lemke and Clark [59], is a linear compact, lightweight, coaxial M-type GW-class HPM-MWT. The device accrues on one hand the advantage of very high current capacity of modern pulsed power systems and on the other hand the advantage of the property of very high power transmission lines (figure 8.20). The device uses a self-generated magnetic field to control electronic motion, removing the need for an external magnetic field and hence its power supply and cooling arrangement; it also allows designs with large cross-sectional areas [24, 60]. The intrinsic electron current generates the azimuthal magnetic field which prevents the electron flow from reaching the anode and thus providing self insulation before the phenomenon of oscillation could take place in the device. Further, this self insulation also prevents electrical breakdown of the anode-to-cathode gap of the

device. The device can operate at low impedances ~10 Ω, allowing for good impedance-match coupling to low-impedance pulsed-power sources such as explosive generators [24, 60]. Typically, in the L band, a power of 2 GW, pulse energies of ~1 kJ, and repetition rates as high as 100 Hz have been achieved though with somewhat lower efficiencies ~10%, due in part to challenges in extracting the output [24].

The basic parts of the *MILO* are: the cathode, the anode, the beam dump or collector, and the choke and the SWS cavities, each bounded by radial vanes of the same periodicity (figure 8.20). The inner diameters of the vanes of the choke cavities are kept the same. The SWS cavities, usually, three or more in number, are excited in the fundamental π-mode in which each cavity behaves as a quarter-wave oscillator shifted in phase by approximately π from the cavity adjacent to it. In these oscillations, maximum magnetic field exists at the cavity top while maximum electric field is close to the electron flow [24, 61]. The inner diameters of the vanes of the SWS cavities are kept the same except for the inner diameter of rightmost vane, at the output end, called the extractor vane, which is made somewhat larger in inner diameter than those of the rest. This helps the vane in functioning as a transition into the coaxial extractor section; the optimized design of which significantly improves the device efficiency (figure 8.20) [24]. The choke-vanes, which are somewhat deeper (with a smaller inner diameter) than the SWS-vanes, perform the function of reflecting RF waves back into the SWS-vane section thereby preventing these waves from propagating upstream into the pulsed power system. Moreover, the impedance mismatch between the choke-vane and SWS-vane sections creates a higher downstream current in the device [24]. Electrons, in the crossed electric and self-generated magnetic field, drifting parallel and adjacent to the cathode while at the same time moving towards the anode-come-SWS, form electron spokes (figure 8.20(b)) and transfer the potential energy of electrons to RF waves (see section 3.7 in chapter 3, volume 1 for the conservation of kinetic energy). In the device, either of the power extraction mechanisms can be used—radial extraction through resonator slots and the axial extraction down the transmission line. The magnetic cutoff for the optimized operation of the device is decided by the cathode-collector distance. In practice, the operating mode, for instance, the fundamental π-mode in the SWS comprising typically three or more cavities, needs to be converted to the radiating mode, for instance, the TE_{11} mode by introducing a mode converter between the MILO and the radiating antenna [60].

The efficiency of the MILO has been reportedly enhanced by innovative designs of its parts and improved mechanisms of power extraction [60]. For instance, some of these innovations with respect to the cathode design are: a tapered cathode shank in the choke-vane region with constant radius cathode over the entire length of the tube; improved cathode surface emission; reduction of the anode plasma formation by maximizing the emission uniformity in the launch point region of the cathode; repetitive operation using a graphite cathode; improved power extraction mechanisms were also explored such as the use of the plate-inserted mode converter and a coaxial horn, the use of a choke vane with tapered extraction region, etc. There is yet another innovation that can be found in *combined MILO-vircator* configurations

which allows independently controlled dual-frequency output at higher efficiencies; this is implemented by combining a MILO with a downstream vircator that adds to the conversion of electron energy in the downstream vircator [22, 24, 60, 62–66]. Some of the experimental outputs of MILOs are: 2.0 GW at 1.5 GHz (with 10% efficiency) (using 400 kV, 50 kA beam) [59]; 110 MW at 9.7 GHz (using 400 kV, 50 kA beam) [67]; and 3.1 GW at 1.755 GHz (with 10.4% efficiency) (using 550 kV, 54 kA beam) [67].

The tapered MILO came into being with the advent of an innovative tapering method of the SWS-vanes (figure 8.21) [61, 68]. The *tapered MILO* alleviates the problem of power extraction from the π-mode excited SWS cavity of a conventional MILO where the group velocity of RF waves is nearly nil. The cathode region of a *tapered MILO* consists of an upstream three-cavity driver section, excited in the π-mode with zero group velocity. The driver section of the cathode region, besides significantly contributing to electron emission being part of the cathode, performs the function of pre-bunching the electron flow and establishing the operating frequency. The cathode region also contains a gentle-taper vane section comprised of a set of MILO cavities tuned to increasingly high-mode frequencies. The amount of power that can be extracted along the axis can be increased by increasing the RF group velocity, which can be implemented by increasing the taper. However, too large an increase in the taper causes a rapid increase in the axial RF phase velocity, which in turn makes effective energy transfer from electrons to RF waves more difficult, conditions for phase focusing of electrons become less favorable and an increasingly large fraction of the electron flow is below the resonance threshold. The anode region of the device consists of a sharp-taper vane section (figure 8.21). The group velocity in the gentle and sharp taper sections is increased in order to facilitate the downstream propagation of microwave energy, however, taking due care not to increase it too quickly and deteriorate the coupling between the drifting electrons and the SWS. The anode region of the device also contains a coaxial output section

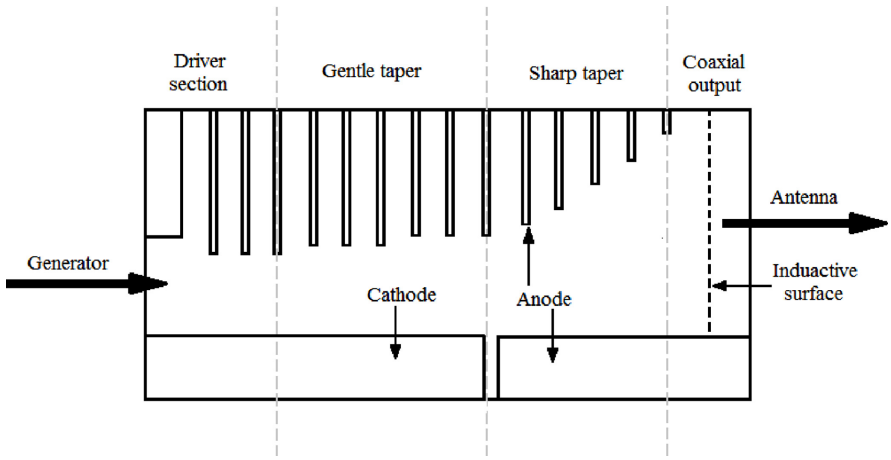

Figure 8.21. Schematic of a typical tapered MILO [24, 61].

in which the central conductor of the coaxial structure is attached to its outer conductor by an inductive surface (figure 8.21).

Closely related to HPM-MWTs is the flux compression generator (FCG) [24, 69]. FCGs can be used as single devices capable of delivering single shots ~10s of MJ of energy in ~10s–100s μs of time and ~TWs-to-tens of TW of peak power. They can be used in cascade, for instance, a smaller FCG priming a larger FCG to fulfill the requirement of the smallest possible start current sources to operate them in applications where space and weight is a bounden necessity. Further, FCGs produce high currents at low voltages with low impedances and thus are suitable for being coupled to and powering low-impedance HPM-MWTs such as the vircator and the MWCG.

The operation of an FCG is based on the transfer of energy from the explosive to the magnetic field. A typical FCG consists of an inner hollow armature tube filled in by an explosive, typically, machined PBX-9501, surrounded by a stator, which, in turn, is enclosed in a dielectric structural jacket. The helically wound wire, typically made of copper of the stator coil, is separated from the armature tube by an insulator block. The stator coil is connected to an external high voltage pulse power source, such as a Marx generator, to provide the start current producing an initial magnetic field in the coil. The explosive is initiated when the start current peaks and is accomplished with an explosive lens plane wave generator producing a uniform plane wave burn or detonation front in the explosive. Consequently, the armature tube distorts and expands into a conical shape to the full diameter of the stator coil thereby short-circuiting the armature tube and the stator coil and trapping the current within the device. With the progress of time, the short propagates and compresses the magnetic flux density and hence reduces the inductance of the stator coil and consequently enhances the stator current with time. As a result, an FCG produces a ramping current at the stator output ring which peaks before the device finally disintegrates [24, 67].

Further, FCGs have been used to construct the so-called *electromagnetic bomb* that is used to harm electronic circuitry in DEW/IW, the latter requiring ~1 GW of power at frequencies ~1 GHz in large pulse durations ~100 ns. The parts of a typical *electromagnetic bomb* are the power supply, the capacitor bank, the first-stage vircator, the second-stage vircator, the microwave antenna and the dielectric nosecone [24, 67].

References

[1] Song H J and Nagatsuma T (ed) 2015 *Handbook of Terahertz Technologies: Devices and Applications* (Singapore: Pan Stanford Publishing)

[2] Ives L, Kory C, Read M, Miram G and Booske J 2003 MEMS-based TWT development *Proc. 4th IEEE Int. Conf. on Vacuum Electronics*

[3] Kory C, Ives L, Read M, Booske J, Jiang H, van der Weide D and Phillip P 2005 Microfabricated W-band traveling wave tubes *Proc. Joint 30th Int. Conf. Infrared Millimeter Waves and 13th Int. Conf. Terahertz Electronics (IRMMW-THz)*

[4] Bower C, Zhou O, Zhu W, Ramirez A G, Kochanski G P and Jin S 2000 Fabrication and field emission properties of carbon nanotube cathodes *Amorphous and Nanostructured Carbon Proc. Mat. Res. Soc. Symp.* vol 593 p 215
[5] Srivastava A 2015 Microfabricated terahertz vacuum electron devices: technology, capabilities and performance overview *Europ. J. Adv. Eng. Tech.* **2** 54–64
[6] Barker R J, Luhmann N C, Booske J H and Nusinovich G S (ed) 2005 *Modern Microwave and Millimeter-wave Power Electronics* (Piscataway: Wiley-IEEE Press)
[7] Siegel P H, Fung A, Manohara H, Xu J and Chang B 2001 Nanoklystron: a monolithic tube approach to THz power generation *Proc. 12th Int. Sym. Space Terahertz Tech. (San Diego)* pp 81–90
[8] Read M E, Ives R L, Neilson J, Mizuhara M, Marsden D and Borchard P 2009 A THz gyrotron based on a pulse solenoid *Proc. IEEE Int. Vacuum Electronics Conf.* pp 519–20
[9] Nusinovich G S, Carmel Y, Antonsen T M, Goebel D M and Santoru J 1998 Recent progress in the development of plasma-filled traveling-wave tubes and backward-wave oscillators *IEEE Trans. Plasma Sci.* **26** 628–45
[10] Vavriv D M 2006 Potential of the clinotron for THz-generation *AIP Conf. Proc.* vol 807, pp 367–72
[11] Goebel D M, Carmel Y and Nusinovich G S 1999 Advances in plasma-filled microwave sources *Phys. Plasmas* **6** 2225–32
[12] Santoru J, Butler J, Goebel D M and Schumacher R W 1994 High power single beam plasma wave tube *IEEE Trans. Plasma Sci.* **22** 593–9
[13] Butler J M *et al* 1992 PASOTRON high-energy microwave source *IEEE MTT-S Int. Microwave Symp. Dig.*
[14] Goebel D M, Adler E A, Ponti E S, Feicht J, Eisenhart R and Lemke R W 1999 Efficiency enhancement in high power microwave oscillators *IEEE Trans. Plasma Sci.* **27** 800–8
[15] Shkvarunets A G, Rodgers J, Carmel Y and Nusinovich G S 2006 Long-pulse operation of a megawatt-class plasma-assisted slow-wave oscillator *Appl. Phys. Lett.* **89** 103503
[16] Goebel D M, Ponti E S, Feicht J R and Watkins R M 1996 Pasotron high-power microwave source performance *Proc. SPIE* **2843** 69–78
[17] Schumacher R W, Hyman J Jr, Harvey R and Santoru J 1990 Plasma-assisted high-power microwave generator *US Patent* No. US4912367 A (Hughes Aircraft Company)
[18] Zavjalov M A, Mitin L A, Perevodchicov V I, Tskhai V N and Shapiro A L 1994 Powerful wideband amplifier based on hybrid plasma-cavity slow-wave structure *IEEE Trans. Plasma Sci.* **22** 600–7
[19] Thumm M 2017 State-of-the-art of high power gyro-devices and free electron masers update 2016 *KIT Scientific Reports* 7735
[20] Kirkpatrick D A, Gold S H, Manheimer W M, Black W M and C 1990 Measurement of plasma-neutralized super-vacuum currents in a gyrotron configuration *Appl. Phys. Lett.* **57** 437–9
[21] Kirkpatrick D A, Gold S H, Ting A C, Manheimer A K, Kinkead A K, Hardesty D L, Killian K W and Sucy M 1990 Microwave measurements from a gyrotron operating with a neutralizing background plasma *IEEE Conf. Record Int. Conf. Plasma Sci.* p 2P3-19
[22] Benford J and Swegle J A 1991 *High Power Microwaves* (Boston: Artech House)
[23] Gaponov-Grekhov A V and Granatstein V L (ed) 1994 *Applications of High-Power Microwaves* (Boston: Artech House)

[24] Benford J, Swegle J A and Schamiloglu E 2015 *High Power Microwaves* 3rd edn (New York: CRC Press)
[25] Choyal Y, Gupta L, Vyas P, Deshpande P, Chaturvedi A, Mittal K C and Maheshwari K P 2005 Development of a 300-kV Marx generator and its application to drive a relativistic electron beam *Sadhana* **30** 757–64
[26] Sharma A *et al* 2012 Marx generator and reflex triode based high power pulsed microwave source *BARC News Lette* pp 37–42
[27] Basu B N 1996 *Electromagnetic Theory and Applications in Beam-wave Electronics* (Singapore: World Scientific)
[28] Pierce J R 1950 *Traveling-wave Tubes* (New York: D Van Nostrand)
[29] Wang P, Xu Z, Nation J A, Banna S and Schachter L 2000 Symmetric and asymmetric mode interaction in high-power traveling wave amplifiers: experiments and theory *IEEE Trans. Plasma Sci.* **28** 2262–71
[30] Bykov N M *et al* 1990 Relativistic periodically-pulsed microwave oscillators *Proc. 8th IEEE Int. Conf. High-Power Particle Beams* pp 1141–6
[31] Miller R B, McCullough W F, Lancaster K T and Muehlenweg C A 1992 Super-reltron theory and experiments *IEEE Trans. Plasma Sci.* **20** 332–43
[32] Bekefi G and Orzechowski T J 1976 Giant microwave bursts emitted from a field-emission, relativistic-electron-beam magnetron *Phy. Rev. Lett* **37** 379–82
[33] Didenko A N, Sulakshin A S, Fomenko G P, Shtein Y G and Yushkov Y G 1978 Intense microwave emission from a relativistic magnetron *Sov. Tech. Phys. Lett.* **4** 3–4
[34] Craig G, Pettibone J and Ensley D 1979 A symmetrically loaded relativistic magnetron *Conf. Record IEEE Int. Conf. Plasma Sci. (Montreal, Canada)* p 44
[35] Didenko A N, Sulakshin A S, Fomenko G P, Tsvetkov V I, Shtein I G and Iushkov I G 1978 Relativistic magnetron with microsecond pulse lengths *Pis'ma Zh. Tekh. Fiz.* **4** 823–6; 1978 *Sov. Tech. Phys. Lett.* **4** 331–2
[36] Treado T A, Smith R S, Shaughnessy C S and Thomas G E 1990 Temporal study of long-pulse relativistic magnetron operation *IEEE Trans. Plasma Sci.* **16** 594–602
[37] Vasil'ev V V, Vintizenko I I, Didenko A N, Lukonin E I and Sulakshin A S 1987 A relativistic magnetron operating in the pulse train mode *Pis'ma Zh. Tekh. Fiz* **13** 762–6
[38] Lopez M R *et al* 2002 Cathode effects on a relativistic magnetron driven by a microsecond e-beam accelerator *IEEE Trans. Plasma Sci.* **30** 947–55
[39] Didenko A N *et al* 1979 Generation of high power RF-pulses in magnetron and reflex triode systems *Proc. 3rd Int. Topical Conf. High Power Electron Ion Beam Res. Tech. (*Novosibirsk, Soviet Union) vol 2, pp 683–91
[40] Fuks M I and Schamiloglu E 2002 Relativistic magnetron with diffraction antenna *AIP Conf. Proc.* vol 625 p 169
[41] Vlasov A N *et al* 2000 Overmoded GW-class surface-wave microwave oscillator *IEEE Trans. Plasma Sci* **28** 550–60
[42] Bugaev S P, Cherepenin V A, Kanavets V I, Koshelev V I, Popov V A and Vlasov A N 1990 Investigation of a millimeter-wavelength-range relativistic diffraction generator *IEEE Trans. Plasma Sci.* **18** 518–24
[43] Bugaev S P, Kanavets V I, Klimov A I, Koshelev V I and Cherepenin V A 1987 Interaction of an electron beam and an electromagnetic field in a multiwave 1010 W Cherenkov generator *Radiotehk. Elektron.* **32** 1488–98; 1987 *Sov. J. Commun. Tech. Electron.* **32** 79–89

[44] Bugaev S P, Kanavets V I, Koshelev V I, Popov V A, Slepkov A I, Fedorov A V and Cherepenin V A 1989 Investigation of a multiwave Cerenkov millimeter-wave oscillator producing gigawatt power levels *Radiotekh. Elektron.* 400; 1989 *Sov. J. Commun. Tech. Electron.* **34** 119

[45] Bugaev S P, V Cherepenin V A, Kanavets V I, Klimov A I and Kopenkin A D 1990 Relativistic multiwave Cerenkov generators *IEEE Trans. Plasma Sci.* **18** 525–36

[46] Bugaev S P, Kanavets V I, Klimov A I, Koshelev V I and Cherepenin V A 1983 Relativistic multiwave Cerenkov generators *Pis'ma Zh. Tekh. Fiz.* **9** 1385–9; 1983 *Sov. Tech. Phys. Lett.* **9** 596–7

[47] Kopp C 1996 *Electromagnetic Bomb–A Weapon of Electromagnetic Mass Destruction* (Clayton, Australia: Monash University)

[48] Barkhausen H and Kurtz K 1929 The shortest waves that can be produced in vacuum tubes *Phys. Zs* **21** 1–6 in German

[49] Thode L E 1987 Virtual cathode microwave device research: Experiment and simulation *High-Power Microwave Sources* ed V L Granatstein and I Alexeff (Boston and London: Artech House)

[50] Huttlin G A *et al* 1990 The reflex-diode HPM source on Aurora *IEEE Trans. Plasma Sci.* **18** 618–25

[51] Didenko A N, Zherlitsyn A G, Sulakshin A S, Fomenko G P, Tsvetkov V I and Shtein I G 1983 Intense microwave emission by a high-current microsecond electron beam in a triode system *Pis'ma Zh. Tekh. Fiz.* **9** 1510–3; 1983 *Soviet Tech. Phys. Lett.* **9** 647–8

[52] Pincosy P, Morrison J and Poulsen P 1991 Progress toward steady-state, high-efficiency vircators *Proc. SPIE* **1407** 172

[53] Kwan T J T, Davis H A, Fulton R D and Sherwood E G 1988 Theoretical and experimental investigation of reditrons *Proc. SPIE* **0873**

[54] Davis H A, Bartsch R R, Thode L E, Sherwood E G and Stringfield R M 1985 High-power microwave generation from a virtual cathode device *Phys. Rev. Lett.* **55** 2293

[55] Davis H A, Bartsch R R, Kwan T J T, Sherwood E G and Stringfield R M 1988 Experimental confirmation of the reditron concept *IEEE Trans. Plasma Sci.* **16** 192–8

[56] Davis H A, R Fulton R D, Sherwood E G and Kwan T J T 1990 Enhanced-efficiency, narrow-band gigawatt microwave output of the reditron oscillator *IEEE Trans. Plasma Sci.* **183** 611–7

[57] Benford J, Price D, Sze H and Bromley D 1987 Interaction of a vircator microwave generator with an enclosing resonant cavity *J. Appl. Phys.* **61** 2098–100

[58] Haworth M D *et al* 1998 Significant pulse-lengthening in a multi gigawatt magnetically insulated transmission line oscillator *IEEE Trans. Plasma Sci.* **26** 312–9

[59] Clark M C and Lemke R W 1987 Theory and simulation of high power microwave generation in magnetically insulated transmission line oscillator *J. Appl. Phys.* **62** 3436–40

[60] Nallasamy V, Datta S K, Reddy S U M and Jain P K 2017 Advances and present trends in magnetically insulated line oscillator *J. Electromagn. Waves Appl* **31** 1864–74

[61] Eastwood J W, Hakins K C and Hook M P 1998 The tapered MILO *IEEE Trans. Plasma Sci.* **26** 698–713

[62] Haworth M D, Luginsland J W and Lemke R W 2001 Improved cathode design for long pulse MILO operation *IEEE Trans. Plasma Sci.* **29** 388–92

[63] Haworth M D *et al* 1997 Recent progress in the hard-tube MILO experiment *Proc. SPIE* **3158** 28–39

[64] Ju J C, Fan Y W, Zhong H H and Shu T 2009 An improved X-band magnetically insulated transmission line oscillator *Phys. Plasmas* **16** 073103
[65] Fan Y W, Zhong H H, Li Z Q, Shu T, Yang H W, Zhou H, Yuan C W, Zhou W H and Luo L 2008 Repetition rate operation of an improved magnetically insulated transmission line oscillator *Phys. Plasmas* **15** 083102
[66] Fan Y W, Yuan C W, Zhong H H, Shu T, Zhang J D, Yang J H, Yang H W, Wong Y and Luo L 2007 Experimental investigation of an improved MILO *IEEE Trans. Plasma Sci.* **35** 1075–80
[67] Fan Y W, Zhong H H, Shu T and Li Z Q 2008 Investigation of an X-band magnetically insulated transmission line oscillator *Chin. Phys.* B **17** 1804–8
[68] Li Z Q, Zhong H H, Fan Y W, Shu T, Qian B L, Xu L R and Zhao Y S 2009 Investigation of an S-band tapered magnetically insulated transmission line oscillator *Chin. Phys. Lett.* **26** 055201
[69] Chung B H 2009 RF & microwave tubes (high power klystron) 40th Anniversary Korean Nuclear Soc. and Spring Meeting (Jeju, Korea, 18–23 May, 2009)

IOP Concise Physics

High Power Microwave Tubes: Basics and Trends

Volume 2

Vishal Kesari and B N Basu

Chapter 9

Frequency and power ranges of common microwave tubes

We have listed the designated frequency ranges of the electromagnetic spectrum for various applications in table 9.1.

With reference to microwave tubes (MWTs) we encounter different terminologies related to their powers: continuous-wave (CW) power, peak power and average power. Thus, the average power of CW radar, which operates continuously in CW mode, can be easily figured out. However, for a pulsed system like pulsed radar, in which the transmitter is switched on and off in pulsed mode and the radar echo is detected during the interval between successive pulses, the average power P_{average} can be calculated by dividing the amount of energy content of a pulse by the duration of a pulse cycle:

$$P_{\text{average}} = \frac{\text{energy content of a pulse}}{\text{duration of a pulse cycle}}. \tag{9.1}$$

Since the energy of a pulse is equal to the product of the peak power P_{peak} and the time of pulse duration τ, and the duration of a pulse cycle (T) is equal to the reciprocal of pulse repetition frequency (that is, $T = 1/\text{prf}$), we can express (9.1) as

$$P_{\text{average}} = \frac{P_{\text{peak}}\tau}{T} = \frac{P_{\text{peak}}\tau}{1/\text{prf}} = \left(P_{\text{peak}}\right)(\tau)(\text{prf}). \tag{9.2}$$

The relation (9.2) between P_{average} and P_{peak} of a pulsed system may be alternatively expressed in terms of the duty cycle, which is the fraction of time during which the system is in an active or operating state, given by:

$$\text{duty cycle} = (\tau)(\text{prf}) = (\tau/\text{T}). \tag{9.3}$$

doi:10.1088/978-1-6817-4704-0ch9

Table 9.1. Designation of frequency ranges/bands.

Frequency ranges/bands (MHz/kHz/GHz)	Terminology
Radio waves: 3 kHz–3 GHz **Microwaves:** 3–300 GHz **ISM band**: 6.765–6.795 MHz; 13.553–13.567 MHz; 26.957–27.283 MHz; 40.66–40.7 MHz; 433.05–434.79 MHz; 902–928 MHz; 2.4–2.5 GHz; 5.725–5.875 GHz, 24–24.25 GHz **ELF:** <3 kHz; VLF: 3–30 kHz; **LF:** 30–300 kHz; **MF:** 0.3–3 MHz; HF: 3–30 MHz (short radio wave); **VHF:** 30–300 MHz (FM radio, TV); **UHF:** 300–3000 MHz (TV, mobile phone, GPS); **SHF:** 3–30 GHz (radar); EHF: 30–300 GHz (millimetre-wave); Terahertz: 300–3000 GHz (sensing and imaging) **L:** 1.12–1.70 GHz; **S:** 2.60–3.95 GHz; **C:** 3.95–5.85 GHz; **X:** 8.20–12.40 GHz; **Ku:** 12.40–18.00 GHz; **K:** 18.00–26.50 GHz; **Ka:** 26.50–40.00 GHz; **V:** 40.00–60.00 GHz; **E:** 60.00–90.00 GHz; **F:** 90.00–140.00 GHz; **W:** 75–110 GHz (satellite communications, targeting, tracking, active denial system)	ISM: industrial, scientific and medical ELF: extremely low frequency VLF: very low frequency LF: low frequency VHF: very high frequency UHF: ultra high frequency SHF: super high frequency

Substituting (9.3) in (9.2) we then get

$$P_{\text{average}} = \left(P_{\text{peak}}\right)(\text{duty cycle}). \tag{9.4}$$

Obviously, in the limit $\tau \to T$ amounting to duty cycle $= (\tau/T) \to 1$ in (9.3), for a CW system, the peak and the average powers, as can be seen from (9.4), become one and the same: $P_{\text{average}} = P_{\text{peak}}$. Thus, typically, a C-band 60 W (CW) TWT gives a 60 W peak as well as 60 W average power. However, the duty cycle needs to be specified in (9.4) to determine the average power capability of a C-band 50 kW pulsed CCTWT for which $P_{\text{peak}} = 50$ kW.

Pulsed MWTs are extensively used in pulse radars for military applications. Major applications include target detection, target recognition in surveillance radars, weapon control in fire-control radars, weapon guidance in missile systems, identifying enemy locations using imaging radars etc. Pulsed MWTs also find applications in other pulsed radars for air traffic control, weather observation (precipitation radar), satellite-based remote sensing, etc. The applications of CW MWTs are in unmodulated CW radars for traffic control, speed gauges, Doppler motion sensors, motion monitoring, etc, and also in frequency-modulated-continuous-wave (FMCW) radars for imaging and non-imaging applications, such as high-resolution imaging, navigation, radar altimeter, aircraft radio altimeter, etc. Similarly, in satellite communication, we can use CW TWTs for multi-carrier communication downlinks and pulsed TWTs for remote sensing and imaging. For deep-space applications, we use pulsed

tubes for imaging and both CW and pulsed tubes for the transfer of data to Earth through telemetry. In electronic warfare (EW) systems, while for electronic counter counter measure (ECCM) a pulsed TWT can be used, we can—in order to implement deceptive anti-jamming by mimicking a radar echo in an electronic support measure (ESM) system—use the same TWT to operate in both CW and pulsed modes depending on the threat scenario.

A pulsed TWT is constructed with a provision to modulate the electron beam using the gun electrode: beam focusing electrode (BFE)/grid/intermediate anode. Also, in some high power MWTs, pulsed power is obtained by providing pulsed cathode voltage with respect to the anode, which is kept at the ground potential. A CW-TWT can be operated in pulsed mode by applying pulsed RF input to the TWT for space and EW systems. Further, during the tube development stage at the manufacturer's end, a CW-TWT, following vacuum processing, is usually subjected to cathode voltage pulsing using an external modulator for initial testing.

The attainable maximum power decreases with the operating frequency such that the product of the power and frequency raised to an index of power remains constant; the index varying roughly between 1 and 5 depending on factors such as thermal dissipation, RF loss, CW or pulsed operating conditions, etc [1, 2–6]. It is of interest to note the power capabilities of typical MWTs in different frequency regimes in general (figure 9.1) and TWTs in particular (table 9.2).

It is also of interest to note the operating frequencies and output powers of typical high power MWTs: the multi-cavity klystron, multi-beam klystron (MBK), relativistic klystron (RELTRON), magnetron, and magnetically insulated line oscillator (MILO) (table 9.3).

The power capabilities vis-à-vis operating frequencies of typical gyrotrons should also be noted (table 9.4).

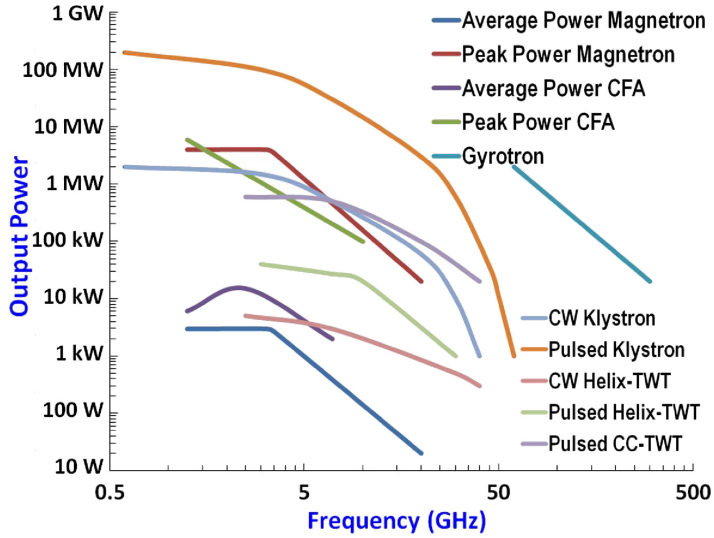

Figure 9.1. Output powers of some MWTs in different frequency regimes [7].

Table 9.2. Power capabilities of typical travelling-wave tubes [8].

TWT	Manufacturer	Band	Power (W)
Satellite communication (ground-station)	Thales	Ku	750
	CPI	Ku	1200 (Peak)/600 (CW)
	Teledyne	C/X/Ku	350/600/350
	NEC	Ka	350 (Peak)/250 (CW)
Satellite communication (space)	L-3	K	50 to 130
	Thales	Ku	100 to 150
	CPI	S	130 k, 8% duty cycle
Radar	e2V	X	20 k, 8% duty cycle
	Thales	Ka	1 k, 12% duty cycle
	L-3	4.5–18 GHz	110
EW	e2V	4.5–18 GHz	100
	Thales	6–16 GHz	1500
		4.5–18 GHz	200
mm-wave CW radar and EW	Hughes (now L-3)	59.7–60.3 GHz	50
mm-wave CW communication (space-type)	Hughes (now L-3)	84–86 GHz	200
mm-wave CW ground terminal	Hughes (now L-3)	91–96 GHz	100

Table 9.3. Power capabilities of typical high power MWTs [3–6].

Device (manufacturer/ developer)	f (GHz)	P_{peak} (MW)	τ (ms/μs/ns)	prf (Hz/single-shot)
Klystron (CPI)	2.998	150	3 μs	60
Klystron (multi-beam) (Thompson CSF)	1.3	10	1.5 ms	10
RELTRON (Titan)	2.85	25	2 μs	10
Magnetron (CPI VMS)	2.845	50	600 ns	10
MILO (AFRL)	1.2	300	600 ns	Single-shot

For the state-of-the gyrotron one can see exhaustive reports prepared and updated by Manfred Thumm from time to time, including the 2016 update on state-of-the-art high power gyro-devices and free electron masers [9]. One can collect

Table 9.4. Power capabilities of typical gyrotrons [9].

Type	Power	Frequency	Efficiency
Conventional pulsed power	340 kW	Ka-Band	
	1.1 MW	100 GHz	
	645 kW	140 GHz	
Conventional short-pulse gyrotrons (<10 ms)	2.1 MW	100 GHz	30%
	1.2 MW		
	1.2 MW	231 GHz	20%
Conventional CW power	200 kW	28–60 GHz	
	100 kW	140 GHz	
Conventional Quasi-CW (long-pulse)	1.05 MW	8 GHz	
	0.37 MW	110 GHz	
	10 kW	503 GHz	5.5%
Coaxial cavity ($TE_{20,13}$ mode)	2.1 MW	100 GHz	
QOG (quasi-optical)	1 kW CW	34 GHz (9% frequency tunability)	
	600 kW (pulse length: 0.013 ms)	120 GHz	9%
Relativistic (beam voltage: 3.3 MV, beam current: 80 kA)	1000 MW	8.35–13	0.4%
Commercial	200 kW	60 GHz	
	100 kW	140 GHz	

Table 9.5. Power capabilities of typical gyrotrons [9].

Manufacturer/developer	f (GHz)	P_{peak} (MW)	Pulse width (ms/s/min)	Efficiency (%)
CPI and European KIT-CRPP-TED collaboration	140	0.92	30 min	44
JAEA-TOSHIBA	110	1.5	4.0 s	45
ITER (Japan)	170	1.0	800 s	55
ITER (Russia)	170	1.0	1000 s	53
	170	1.75	0.1 s	50

Terminology: CPI: Communications and Power Industries; KIT: Karlsruhe Institute of Technology; CRPP: Centre de Recherche de Physique des Plasmas; TED: Thales Electron Devices; JAEA: Japan Atomic Energy Agency; ITER: International Thermonuclear Experimental Reactor

from [9] some typical data for the power, frequency, pulse width, and efficiency of gyrotrons from typical manufactures/developers of gyrotrons (table 9.5).

The power capabilities of some HPM tubes for radar, communication, EW and information warfare involving direct energy weapons (DEWs), which can generate

gigawatts with hundreds of J s^{-1} of energy per pulse, have already been enumerated (see table 8.5 in chapter 8, volume 2).

References

[1] Spangenberg K 1948 *Vacuum Tubes* (New York: McGraw Hill)

[2] Gilmour A S Jr 1986 *Microwave Tubes* (Norwood: Artech House)

[3] Benford J and Swegle J A 1991 *High Power Microwaves* (Boston: Artech House)

[4] Gaponov-Grekhov A V and Granatstein V L (ed) 1994 *Applications of High-Power Microwaves* (Boston: Artech House)

[5] Benford J, Swegle J A and Schamiloglu E 2015 *High Power Microwaves* 3rd edn (New York: CRC Press)

[6] Barker R J, Luhmann N C, Booske J H and Nusinovich G S (ed) 2005 *Modern Microwave and Millimeter-wave Power Electronics* (Piscataway: Wiley-IEEE Press)

[7] Chung B H 2009 RF & microwave tubes (high power klystron) 40th Anniversary Korean Nuclear Soc. and Spring Meeting (Jeju, Korea, 18–23 May, 2009)

[8] 1997 *Industrial Assessment of the Microwave Power Tube Industry* Department of Defence, National Technical Information Centre (Washington, DC, USA)

[9] Thumm M 2017 State-of-the-art of high power gyro-devices and free electron masers update 2016 *KIT Scientific Reports* 7735

IOP Concise Physics

High Power Microwave Tubes: Basics and Trends

Volume 2

Vishal Kesari and B N Basu

Chapter 10

Epilogue

Our aim in this monograph is to present an overview of microwave tubes (MWTs), which continue to be important despite competitive incursions from solid-state devices (SSDs). We have presented a broad and introductory survey which we hope readers will be encouraged to read, rather than going through lengthier tomes, and explore the field further.

We have appreciated that MWTs enjoy superiority over SSDs in terms of lesser heat generated due to collision in the bulk of the device, higher breakdown limit on the maximum electric field inside the device, smaller base-plate size determined by the cooling efficiency, higher peak pulsed-power operability and ultra-bandwidth performance above a GHz (chapter 1, volume 1). Moreover, MWTs that are fabricated out of metals and ceramics are inherently hardened against radiation and more capable than SSDs in withstanding temperature and mechanical extremes. Leaving aside the high power application areas of MWTs, there are applications where SSDs cannot yet substitute MWTs. For example, though attempts were made to replace space-qualified TWTs by SSDs, such attempts declined after noting that SSDs could not meet the required MTBF $\sim 5 \times 10^6$ h, as achieved by space TWTs (chapter 1, volume 1).

The development of MWTs has been intensified in view of their wide range of applications in civilian and military sectors (chapter 2, volume 1). MWTs find applications in military radar, electronic warfare (EW), missile guidance and tracking, and ADS—active denial system. High power microwave (HPM) tubes are used for directed energy weapons (DEWs) and information warfare (IW). Civilian radars employing MWTs are used for weather detection, avoidance of highway collisions and air-traffic control. They are also used in remote sensing, imaging in atmospheric and planetary science, space debris phased-array mapping, analysis of clouds, life detection systems to sense heart beats and breathing under earth-quake rubbles, and so on (chapter 2, volume 1). Some of the peaceful applications of MWTs are in material processing such as ceramic sintering and

doi:10.1088/978-1-6817-4704-0ch10

joining, and production of stronger and less brittle composite ceramics, which could be used to construct lightweight ceramic engines for aircraft and automobiles as well as strong, long-lasting ceramic walls for thermonuclear power reactors. Other applications of MWTs are in waste remediation, breaking of rock and concrete, tunnel boring, soil treatment and fusion plasma heating for controlled thermonuclear reactors, besides industrial heating covering paper, leather, textile, tea, etc. In the terahertz regime, applications include imaging, security inspection, enhanced sensitivity spectroscopy and dynamic nuclear polarization enhanced nuclear magnetic resonance. The applications of MWTs in scientific applications include RF linear accelerators, plasma diagnostics and chemistry, and nonlinear spectroscopy. Applications in the medical sector are also broad. Medical applications include hyperthermia that locally heats tumor cells selectively and raptures their membrane leading to the destruction of cancerous cells, without harming healthy ones. Hyperthermia can also be used in ablation that dries up or desiccates tumors with localized application of heat for the removal of unwanted tissues. Some of the unconventional areas of applications in which MWTs have been explored are satellite power stations, creation of artificially ionized layers for the extension of radio range, city lighting, nitrogen-fertilizer raining, and environmental control by both ozone generation and atmospheric purification of admixtures such as chlorofluorocarbons that destroy the ozone layer (chapter 2, volume 1).

MWTs can be classified according to various viewpoints—the kinetic energy conversion type such as the klystron and the potential energy conversion type such as the magnetron; the O type such as the TWT, in which an external DC magnetic field is used to confine the electron beam in the axial direction of the device and the M type such as the magnetron, in which the magnetic field takes part in crossed-field beam-wave interaction (chapter 2, volume 1). From another viewpoint, MWTs have been classified as the Cerenkov radiation type such as the TWT, the transition radiation type such as the klystron, and the bremsstrahlung radiation type such as the gyrotron. MWTs have also been classified as the slow-wave type such as the TWT, and the fast-wave type such as the gyrotron, in which the interaction structures used are the slow-wave structure such as the helix, and the fast-wave structure such as the waveguide resonator, respectively. Similarly, from the viewpoint of the bunching mechanism, MWTs have been classified as the relativistic bunching type in which the relativistic dependence of the mass of an electron on its velocity becomes dominant and the non-relativistic bunching type in which such dependence becomes insignificant (chapter 2, volume 1). The cathode, which is considered to be the life of a MWT, has been outlined starting from the evolution of indirectly heated cathodes, namely, M and MM cathodes via L, A, and B cathodes (chapter 3, volume 1). While the cathodes of conventional MWTs are operated under a space-charge limited condition that provides a control of the beam current by the beam voltage, the cathodes of a magnetron injection gun (MIG) of fast-wave tubes such as the gyrotron are operated under temperature-limited conditions to minimize the beam velocity spread (chapters 3 and 4, volume 1). We have introduced the basic Child–Langmuir and Richardson–Dushman relations for space-charge-limited and temperature-limited conditions of emission, respectively

(chapter 3, volume 1). We have identified and outlined some enabling concepts and outlined them as they prove to be useful in the understanding of the behavior of MWTs (chapter 3, volume 1). Thus, space-charge waves and cyclotron waves have been introduced that help one to understand the behaviors of MWTs such as the TWT and the gyrotron, respectively. In MWTs (with exceptions, such as in the peniotron), the electrons need to be bunched before their kinetic energy, as in a gyrotron, or their potential energy, as in a magnetron, is converted into RF energy. The bunching of electrons may be non-relativistic for instance, in a TWT, and relativistic for instance, in a gyrotron (chapter 3, volume 1). Understanding the principles of MWTs, for instance, klystron is based on the concept of induced current on electrodes. Currents are induced on the electrodes, such as the grids of the device due to the electron beam flowing between the electrodes and subsequently realized as an external circuit current, even when the electrons do not actually strike an electrode, provided the number and/or velocity of electrons approaching the electrode is different from that receding from it (chapter 3, volume 1). It is useful to analytically appreciate the upper limit of the beam current, and hence beam power, in MWTs set by the space-charge limiting current which is found to depend on the radius of the beam relative to that of the drift tube surrounding the beam in the device. The space-charge limiting current can be increased by placing the beam closer to the drift tube, say, the metallic boundary of an interaction structure of a tube as can be done, for instance, in a gyrotron. In contrast, in a tube like the virtual cathode oscillator (vircator), the space-charge limiting current is reduced to encourage the formation of a virtual cathode by placing the beam far from the metallic boundary (chapter 3, volume 1). It is also useful to analytically appreciate that in crossed-field tubes like the magnetron, it is the potential energy that is converted into RF energy rather than the kinetic energy, since in such a device on average the kinetic energy gained by an electron in its motion along a direction is also lost by it in its motion in a transverse direction (chapter 3, volume 1). That the beam current becomes insignificantly small if an interaction structure of a tube separates a cathode and an anode, which can be appreciated by the Child–Langmuir relation (chapter 3, volume 1), therefore calls for an electron gun in an O-type MWT (chapter 4, volume 1). The electron gun throws the beam of the desired parameters into the interaction structure of a device and it is confined by a focussing structure and collected by a beam dump or collector. The Child–Langmuir relation is the starting point of the synthesis of the extensively used gun, called the Pierce gun, derived from a flat planar cathode including the prediction of the electrode shapes from the solution of a two-dimensional Laplace equation. Similarly, the Langmuir–Blodgett relation is the starting point for the synthesis of the Pierce gun derived from a large-area curved cathode, which can be synthesized for its output parameters, including its electrode shapes found by conformal mapping (chapter 4, volume 1). However, in order to form a hollow annular beam of gyrating electrons we use an electron gun called the magnetron injection gun (MIG), so named because of its cathode assembly resembling a magnetron. The MIG forms small helical beamlets drawn off from the annular emitting portion of the conical cathode surface and subjected to a system of a crossed electric and magnetic fields. For this purpose, the

first anode or gun anode and the gun solenoid of the MIG provide the required electric and magnetic fields, respectively. The non-emitting portion of the cathode of the MIG serves as a focusing electrode and the second anode of the MIG accelerates electrons in the axial direction. In yet another gun, called the cusp gun, which finds use in a large-orbit gyrotron (LOG) that is suitable for the beam harmonic operation of a gyrotron allowing the latter to operate with a lower magnetic field (chapter 7, volume 2), a beam of axis-circling electrons is formed (chapter 4, volume 1). The electron beam formed by a gun needs to be confined in the interaction structure by means of a magnetic focussing structure. According to one of the conditions, called Brillouin conditions, for beam focussing for no beam scalloping, the cathode of the gun should be magnetically shielded. The other conditions to be satisfied at the entrance of the focussing structure are that the beam should have a radius equal to one to be maintained constant throughout the beam transport; that there should be no radial component of beam velocity; and that the magnetic flux density in the focussing structure should be related to the beam parameters, namely, the beam voltage, current and radius by a relation called the Brillouin relation (chapter 4, volume 1). In another approach of beam confinement, called the confined-flow focussing, unlike in Brillouin focussing, the magnetic flux lines are allowed to thread into the cathode. Moreover, in this approach, the stringent Brillouin conditions are relaxed and, at the same time, the beam radius becomes much less sensitive to the variation of beam current density. Further, the advent of periodic permanent magnet (PPM) as well as that of lightweight magnetic materials such as samarium-cobalt and ALNICO-5 has made it possible to replace heavy magnetic solenoid focussing with PPM focussing thereby expanding the scope of MWTs to many applications including space applications (chapter 4, volume 1).

We have also provided an analytical appreciation of beam-absent or cold behaviors of interaction structures exemplified with reference to helical structures in the slow-wave regime and disc-loaded waveguides in the fast-wave regime (chapter 5, volume 1). Both the approaches of field and equivalent circuit analyses have been made to analyze helical structures. The model for dielectric helix-supports and that for finite number of metal vanes of the envelope of the structure have been developed based on field analysis. The rigor to the analysis has been added by including the effects of finite helix thickness, non-uniformity of radial propagation over the structure's cross section, structure losses and asymmetry of dielectric helix-support rods. The simple Pierce's sheath-helix model has been improved by Sensiper's tape-helix model, which is valid even for a relatively small number of helix turns per guide wavelength. The tape-helix model can take into account the effect of the finite helix tape width and that of space-harmonics generated due to the axial periodicity of helix turns (chapter 5, volume 1). The analytical expressions for the dispersion relation and interaction impedance of the helical structure have been used to find the optimum structure parameters for the desired dispersion characteristics of the structure at a high value of interaction impedance as required to implement wideband gain-versus-frequency characteristics of a TWT. We have also discussed the non-resonant perturbation technique to experimentally find the

dispersion and interaction versus frequency characteristics of helical structures (chapter 5, volume 1).

The field analysis can also be extended to study fast-wave interaction structures. Here, for analysis, we have typically chosen the disc-loaded circular waveguides, which have potential application in wideband gyro-TWTs (chapter 5, volume 1). We have provided steps for obtaining the dispersion relation and dispersion characteristics and the expression for interaction impedance and interaction impedance versus frequency characteristics of a basic disc-loaded circular waveguide with metal discs of uniform hole-radius and uniform axial periodicity. With reference to a disc-loaded structure, the interaction impedance is referred to as the azimuthal interaction impedance since in a gyro-device it is the azimuthal RF electric field that takes part in beam-wave interaction. The analysis has been outlined first for infinitesimally thin metal discs and then for metal discs of finite thickness. Further, two variants of the basic disc-loaded circular waveguide have been analysed. The first of these variants is the interwoven-disc-loaded circular waveguide comprising two interwoven groups of annular metal discs such that the discs of any of these groups have the same hole-radius though the two groups themselves differ in hole-radii. The second variant analysed consists of a circular waveguide loaded with alternate dielectric and metal discs. The structure parameters of a disc-loaded waveguide, namely, the waveguide radius, the disc-hole radius and the structure periodicity can be optimized to shape the dispersion characteristics of the waveguide and hence obtain wideband coalescence between the waveguide-mode and beam-mode dispersion characteristics at a high value of azimuthal interaction impedance, which can be used to implement wideband gain-versus-frequency characteristics of a gyro-TWT (chapter 5, volume 1).

The analysis of the beam-present interaction structure has also been outlined, which leads to the derivation of the dispersion relation of the structure in the presence of an electron beam (chapter 5, volume 1). Typically, the analysis gives the dispersion relation of a TWT following the approach of Pierce by combining the circuit and electronic equations. Similarly, the dispersion relation of a gyro-TWT is obtained starting from the wave equation for the axial component of the RF magnetic field in the presence of a thin hollow, annular, electron beam in helical trajectories in a waveguide excited in TE mode. The solution of the beam-present dispersion relation for the propagation constant referring to a growing wave can be interpreted to obtain the gain relation of a TWT or gyro-TWT. The gain relation has been typically exemplified in a tapered disc-loaded gyro-TWT in which the disc parameters are optimized for wideband coalescence between the waveguide-mode and beam-mode dispersion characteristics and, at the same time, the waveguide cross section is tapered thereby resulting in a wideband gain-versus frequency response of the device bandwidth at a reasonably large gain (chapter 5, volume 1).

In this book we have explored both conventional and unconventional MWTs. The conventional MWTs have included TWTs with an emphasis on helix TWTs; klystrons including multi-cavity and multi-beam types; and crossed-field tubes, namely, the magnetron, crossed-field amplifier (CFA) and carcinotron. We have also discussed klystron variants including the reflex klystron, inductive output tube

(IOT), extended interaction klystron (EIK), extended interaction oscillator (EIO) and twystron (chapter 6, volume 2). Further, the advent of fast-wave tubes such as the gyrotron has made it possible to design MMTs with larger sizes in the millimeter-wave frequency regime (chapter 7, volume 2). This has alleviated the problem of extending the operating frequencies of slow-wave conventional MWTs to the millimeter-wave and higher ranges of frequencies where such tubes become so tiny that makes it difficult to handle large power and provide the required thermal management. At the same time, the evolution of such fast-wave tubes gives one an option to do away with the method of reducing the frequencies of light-wave quantum mechanical devices (such as the laser) down to microwave frequencies—a method that would be associated with the reduction of energy of each quantum as well as with the difficulty in sustaining population inversion. Thus, the development of fast-wave tubes has filled the millimeter-wave technology gap (chapter 7, volume 2). Fast-wave tubes that have received attention encompass the gyrotron, gyro-BWO, gyro-klystron and gyro-TWT, in which cyclotron resonance maser (CRM) instability dominates over Weibel instability. We have also discussed fast-wave tubes, namely, the cyclotron auto-resonance maser (CARM), in which CRM and Weibel instabilities are present in equal proportions, and the slow-wave cyclotron amplifier (SWCA), in which Weibel instability dominates over CRM instability. Hybrid gyro-tubes, namely, the gyro-twystron, harmonic multiplying gyro-TWT, triplet gyrotron amplifier (gyro-triotron) and phigtron have also been discussed (chapter 7, volume 2). We have also discussed the peniotron which, unlike conventional gyro-tubes such as the gyrotron, does not require relativistic bunching of electrons for its operation. In a peniotron, both initially accelerated and initially decelerated electrons are made to deliver kinetic energy to the RF waves thereby making the device highly efficient (chapter 7, volume 2).

The book has further brought within its purview vacuum microelectronic (VME) MWTs, which can operate in W and terahertz bands. These tubes are micro-fabricated using vacuum-microelectronic technology in which both vacuum-tube and solid-state microelectronic technologies coexist (chapter 8, volume 2). The VM-MWTs discussed are the klystrino module comprising typically separate electron guns but a common vacuum and collector with cavities fabricated using LIGA technology, and the nanoklystron that uses a CNT field-emission cold cathode and a cavity structure formed monolithically from silicon wafers using DRIE technology. There is yet another example of the coexistence of these two technologies in a compact microwave power module (MPM), in which the overall gain of the MPM is equally shared between a TWT and a solid-state power amplifier (SSPA); the former boosting up the latter in RF power output, while a built-in power supply provides DC power to both. In the terahertz regime, there is yet another device discussed, namely, the clinotron, which is basically a BWO with an inclined electron beam impinging on a grating interaction structure that has a larger beam thickness than the conventional BWO allowing thereby each layer of the inclined beam to take part in beam-wave interaction effectively. The device enjoys large tunability by the successive excitation of the resonator modes obtained by varying the beam voltage (chapter 8, volume 2).

Furthermore, the evolution of high power microwave (HPM) MWTs has made it possible to develop lethal and non-lethal directed energy weapons (DEWs) for information warfare (IW) to cause burnout and lethal damage to electronic systems or for the deception/spoofing of enemy systems to mission failure. Intensive relativistic beams (IREBs) have been used in HPM-MWTs (chapter 8, volume 2). Some IREB-driven HPM-MWTs discussed are: the 'relativistic' versions of conventional MWTs such as the magnetron, klystron, TWT and BWO, RELTRON (being a kind of relativistic klystron). In this category, we have also discussed the virtual cathode oscillator (vircator), which is a bremsstrahlung radiation type of MWT in which a bremsstrahlung of electrons takes place in the electrostatic field, unlike in a gyrotron where such bremsstrahlung takes place in the magnetic field. We have also discussed the magnetically insulated line oscillator (MILO) that uses a self-generated magnetic field to control electronic motion requiring no external magnetic field. Other such HPM-MWTs discussed are: the surface-wave oscillator (SWO), orotron or radiation diffraction generator (RDG); multiple-wave Cerenkov generator (MWCG) and multi-wave diffraction generator (MWDG). Moreover, we have also discussed HPM-MWTs that accrue the advantage of plasma assistance in enhancing their space-charge limiting current thereby increasing their beam current and hence beam power. Those discussed are: the plasma-wave tube (PWT), plasma-assisted slow-wave oscillator (PASOTRON), plasma-filled TWTs and gyrotrons (chapter 8, volume 2). Further, in the present monograph, we have presented a glimpse of representative frequency and power ranges of common MWTs (chapter 9, volume 2), though more device performance data have been provided as and where necessary in the rest of the chapters of this book.